

Taewoo Kim

Installation of an offshore wind turbine blade using a jack-up installation vessel in water depth of 60m

Master's thesis in Marine Technology

Supervisor: Zhen Gao

June 2021

Taewoo Kim

Installation of an offshore wind turbine blade using a jack-up installation vessel in water depth of 60m

Master's thesis in Marine Technology
Supervisor: Zhen Gao
June 2021

Norwegian University of Science and Technology
Faculty of Engineering
Department of Marine Technology



Norwegian University of
Science and Technology

Abstract

Offshore wind turbines are important sources of renewable energy. The offshore wind turbine industry grows very rapidly. The global offshore wind is expected to grow with an annual growth rate of 18.6% until 2024 and 8.2% to 2030. The size of the wind turbine gets larger. 10MW and 15MW wind turbines have been released. The blade length reaches about 100 meters. The hub height is above 100 meters. The parts of wind turbines become heavier. The blade of a 10MW wind turbine weighs 42 tons. The nacelle weight of the 10MW wind turbine is 446 tons. The installation number of the offshore wind turbines becomes larger. Recently constructed wind farms had 50 ~ 180 wind turbines. Because of these trends of offshore wind turbines, the installation of offshore wind turbines becomes important. One of the most critical phases of the offshore wind turbine installation is the blade installation. Since the blade is a very large and slender body, it can be highly affected by environmental forces.

In this thesis, the installation of the blade is investigated. The blade motions are simulated by SIMA. The blade of DTU 10MW wind turbine is used. A jack-up vessel is used for the blade installation. The aerodynamic force on the blade is simulated by TurbSim. The hydrodynamic load on the jack-up vessel is simulated by SIMA.

In 2~5m/s constant wind conditions, the translational change of the blade is less than 0.5m. The rotational angle is less than 2 deg. The initial pitch angle of the blade gives an effect on the applied forces and moments. They are smallest when the initial pitch angle is -15 ~ 0 deg. The wind affects the average and the standard deviation of the blade position. The wave affects the standard deviation of the blade position. The natural period of the jack-up vessel is about 3 sec. The surge, heave, and pitch motion of the blade have peak frequency at the natural frequency of the jack-up vessel. The peak frequencies of the sway, roll and yaw motions are zero. Wave is important for a blade installed by a semi-submersible. The surge, heave, pitch, and yaw motion of the blade have the same peak frequency as the peak frequency of the wave.

Sammendrag

Vindturbiner til havs er viktige kilder til fornybar energi. Vindturbinindustrien til havs vokser veldig raskt. Den globale havvinden forventes å vokse med en årlig vekstrate på 18,6% fram til 2024 og 8,2% til 2030. Vindturbinens størrelse blir større. 10MW og 15MW vindturbiner er frigitt. Knivlengden når omtrent 100 meter. Navhøyden er over 100 meter. Delene av vindturbiner blir tyngre. Bladet til en 10 MW vindturbin veier 42 tonn. Nacellevekten til 10MW vindturbinen er 446 tonn. Installasjonsnummeret på havvindturbinene blir større. Nylig konstruerte vindparker hadde 50 ~ 180 vindturbiner. På grunn av disse trendene med havvindturbiner blir installasjonen av havvindturbiner viktig. En av de mest kritiske fasene i offshore vindturbininstallasjonen er bladinstallasjonen. Siden bladet er en veldig stor og slank kropp, kan det bli sterkt påvirket av miljøkrefter.

I denne oppgaven blir installasjonen av bladet undersøkt. Knivbevegelsene er simulert av SIMA. Bladet til DTU 10MW vindturbin brukes. Et oppjekkningsfartøy brukes til bladinstallasjonen. Den aerodynamiske kraften på bladet er simulert av TurbSim. Den hydrodynamiske belastningen på jack-up fartøyet er simulert av SIMA.

I 2 ~ 5m / s konstante vindforhold er bladets translasjonsendring mindre enn 0,5m. Rotasjonsvinkelen er mindre enn 2 grader. Den opprinnelige stigningsvinkelen til bladet gir en effekt på de påførte kreftene og momentene. De er minste når den første stigningsvinkelen er -15 ~ 0 grader. Vinden påvirker gjennomsnittet og standardavviket til bladposisjonen. Bølgen påvirker standardavviket til bladposisjonen. Den naturlige perioden med oppjekkningsfartøyet er omtrent 3 sek. Bladets overspenning, heving og stigning har toppfrekvens ved den naturlige frekvensen til oppjekkningsfartøyet. Toppfrekvensene til sving-, rull- og girbevegelsene er null. Bølge er viktig for et blad installert av en nedsenkbar del. Bladets sving, heving, stigning og gjenging har samme toppfrekvens som toppfrekvensen til bølgen.

Preface

This thesis is done as a master's degree program of the Marine Technology Department of the Norwegian University of Science and Technology (NTNU). The relevant course is 'TMR4930 Marine Technology, Master's Thesis'. The thesis work has been conducted under the supervision of Professor Zhen Gao and by collaboration with Shuzhou Jiang. Shuzhou Jiang is a master's degree course student. This thesis deals with the blade installation by a jack-up vessel. Jiang's research deals with the same subject by a semi-submersible.

Acknowledgment

First, I would like to express my sincere appreciation to my supervisor Prof. Zhen Gao. His excellent guidance helps me to understand and investigate the subject. I would also like to thank my teaching assistant Ms. Menging Wu. She answered my questions with patience and kindness.

I am highly grateful to Shuzhou Jiang. He and I have collaborated on this study from the beginning. Thanks to his dedicated efforts, we were able to solve the difficulties one by one.

I also thanks Juyoung and Jaehyung who entered NTNU together with me. They helped me a lot to study. It is my good memory to study with them in Tyholt.

I appreciate my mother and my sister in South Korea. They always considered me so that I stayed well in Norway.

Last but the most important, I would like to thank my family. My two wonderful daughters and my wife help me concentrate on my studies during whole my master's degree course period.

Table of Contents

List of Figures	xi
List of Tables.....	xii
1 Introduction	14
1.1 Introduction of wind turbine.....	14
1.2 Growth of offshore wind turbines.....	15
1.2.1 New installation trend of offshore wind turbine	15
1.2.2 Trend of wind turbine size.....	16
1.2.3 Dimension trend of wind turbine	17
1.2.4 Installation number trend of wind turbine	18
1.3 Classification of wind turbines by foundation	19
1.3.1 Bottom fixed wind turbines	19
1.3.2 Floating wind turbines	20
1.4 Overall wind turbine installation	23
1.4.1 Installation procedure.....	23
1.5 Single blade installation	26
1.6 Installation vessels	29
1.7 Research purpose	30
2 Theories of the blade installation.....	31
2.1 Description of a coupled system of blade installation.....	31
2.2 Aerodynamic loads	33
2.2.1 Aerodynamic loads on the blade	33
2.2.2 Wind loads on the jack-up hull.....	36
2.3 Hydrodynamic loads	37
2.3.1 Wave loads on the jack-up legs	37
2.4 Jack-up soil-structure interaction.....	38
2.5 Structural modeling	38
2.6 Mechanical couplings	39
2.7 Time-domain simulations.....	39
2.8 Extreme value analysis by use of Gumbel distribution	39
3 Numerical model.....	41
3.1 Model components specifications	41
3.1.1 Coordinate systems.....	41
3.1.2 Blade and lifting arrangements	41
3.1.3 Jack-up vessel specification.....	42

3.1.4	Crane specification.....	42
3.2	Loading and coupling methods	43
3.2.1	Wind load	43
3.2.2	Hydrodynamic loads.....	44
4	Results and discussion.....	45
4.1	Installation system characteristics	45
4.1.1	No external load condition.....	45
4.1.2	The blade position in the constant winds.....	45
4.1.3	The blade position in regular wave loads.....	46
4.1.4	The effect of the initial blade pitch angles	50
4.1.5	The effect of the turbulent wind and the irregular waves.....	51
4.1.6	Simulations with different wind and wave seeds	58
4.1.7	Comparison of the blade installation simulation results of the jack-up vessel and the semi vessel (collaboration research)	66
5	Conclusions.....	70
5.1	The summary of the discussion about results	70
5.2	Future work suggestion	70
6	Reference	71
7	Appendices	74

List of Figures

Figure 1.1: Global levelized cost of generation [2]	14
Figure 1.2: Offshore wind turbine installation present conditions as of 2019 [6]	15
Figure 1.3: New installation trend of offshore wind turbines [6].....	15
Figure 1.4: Global offshore wind growth expectation to 2030 [6]	16
Figure 1.5: Offshore wind turbine project size trend [6]	16
Figure 1.6: Trend of wind turbine size [10]	17
Figure 1.7: Some typical foundation concepts and their respective share on commercial projects as of December 2012 [4] (a) Gravity-based foundation (16%), (b) monopile foundation (74%), (c) caisson foundation (0%),(d) multi pile foundation (5%), (e) multi caisson foundation (0%) and (f) jacket foundation (5%)	19
Figure 1.8: Different types of floating turbines [6]	21
Figure 1.9: Procedure of monopile offshore wind turbine [22]	24
Figure 1.10: Offshore wind turbine installation strategies [23]	26
Figure 1.11: Flowchart of the typical single blade installation [24]	27
Figure 1.12: Blade lifting [22]	27
Figure 1.13: Alignment phase [24]	28
Figure 1.14: (a) Schematic of the main components involved in the mating process (b) Positions of the guide pin and flange hole in the yz-plane [24]	29
Figure 1.15: Wind turbine installation vessels	29
Figure 2.1: The structural and external force models of a typical elevated jack-up crane vessel [37]	32
Figure 2.2: Definition of coordinate systems $O - XYZ$, $O - XbYbZb$ and $O - XcYcZc$ are respectively the global, blade-related and local blade element coordinate systems [40]	33
Figure 2.3: Illustration of cross-flow principle: $VA, i = VA, i, xc VA, i, yc VA, i, zcT$ [40]	34
Figure 2.4: Flow chart for aerodynamic modeling	35
Figure 2.5: Distribution of lift and drag forces on a blade under rotating condition and lifting condition: blade pitch angle 0; rotational speed for the rotating blade 8.029 rpm; constant wind 10m/s [34]	36
Figure 2.6: Illustration of wind area and relative wind inflow angle (top view)	37
Figure 2.7: Wave loads on jack-up legs[40]	37
Figure 2.8: Modeling of soil resistance force on the spud can using linear springs and dampers [34].....	38
Figure 3.1: Definition of coordinate systems for the blade installation system[34]	41
Figure 3.2: Illustration of the tugger line system	42
Figure 3.3: Illustration of a typical offshore pedestal crane [37]	43
Figure 3.4: Overview of the coupled simulation method [34]	44
Figure 4.1: An example of the incident wave.....	46
Figure 4.2: The responses of the jack-up hull for an incident wave with 1m amplitude ..	47
Figure 4.3: The responses of the blade for an incident wave with 1m amplitude	48
Figure 4.4: The name of the leg components	48
Figure 4.5: The fluctuating axial forces and the bending moments due to regular waves	49
Figure 4.6: Time series and spectral density plots of the blade motion ($H_s = 1.0m$, $T_p = 9$ sec, $U_w = 5m/s$)	54
Figure 4.7: Time series and spectral density plots of the jack-up hull motion ($H_s = 1.0m$, $T_p = 9$ sec, $U_w = 5m/s$)	55
Figure 4.8: Lift Wire.....	60

Figure 4.9: The Gumbel distribution plots of the maximum and the minimum of the 6 D.O.F motions of the blade	65
Figure 7.1: Time series and spectral density plots of run #1	76
Figure 7.2: Time series and spectral density plots of run #2	77
Figure 7.3: Time series and spectral density plots of run #3	78
Figure 7.4: Time series and spectral density plots of run #4	79
Figure 7.5: Time series and spectral density plots of run #5	80
Figure 7.6: Time series and spectral density plots of run #6	81
Figure 7.7: Time series and spectral density plots of run #7	82
Figure 7.8: Time series and spectral density plots of run #8	83
Figure 7.9: Time series and spectral density plots of run #9	84
Figure 7.10: Time series and spectral density plots of run #10	85
Figure 7.11: Time series and spectral density plots of run #11	86
Figure 7.12: Time series and spectral density plots of run #12	87
Figure 7.13: Time series and spectral density plots of run #13	88
Figure 7.14: Time series and spectral density plots of run #14	89
Figure 7.15: Time series and spectral density plots of run #15	90
Figure 7.16: Time series and spectral density plots of run #16	91
Figure 7.17: Time series and spectral density plots of run #17	92
Figure 7.18: Time series and spectral density plots of run #18	93
Figure 7.19: Time series and spectral density plots of run #19	94
Figure 7.20: Time series and spectral density plots of run #20	95

List of Tables

Table 1.1: Global levelized cost of generation (USD per MWh) [2]	14
Table 1.2: Dimensions of wind turbines [11]	17
Table 1.3: Major wind turbine specifications	18
Table 1.4: Recent offshore wind farms [5]	18
Table 1.5: Proposed offshore wind farms [15]	18
Table 1.6: Comparison of mainstream floating foundation [6]	22
Table 1.7: Jack-up vessel specifications	29
Table 1.8: Floating vessel specifications	30
Table 1.9: Wind turbine jack-up vessel generations [33]	30
Table 3.1: Main properties of the blade lifting system[34]	42
Table 3.2: Main parameters of the jack-up vessel[37]	42
Table 3.3: Main parameters of the crane	43
Table 3.4: TurbSim input setting	43
Table 4.1: The blade positions in no wind and no wave condition	45
Table 4.2: The blade position change due to the wind speed and the wind direction	45
Table 4.3: The forces and the moments on the blade due to the blade pitch angles (dynamic calculation)	50
Table 4.4: The translational and the rotational displacement of the blade due to the blade pitch angles (dynamic calculation)	50
Table 4.5: The translational and the rotational displacement (static calculation)	50
Table 4.6: The real blade pitch angle due to the initial blade pitch angle	51
Table 4.7: The blade position and angle due to the turbulent wind speed (winds only) ..	51

Table 4.8: The blade motions due to the significant wave heights	52
Table 4.9: The blade position and angle due to the wave peak periods	53
Table 4.10: The environmental conditions (the turbulent wind and irregular wave combinations)	54
Table 4.11: The blade motion due to the turbulent winds and irregular waves combinations	56
Table 4.12: The influence of the environmental factors on each motion	57
Table 4.13: The seeds of the wind and wave of simulations	58
Table 4.14: Statistical result of 6 D.O.F. motions of the blade in the 20 simulations with different seeds ($H_s = 2.0\text{m}$, $T_p = 9\text{sec}$, $U_w = 10\text{m/s}$)	59
Table 4.15: Peak frequency of the blade motion, the wave elevation, and the axial force of the lift wire of the irregular waves and turbulent wind environment [rad/s]	61
Table 4.16: Axial force of the lift wire of the irregular waves and turbulent wind environment ($H_s = 2.0\text{m}$, $T_p = 9\text{sec}$, $U_w = 10\text{m/s}$)	62
Table 4.17: The axial force of the tugger line	63
Table 4.18: The maximum and the minimum values of the blade position and angle	63
Table 4.19: Coefficients of the Gumbel distribution of the maximum of the 6 D.O.F motions of the blade	64
Table 4.20: The blade positions of the semi in no wind and no wave condition	66
Table 4.21: Statistical values of the blade position and angle in the 20 simulations with different seeds ($H_s = 2.0\text{m}$, $T_p = 9\text{sec}$, $U_w = 10\text{m/s}$) [semi-submergible]	66
Table 4.22: The maximum values of the blade position and angle of the semi (The values are corrected by the static results in the calm sea)	68
Table 4.23: The spectral density peak frequency of the position and angle of the blade installed by a semi-submersible vessel	69

1 Introduction

1.1 Introduction of wind turbine

A wind turbine is an electricity generator that converts the wind's kinetic energy to electrical energy. Wind farms are a cluster of many wind turbines. They are one of the important sources of renewable energy to reduce greenhouse gases. [1]

Wind turbines are already competitive among electricity generation. In 2020, the investment bank Lazard, Bloomberg New Energy Finance(BNEF), and International Renewable Energy Agency (IRENA) investigated cost according to generation methods, respectively. [2]

Table 1.1: Global leveled cost of generation (USD per MWh) [2]

Source	Solar (utility)	Wind onshore	Gas combined cycle	Geothermal	Wind Offshore	Coal	Nuclear	Gas peaker	Solar (residential)
Lazard	36	40	59	80	86	112	164	175	186
BNEF	50	44							
IRENA	68	53		73	113				
Lazard (ranges)	29 - 42	26-54	44-73	59-101	86	65-159	129-198	151-198	132-245

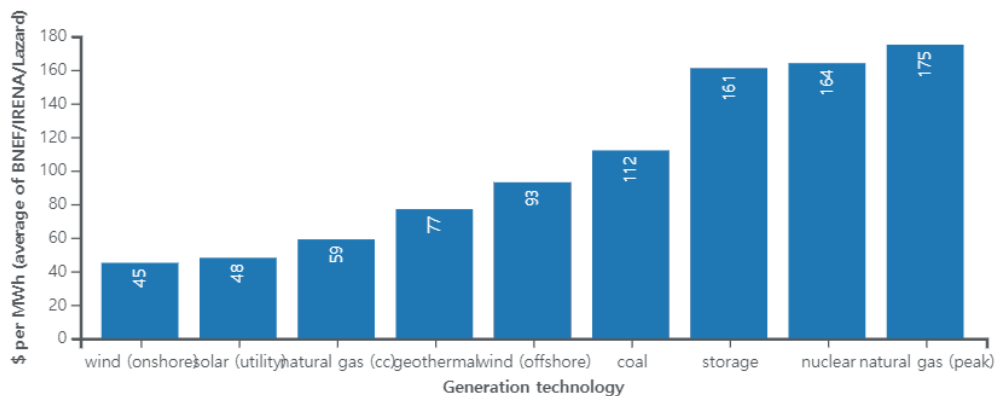


Figure 1.1: Global leveled cost of generation [2]

Offshore wind turbines are installed in the sea. This can lead to some advantages. Since higher wind speeds are available compared to on land, the electricity generation in the sea can get higher per amount of capacity installed,[3] and NIMBY opposition to the wind turbines is usually smaller. Offshore wind may be stronger in the afternoon when people are using the most electricity. Furthermore, offshore turbines can also be located near large cities with coasts. This reduces transmission costs and facilities for transmission.[4] However, there are some disadvantages to offshore wind turbines. It is more expensive to install them and difficult to access. They may operate in harsher conditions. [5]

1.2 Growth of offshore wind turbines

As of the end of 2019, the total wind power was 29.1 gigawatt(GW) in the world. All the largest offshore wind farms are in northern Europe. The United Kingdom and Germany take over two-thirds of the total offshore wind power installed worldwide. Almost 60% of new offshore wind installations and about 75% of existing offshore wind installations are in Europe. As of 2020, the 1.2GW Hornsea Project One in the United Kingdom is the largest offshore wind farm in the world. [7] Dogger Bank in the United Kingdom at 4.8 GW and Greater Changhua in Taiwan at 2.4GW are in the planning stage. [8]

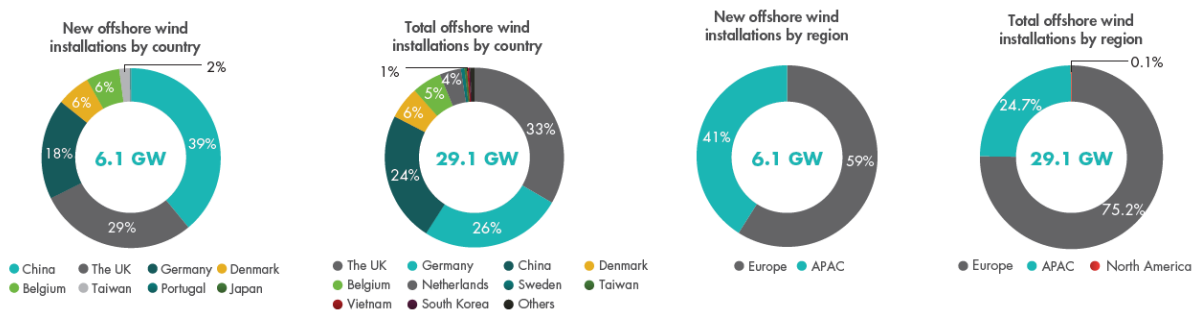


Figure 1.2: Offshore wind turbine installation present conditions as of 2019 [6]

Wind power generation takes 4.7% of the world's electricity output in 2018. It is expected that wind power generation increases from 1,280 TWh/yr in 2017 to 18,500 TWh/yr in 2050. By 2050, the wind is expected to supply more than 40% of electricity in OECD Pacific and Europe, and more than 30% of electricity in China, Latin America, and North America. The portion of offshore wind in the total wind electricity generation will increase steadily, rising globally from 5.5% in 2018 to 28% in 2050, a fifth of which is floating offshore. [9] Due to the high demand for wind energy, both the installation number and size of a wind turbine are expected to dramatically increase.

1.2.1 New installation trend of offshore wind turbine



Figure 1.3: New installation trend of offshore wind turbines [6]

The global offshore market has grown 24% annually since 2013 that the total installations reach 29.1 GW, which amounts to 5% of the total capacity of the global wind as the end of 2019. Europe will remain the largest offshore market at the end of 2019. It makes up

75% of total global offshore wind installation. The installation of offshore wind turbines is also increasing in Asian countries, China, Taiwan, Vietnam, Japan, and South Korea. North America has only 30MW offshore wind generation, but its capacity is increasing. The top five offshore wind installation markets are the UK, Germany, China, Denmark, and Belgium.[6]

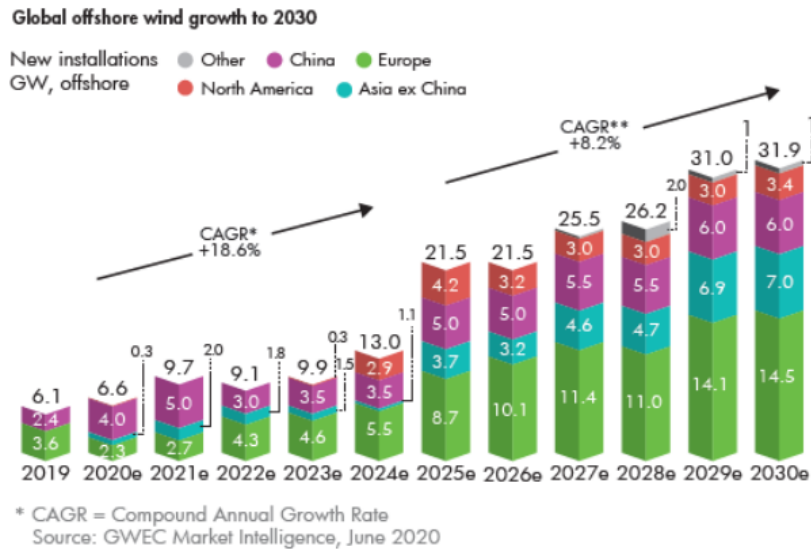


Figure 1.4: Global offshore wind growth expectation to 2030 [6]

The global offshore wind is expected to grow with an average annual growth rate of 18.6% until 2024 and 8.2% to 2030. New annual installations are expected to come to 20GW in 2025 and 30 GW in 2030. New offshore wind capacity will be added over 205GW until 2030. Three-quarters of this new volume will be added in 2025-2030 due to plans to connect to the grid. Offshore wind will be 10% of global new wind power installations in 2019. Due to the acceleration of the growth of offshore wind turbines, it is expected that offshore wind will take more than 20 percent of total wind installations by 2025. [6]

1.2.2 Trend of wind turbine size

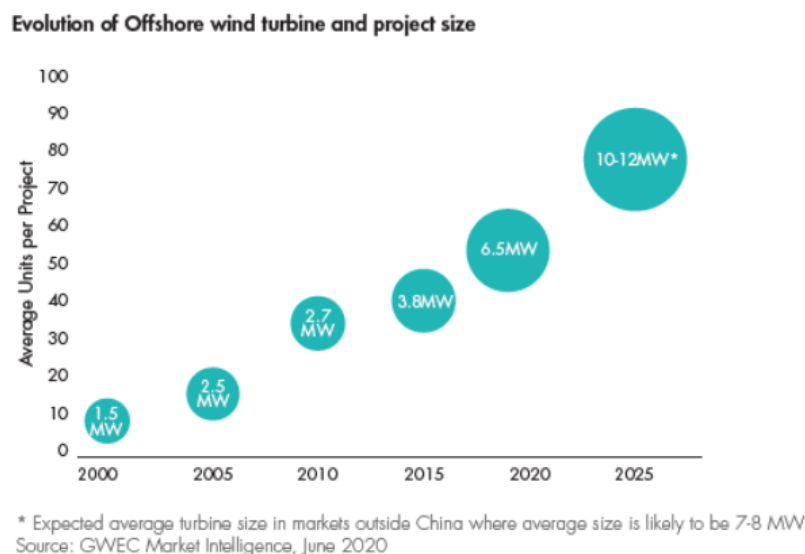


Figure 1.5: Offshore wind turbine project size trend [6]

The size of a wind turbine has been increasing. When the world’s first offshore wind farm, Vindeby, was installed in Denmark in 1991, the turbine size was only 450kW (Bonus B35). Since then, the offshore wind turbine size has grown significantly with the global average offshore wind turbine size reaching 1.5 MW in 2000 and 6.5 MW in 2018. In Europe, the average turbine size for new installations in 2019 becomes higher, 7.2 MW. GE Renewable Energy introduced *Haliade X 12 MW DD* turbine 2018 with the prototype installed in Rotterdam for onshore testing from November 2019.

Siemens Gamesa released its *SG14- 222 DD* model in May 2020. This new turbine which can reach 15 MW with Power Boost will be available on the market from 2024. It was predicted in GWEC’s recent Global Offshore Wind Technology webinar that the next generation of offshore turbine technology could probably be around 20 MW with a 275m rotor diameter by 2030.[6]

1.2.3 Dimension trend of wind turbine

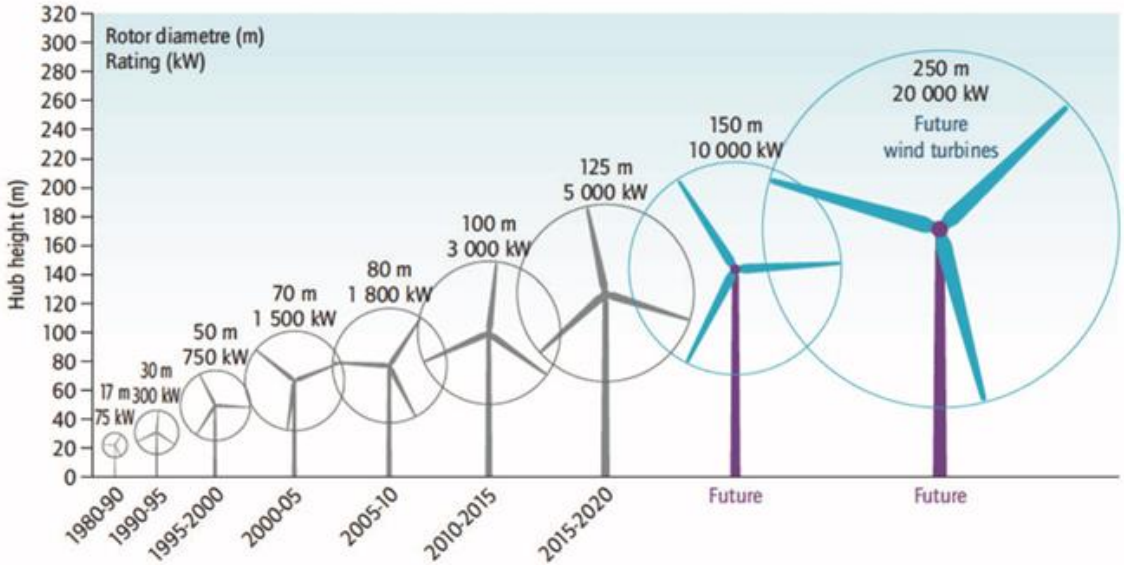


Figure 1.6: Trend of wind turbine size [10]

Table 1.2: Dimensions of wind turbines [11]

	Vindby 450kW	2MW	NREL 5MW [12]	8MW	DTU 10MW [13]	12MW	IEA 15MW [14]
Blade length [m]	rotor dia. 35	44	61.5	82	86.4	108	117
Blade weight [ton]	-	10	17	35	41.7	55	65
Hub height [m]	35	78	90	138	119	135	150
Nacelle weight [ton]	-	75	240	390	446	500	630

Due to the high demand for renewable energy and economical reason, the size of a wind turbine has been increased. [Figure 1.6] Main parameters due to capacities are shown in Table 1.2.

Table 1.3: Major wind turbine specifications

Description	NREL 5MW [12]	DTU 10MW [13]	IEA 15MW [14]
Rating	5MW	10MW	15MW
Rotor orientation, configuration	Upwind, 3 blades	Upwind, 3 blades	Upwind, 3 blades
Rotor, hub diameter	126m, 3m	178.3m, 5.6m	240m, 7.94m
Hub height	90 m	119m	150m
Blade length	61.5	86.4m	117m
Cut-in, Rated, Cut-out wind speed	3m/s, 11.4m/s, 25m/s	4m/s, 11.4m/s, 25m/s	3m/s, 10.59m/s, 25 m/s
Cut-in, Rated, rotor speed	6.9 rpm, 12.1 rpm	6 rpm, 9.6 rpm	-
Rated tip speed	80 m/s	90 m/s	-
Overhang, shaft tilt, Pre-cone	5m, 5°, 2.5°	7.07m, 5°, 2.5°	-
Blade weight	17 tons	41.7 tons	65.2 tons
Rotor mass	100 tons	229 tons	-
Nacelle mass	240 tons	446 tons	-
Tower mass	347 tons	605 tons	860 tons

1.2.4 Installation number trend of wind turbine

It is predicted by GWEC Market Intelligence that over 205GW of new offshore wind capacity is added over the next decade. This means that approximately 2000 wind turbines will be newly installed every year. 600 wind turbines will be installed in 2020, and the installation number continuously increases. More than 3000 wind turbines are expected to be installed in 2030.

For recent wind farms, the number of wind farms is usually 50 ~ 100 as shown in Table 1.4. However, according to Table 1.5, the capacities of each wind farm are expected to increase a few times. Hence, the number of wind turbines per wind farm will increase explosively. This may accelerate the enlargement of wind turbine size. The required number of wind turbines can be reduced by increase wind turbine size.

Table 1.4: Recent offshore wind farms [5]

Wind farm	Capacity	Turbines & model	Commissioning date
Hornsea 1	1,218	174 x Siemens SWT-7.0-154	2020
Beatrice	588	84 x Siemens SWT-7.0-154	2019
Hohe See	497	71 x Siemens SWT-7.0-154	2019
Borkum Riffgrund 2	450	56 x MHI Vestas V164-8.0 MW	2019
Horns Rev 3	407	49 x MHI Vestas V164-8.3 MW	2019
Walney Extension	659	40 x MHI-Vestas 8.25 MW 47 x Siemens Gamesa 7 MW	2018
Race Bank	573	91 x Siemens SWT-6.0-154	2018

Table 1.5: Proposed offshore wind farms [15]

Wind farm	Location	Capacity [MW]
IJmuiden Ver	Netherlands	4,000
East Anglia (formerly Norfolk Bank)	United Kingdom	3,100
Coastal Virginia O_shore Wind	United States	2,640
Hornsea Project Three	United Kingdom	2,400
Formosa III	Taiwan	2,000
Moray Firth	United Kingdom	1,866

1.3 Classification of wind turbines by foundation

1.3.1 Bottom fixed wind turbines

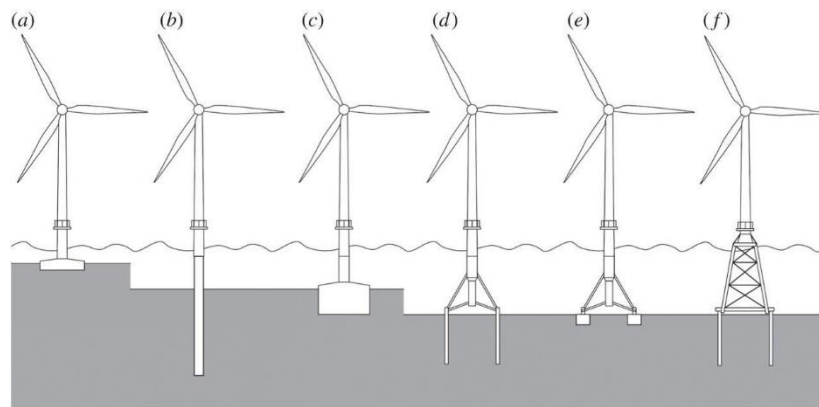


Figure 1.7: Some typical foundation concepts and their respective share on commercial projects as of December 2012 [4] (a) Gravity-based foundation (16%), (b) monopile foundation (74%), (c) caisson foundation (0%), (d) multi pile foundation (5%), (e) multi caisson foundation (0%) and (f) jacket foundation (5%)

- Monopile

An offshore wind turbine is composed of a wind turbine, tower, and foundation. A monopile structure is the most common foundation because of its simple and robust design. It is appropriate for mass fabrication. Conventional impact driving is a simple and suitable installation method for most soil conditions. Monopiles are easy to store, transport, and treat. The monopile is the best method in economic and technical view in shallow water. Therefore, most developments have been achieved in shallow water. For deeper water, other foundations and structures are preferred.

Many wind farms in both German and the UK are below 40m water depth. For example, 90% of the 9GW Dogger Bank development is below 35m and about 50% of the 4GW Hornsea development is below 40m water depth. By advanced finite element modeling and the development of new more highly optimized design methods, a monopile that can support 6~8MW wind turbines can be installed within most of these sites. Monopiles supporting 6MW wind turbines have been designed for water depth up to 35m, including those recently constructed for the Gode Wind Offshore Wind Farm. This monopile is 7.5m in diameter. Monopiles are developed to apply for water depths up to 60m. However, larger turbines and deeper water will challenge the technical feasibility of the monopile, particularly as wave increasingly acts with the dynamics of the turbine structure. [16]

- Gravity based foundation (also gravity-based structures)

According to Wind Europe's report (2017), monopile foundation was the most common of the classification in Europe, with 3720 units (81.7%). The jacket is next, with 315 units. The third is the gravity-based foundation, with 283 units. This characteristic of monopiles, together with their reduced cost, has displaced other types of foundations from a strategic position in the sector.

However, as water depth increases, monopiles show some limitations. These make other types of foundations increase in use. GBF can be an alternative to monopile in locations with the terrain where the driving-in of monopiles is difficult.

The GBF has some advantages. It is suitable in rocky or sandy soils with high bearing capacity. It can be an alternative that can enrich market competitiveness. Its performance is proven by the oil and gas industries. The GBF has some disadvantages. It is not much accepted in the wind industry at present. It needs soil with specific geotechnical properties, such as high bearing capacity. In general, previous soil preparation is needed for the correct support of the structure. It claims a large occupation area in the seabed, with its associated environmental impact. It also needs the means of manufacture, transport, and installation. [17]

- Jacket foundation

The jacket substructure is good in the transition-water depth (usually 30~35 meter) because of its comparably lighter structural mass, higher transparency to the wave loading, higher structural stiffness, and lower soil dependency. The jacket has foundations with a lattice framework that feature three or four seabed anchoring points. Furthermore, anchoring increases the levels of safety. The top of the jackets features a transition piece that is connected to the turbine shaft, while the legs are anchored to the seabed with piles. [18] [19] The jacket has some advantages, low wave loads, high capacity to carry turbines, and the ability to stand in very deep water.

It is difficult to manufacture a jacket. The nodes are extremely difficult to manufacture, and the cast with high-tensile steel nodes is very expensive. Furthermore, all the welding on a jacket is handmade and automation is not established well. In contrast, the monopile is largely manufactured using welding robots and a large degree of automation. So, the jacket has a downside, i.e., the price and complexity of manufacturing the jacket. [20]

- Etc.

As with other foundations of wind turbines, there are Caisson foundation, multi pile foundation, and multi caisson foundation. These foundations are not much used in real.

1.3.2 Floating wind turbines

A floating wind turbine uses a floating structure. Hence, it is applied to the place where fixed-foundation turbines are not feasible due to water depth. Floating wind farms have the potential to significantly increase the sea area available for offshore wind farms. Less visual pollution and good-quality winds are advantages of the far offshore area.

The floating foundation can be generally categorized into three configurations by floating principles for static stability: a semi-submersible type, a spar type, and a tension leg platform (TLP) type. [6]

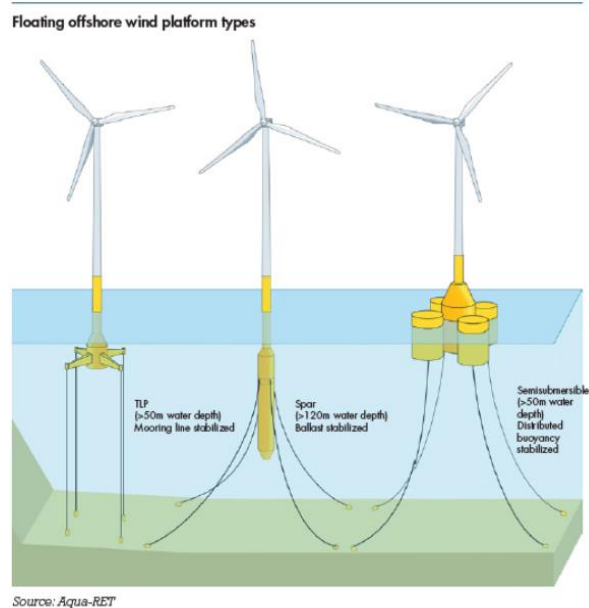


Figure 1.8: Different types of floating turbines [6]

Commercial floating wind turbines are the start phase. Several single turbine trials have been installed since 2007. Hywind Scotland, developed by Equinor ASA is the only operational floating wind farm as of 2018. The farm has five floating turbines with a total capacity of 30 MW. [21] 11.4MW floating wind was installed in 2019. 8.4MW is from Portugal and 3MW from Japan. As of 2019, a total of 65.7 MW floating wind was installed globally. 32MW is in the UK, 19MW in Japan, 10.4MW in Portugal, 2.3MW in Norway, and 2MW in France. [6] Deepwater floating spar was the most common choice in the past. However, semi-submersible floating becomes popular. According to GWEC Market Intelligence’s global floating offshore database, cumulatively 15 floating projects will come into operation by the end of 2020. Ten semi-submersible floaters and five spars will be installed. According to the study by the University of Strathclyde Glasgow, DNV-GL, and other two organizations in 2019, semi-submersible floaters will be the market leader with a share of about 62% by 2022. Though it has flexibility in shallower and deeper waters, TLP has a relatively lower market share due to complex installation. It needs a cost reduction for mooring installation. [6]

- Spar type

A large cylindrical buoy is used to stabilize the spar structure. The heavy lower part of the buoy, i.e. the ballast, and light upper part are combined to lower the center of buoyancy, which leads to a recovering moment when the floating cylinder declines from the preset axis. Hywind tampen wind farm uses spar type wind turbine. [6]

- TLP

The TLP is stabilized by the mooring system. The TLP is moored onto the seabed through a set of tension legs. Since the leg is pre-tensed before the foundation is fully functional, the preset location and posture of the foundation are recovered by the adjustment of tensions among the legs.[6]

- Semi-submersible

Because of the wave cancellation effect, the semi-submersible foundation undergoes less motion than expected. The semi-submersible foundation consists of three or four slender columns that are connected through braces. The wetting surface area of a single column, the height of the buoyancy center, and the distance between two columns affect the forces acting on the floating foundation, which recover the original location and posture of the floating foundation. Moreover, the increase of wetting surface gives more hydrodynamic stability and more structural stiffness to sustain the wave load. For the connections between columns, steel braces/bars, which increase the stiffness of the foundation, are widely used.

Table 1.6: Comparison of mainstream floating foundation [6]

Spar	Semi-submersible	TLP
<p>Overview:</p> <ul style="list-style-type: none"> - Simplest concept and attractive dynamics - Minimum depth 80m during the whole installation process - Achieves stability through ballast installed below its main buoyancy tank - Complex manufacturing and Weight for 6 MW: ~3.500 t 	<p>Overview:</p> <ul style="list-style-type: none"> - Most popular concept and less attractive dynamics - Typically requires moveable water ballast to limit tilt - Requires dry dock for fabrication - Achieves static stability by distributing buoyancy widely at the water plane - Weight for 6 MW: ~3.000 t 	<p>Overview:</p> <ul style="list-style-type: none"> - Attractive dynamics but not widely deployed - Achieves static stability through mooring line tension with a submerged buoyancy tank - Typically requires purpose-built installation vessel - Weight for 6 MW: 2.000 t
<p>Benefits:</p> <ul style="list-style-type: none"> - Inherent stability - Suitable for even higher sea states - Soil condition insensitivity - Cheap & simple mooring & anchoring system - Simple fabrication process - Low operational risk - Little susceptible to corrosion 	<p>Benefits:</p> <ul style="list-style-type: none"> - Heave plates for reducing heave response - Broad weather window for installation - Depth independence - Soil condition insensitivity - Cheap & simple mooring & anchoring system; Overall lower risk - Simple installation & decommissioning as specialized vessel required 	<p>Benefits:</p> <ul style="list-style-type: none"> - High stability, low motions - Having a good water-depth flexibility - Small seabed footprint and Short mooring lines - Simple & light structure, easy for O&M - Lower material costs due to structural weight of the substructure - Onshore or dry dock assembly possible
<p>Challenges:</p> <ul style="list-style-type: none"> - High cost, 5-8 m EUR/MW (based on the 30 MW demo) - Heavyweight, with long mooring lines and long & heavy structure - Deep drafts limit port access and Large seabed footprint - Relatively large motions - Assembly in sheltered deep water challenging and time-consuming - High fatigue loads in the tower base - Specialized installation vessels needed 	<p>Challenges:</p> <ul style="list-style-type: none"> - Non-industrialized fabrication - Higher exposure to waves leads to lower stability and impacts on turbine - Labor intensive and long lead time - Large and complex structure, so complicated in fabrication - Foundation always built-in one piece, requiring dry dock or special fabrication yard with skid facilities - Lateral movement presents potential problems for the export cable 	<p>Challenges:</p> <ul style="list-style-type: none"> - Unstable during assembly, requiring the use of a special vessel - High vertical load moorings - Complex & costly mooring & anchoring system making it the most expensive oater design type - Mooring tendons presenting higher operational risk in case of mooring failure and add requirements on-site seabed conditions

1.4 Overall wind turbine installation

Bottom fixed wind turbines are dominant because floating wind turbines claim higher cost and more difficulty to install. It is not favorable to bring electricity from the deep sea to onshore. Hence, floating wind turbines are not used except under special situations. As aforementioned, the most preferred type is the monopile type because it is relatively easy to install and manufacture. It is also proven technology by many existing cases. In this regard, it is expected that monopile type will remain the most wind turbine constructions in the next decade. So, an installation of a monopile wind turbine is introduced in this section.

1.4.1 Installation procedure

The installation procedure of monopile wind turbine is as follows.

- a. Scour protections installation
- b. Installation of foundations
- c. Transportation of transition pieces
- d. Installation of the turbine tower
- e. Nacelle installation
- f. Blade installation



(a) Scour protection installation



(b) Installation of foundations



(c) Transportation of transition pieces



(d) Installation of turbine tower



(e) Nacelle installation



(f) Blade installation

Figure 1.9: Procedure of monopile offshore wind turbine [22]

- Installation of monopile wind turbine foundations

The monopile is driven into the seafloor by a hydraulic hammer. It is made of steel and manufactured by welding. If the equipment, installation method, site preparations, and soil data are well prepared, monopiles are easy to install.

The pile-driving process will forge the top of the pile due to the constant pounding on the surface with the hammer. This may make the metal brittle and unsuited for any load-bearing. By fitting a transition piece on top of the monopile, the monopile is slotted into the transition piece over 6-8m. The transition piece is then adjusted to true vertical height, and a high-density concrete, grout, is poured to the annulus between the pile and transition piece.

Following equipment are used for the installation:

- Installation vessel the preferred type of installation vessel is the jack-up that can load and transport the monopiles and transition pieces on deck.
- A large hydraulic hammer is used to drive the pile. A power pack is applied. Driving operations are controlled from the control room.
- The Pile-handling tool holds and positions the monopile vertically during driving operation.
- Grouting equipment casts the monopile and transition piece together.
- A drilling rig is used if there are large boulders or the strong ground underneath the pile. A reverse circulation drilling system is placed on top of the pile, and the large diameter drill will then drill internal relief. After that, the pile can be driven once the material has been removed.

The foundation work can be carried out by various types of vessels. A filter layer is a stone layer of small (10-20cm) stones that will be used as a cover layer on top of the seabed to create a solid unscourable surface around the pile. The filter layer is installed by scouring protection installation vessels.

The monopile needs no seabed preparations, unlike the gravity-based foundation. Hence, the monopile method can save time and expense significantly. The monopile will be driven through the filter layer, and once the cable has been fitted, the cover layer will be dumped on top to lock the filter layer to the ground. [20]

- Installation of turbine tower, nacelle, rotor

Turbine tower usually gets cylindrical shape. They are erected vertically on the installation site. A strict operation limit should be observed because towers are heavy and very long. They are assembled with foundations with bolts and nuts.

Rotor and nacelle are delivered and assembled at the installation site. Nacelle usually weighs more than 400 tones and is hoisted more than 100m above, i.e. till hub height. Jack-up crane is used for this job. [20]

- Blade installation

Blade installation is the most critical and challenging phase of the whole installation due to the enormous dynamic effect of the wind blade. For example, a usual blade length accounts for 80 ~ 120m for a 10 ~ 15 MW wind turbine. It weighs 40 ~ 60 tons. Wind and crane motion highly affect the motion of the hanging blade. If the floating vessel is used, the motion of the vessel also affects the blade motion. Due to the heavyweight, large dimensions, and complicated motion of the blade, blade installation is the most critical phase during the whole installation. Blade installation can be divided into four strategies.

Enormous dynamic effects of the wind turbine blade make the blade installation be the most critical and challenging phase of the whole installation. A usual blade length comes to 80 ~ 120m for a 10 ~ 15MW wind turbine. Its weight reaches 40 ~ 60 tons. Wind and crane and the motion of the installation vessel affect the blade motion. There are four methods of blade installation. [23]

1. Each blade is assembled to the hub respectively.
2. Two blades can be preassembled on the hub with a bunny-ear configuration.
3. All blades are assembled on the hub and the rotor is installed altogether.
4. All wind turbine components are preassembled and installed with one lift.

If more offshore operations are required, a longer operation window is necessary. This claims stricter requirements for the weather and onboard equipment. Hence, onshore preassembly may shorten the expensive offshore operations. The most efficient solution is to preassemble all parts. However, as the wind turbine size gets bigger, the preassembly method is limited. This method claims larger vessels and cranes for installation.

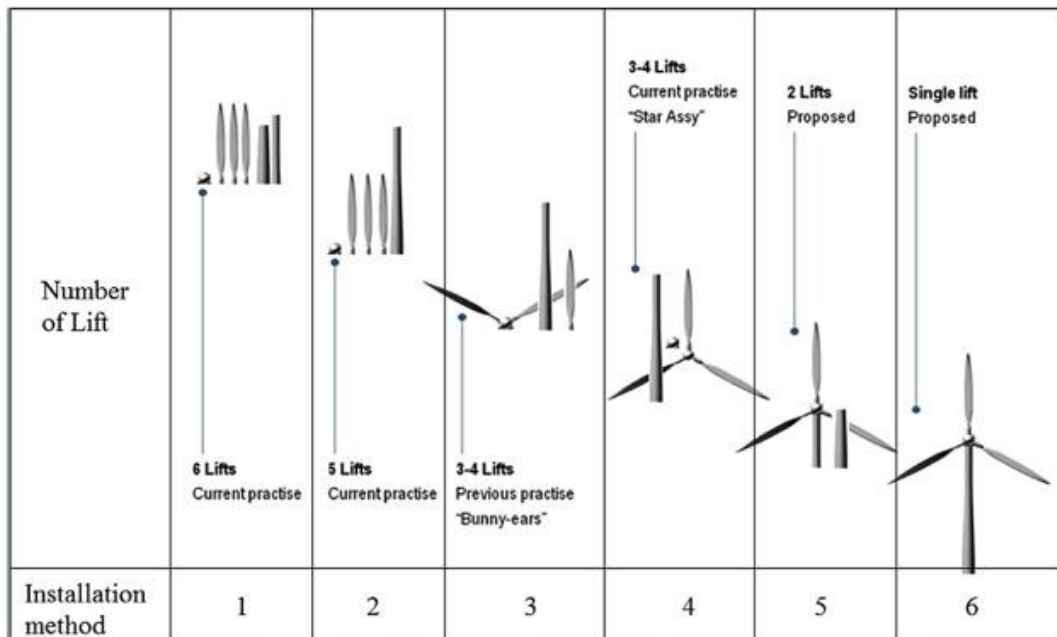


Figure 1.10: Offshore wind turbine installation strategies [23]

1.5 Single blade installation

Though blade installation is just one phase of offshore wind turbine installation, it is the most critical phase among installation phases. The heavy blade should be lifted in about 100m height. It received a big aerodynamic load significantly due to its shape. The installation vessel receives wind and wave loads together. Since blade, crane and vessel are connected and received environmental load, respectively, the motion of each component is coupled with the other components. Furthermore, the blade should be approached to the nacelle with a small gap without collision. If the mechanics of the blade installation can be analyzed by a numerical method, the installation job becomes easier.

Single blade installation is a common procedure for wind turbine installation. It is expected to be more popular as wind turbines get larger. In this chapter, single blade installation is introduced.

- Installation procedure

The single blade installation procedure is described in Figure 1.11. Special tools are often devised to turn the turbine hub to a horizontal position (step 2). Then, a yoke is used to seize the blade and lift it to the hub level (steps 3) and (step 4). The blade-root motion is observed at the alignment phase (step 5). If the motion is beyond criteria, the blade will be kept hanging close to the hub and wait for allowable weather conditions. If, after a certain period, the unfavorable condition is kept, the blade-yoke system will be lowered to the deck (step 10). It can wait until a maximum of 30 min here. If the relative motion satisfies the criteria, the blade root and hub shall be aligned by manual work. Then, the mating phase starts. The guide pin of the blade root will enter the flange hole at the hub (step 6). If this process is completed, the blade will be assembled onto the hub, and the lifting gear will be retracted (step 8). [24]

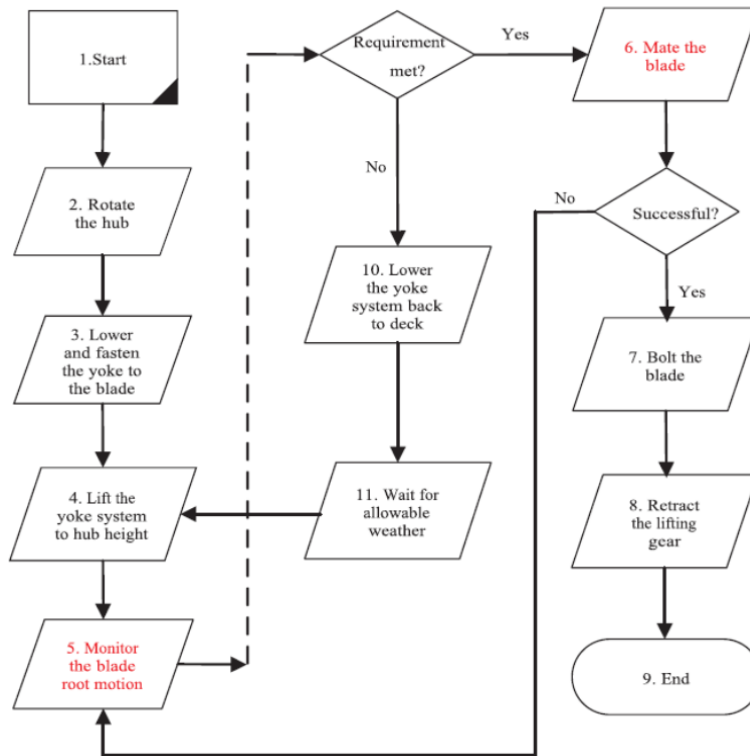


Figure 1.11: Flowchart of the typical single blade installation [24]

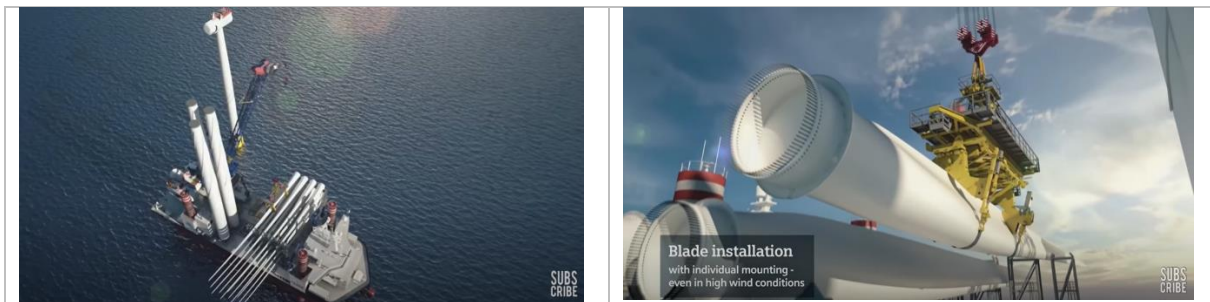
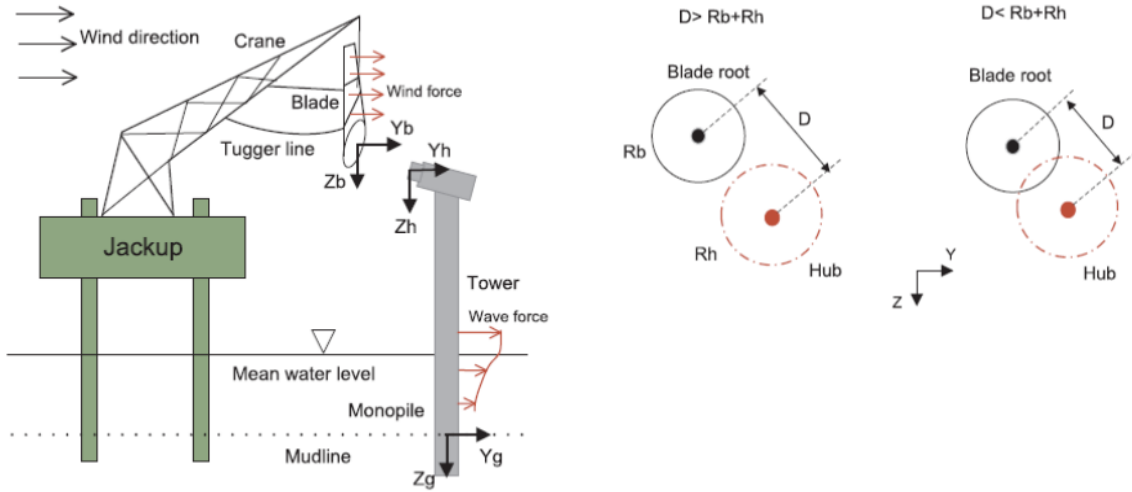


Figure 1.12: Blade lifting [22]

- Alignment phase

After the blade is lifted to the hub height, the alignment phase starts. By moving the crane and adjusting the tugger lines, the blade root is brought closer to the hub location. Figure 1.13(b) shows two possible scenarios during the alignment. R_b and R_h are the radius of the blade root and the hub, respectively. D is the distance between the center of the blade root and the hub. At this stage, the blade root and the hub go through relative motions, and the distance changes with time. In case of $D < R_b + R_h$, the alignment can be done with visual and manual assistance. [24]

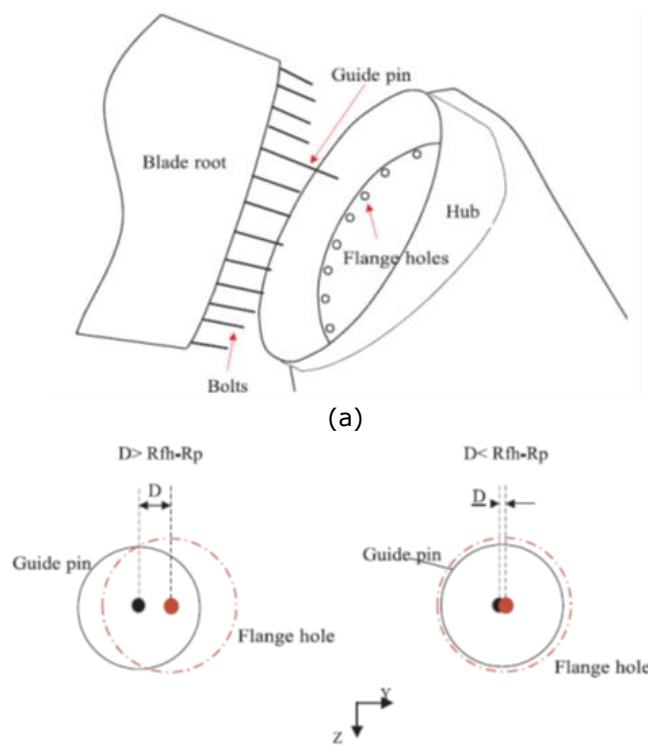


(a) Schematic of the blade alignment plan for a monopile wind turbine (b) Positions of the blade root and hub in the yz-plane

Figure 1.13: Alignment phase [24]

- Mating phase

Figure 1.14 (a) shows the main components of the blade root and hub. "T-bolts" can be used. They are commonly used for blade root connections. The guide pin takes a role to lead the appropriate position by entering a flange hole first. The bolts can then be mated in the right positions. The mating criteria are stricter than the alignment criteria. In Figure 1.14 (b), D is the distance between the two centers, R_{fh} and R_p are the motion radius of the flange hole and of the guide pin, respectively. The mating is possible in the case of $D < R_{fh} + R_p$. [24]



(b)

Figure 1.14: (a) Schematic of the main components involved in the mating process (b) Positions of the guide pin and flange hole in the yz-plane [24]

1.6 Installation vessels

Jack-up vessels and floating vessels are usually used for wind turbine installation. Jack-up vessels can give stability for crane lifting operations because they are supported by their legs. So, the lifting operations are not much affected by wave conditions. However, Jack-up vessels can access only shallow water, needs low sea states to deploy and retrieve their legs. They also spend much time moving. In contrast, floating vessels can operate in deeper water. They can move and prepare installation faster than Jack-up vessels. Their weakness is the motion due to waves. Harsh sea states hinder the floating vessel to install turbines. Since most offshore wind turbines are monopile type installed in shallow water, jack-up vessels are naturally mainstream for installation vessels. Since floating wind farm is not common, dedicated floating vessels for wind turbine installation are not common. Multipurpose crane vessels usually perform installation jobs.



(a) Jack-up vessel installing a blade [25]



(b) Floating installation vessel [26]

Figure 1.15: Wind turbine installation vessels



Table 1.7: Jack-up vessel specifications

	Voltaire [26]	Seajack Scylla [27]	Fred. Olsen Windcarrier [28]	ULSTEIN J103 [29]
Length overall [m]	169.3	139	132	164
Breadth [m]	60	50	39	104
DWT [ton]	21,500	-	9,500	
Crane lifting capacity [ton]	more than 3,000	1,500	800	2,500
Lifting height above deck [m]	162.5	105	-	250
Max. water depth [m]	80	-	60	65
Leg length [m]	130	105	92.4	-
Delivery	Under construction	2015	2012	Design only

Table 1.8: Floating vessel specifications

	Saipem 7000 [30]	Les Alizes [31]	Oleg Strashnov [32]
Length overall [m]	197.95	236.8	183.0
Breadth [m]	87	52	47
Crane lifting capacity [ton]	14,000	5,000	5,000
Lifting height above deck [m]	140	270	98.7
Delivery	1988	Under construction	2011

Table 1.9: Wind turbine jack-up vessel generations [33]

Generation:	1 st	2 nd	3 rd	4 th
Operational:	2005	2010	2015	2022
Description:	<i>First heavy lift jack-ups in offshore wind</i>	<i>New designs primarily for offshore wind</i>	<i>Scaled-up designs for larger turbines</i>	<i>Next generation for future 15MW turbines</i>
Average crane capacity:	500 ton	900 ton	1.400 ton	2.5 - 3.500 ton
Average variable load:	2.000 ton	5.000 ton	8.500 ton	10 - 16.000 ton
Typical Wind Turbine:	3 MW	6 MW	9 MW	15 MW
Example:				

1.7 Research purpose

Since the blade installation is a limited operation influenced by weather conditions, it is important to investigate the motions and the displacements of the vessel and the blade according to the sea conditions. A single blade installation is simulated with the DTU 10MW wind turbine. A jack-up vessel is used as an installation vessel.

In this paper, the kinematics of the blade and the jack-up vessel is simulated with various wind and wave conditions.

2 Theories of the blade installation

The wind and wave load are applied to the installation system. The wind load affects the installation system above the free surface. Especially, the blade received a big effect from the wind since it is a very slim and slender body with a large surface. The wave load is applied to the jack-up legs. Since the blade, the jack-up hull, and the jack-up legs are connected and receive the loads respectively, the whole installation system should be evaluated as a coupled system.

The blade installation is simulated to calculate the system loads and motion/structural responses. These responses can be used to assess possible weather windows for real operations. The theories are related to load calculations (aerodynamic loads on the lifted blade, hydrodynamic loads on the jack-up legs, and the global motion and structural responses.)

2.1 Description of a coupled system of blade installation

A coupled system is that one component affects the motions of other components and affected by the other components at the same time. Each component responds interactively to the effect of other components. Hence, the motion of the system should be solved with coupled equations. As a simple example of a coupled system, let us suggest two masses which is connected by a spring. Each mass receives external forces respectively and this causes each mass motion. However, the relative position between two masses affects their motion due to spring stiffness. Their motion should be solved by coupled differential equations.

During the blade installation, each component of the installation system receives environmental loads, respectively. The blade and the crane receive wind load. The hull of the jack-up vessel above the free surface also receives wind load. Meanwhile, the jack-up legs receive the wave load and the current load. Hydrodynamic loads on the jack-up legs and the wind load to the jack-up hull make the jack-up vessel move. Since the blade is connected to the jack-up vessel via the crane, the blade motion is affected by the motion of the jack-up vessel. On the contrary, the blade motion can also affect the motion of the jack-up vessel. Hence, all components in the installation system should be considered together to solve the motion of the blade and the global motion of the installation system.

Yuna Zhao suggested a method to solve the coupled installation system with SIMO, RIFLEX, and in-house aerodynamic code(Aero)[34]. The SIMO and RIFLEX codes were developed by SINTEF Ocean and have been used to simulate motions of offshore structures in the sea. A jack-up crane is modeled based on the SIMO-RIFLEX. The relevant external load and structural model are shown in Figure 2.1. The structural flexibility of the legs and the crane, the soil-spudcan interaction, the wave loads, and the wind loads acting on the vessel are considered in the vessel model. The load on the wind turbine blade is simulated by SIMO-Aero code.

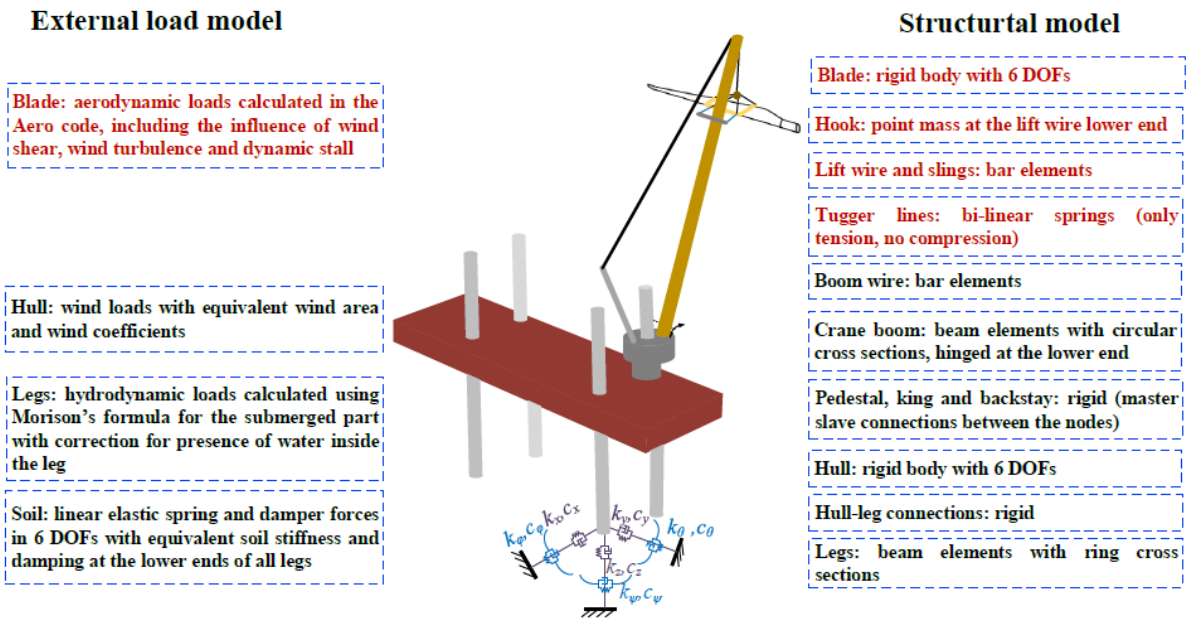


Figure 2.1: The structural and external force models of a typical elevated jack-up crane vessel [37]

The hull of the jack-up is simulated as a rigid body because it is a very big and blunt body comparing other parts. The jack-up legs are simulated as flexible beam elements by use of RIFLEX. The spud cans are considered nodal bodies at the lower end of each leg. The jack-up legs are attached to the hull. It is so stiff that the flexibility of connection is negligible. The hull-leg connections are regarded as rigid connections[37].

It is assumed that the deformation of the crane system is dominated by the flexibility of the boom and boom wires. The deformation of the crane supports, including a king, pedestal, and back-stay is neglected [Figure 3.3]. The lattice boom is simplified into a circular RIFLEX beam with equivalent structural stiffness properties. The lower end of the boom is hinged on the crane base. The boom inclination is controlled by the boom wires which are modeled as RIFLEX bar elements[37].

2.2 Aerodynamic loads

2.2.1 Aerodynamic loads on the blade

The aerodynamic load on a blade element can be calculated according to the cross-flow principle [38, 39]. The coordinate systems are shown in Figure 2.2. It is possible to calculate aerodynamic forces on a wind turbine blade if the local blade element suits a 2D approximation. In the cross-flow principle, the inflow velocity normal to the cross-section, i.e., $V_{A,i}$ along y_c is neglected as shown in Figure 2.3. The relative wind velocity used in the aerodynamic load calculation V_{rel} can be expressed as:

$$\mathbf{V}_{rel} = [V_{A,i,x_c} \ 0 \ V_{A,i,z_c}]^T \quad (2.1)$$

where $V_{A,i}$ is the relative wind velocity by the element i . V_{A,i,x_c} and V_{A,i,z_c} are the projection on x_c and z_c . $V_{A,i}$ can be evaluated by Eq. (2.2).

$$\mathbf{V}_{A,i} = \mathbf{T}_{GC,i}(\mathbf{V}_{WG,i} - \mathbf{V}_i + \mathbf{V}_{IG,i}) \quad (2.2)$$

where $\mathbf{V}_{WG,i}$, $-\mathbf{V}_i$ and \mathbf{V}_{IG} are the global wind velocity, element velocity, and wake-induced velocity at the i th element. The V_{IG} can be negligible for a blade during installation because the motion of the blade is quite small. By the way V_{IG} need to be considered in operation. Thus, Eq. (2.2) can be simplified as

$$\mathbf{V}_{A,i} = \mathbf{T}_{GC,i}(\mathbf{V}_{WG,i} - \mathbf{V}_i) \quad (2.3)$$

The angle of attack α is decided by V_{rel} . α is further used to find the C_L and C_D coefficients based on a 2D look-up table which defines the relationship between C_L , C_D , and α . Furthermore, there is an option to include the dynamic stall effect before the table look-up [34].

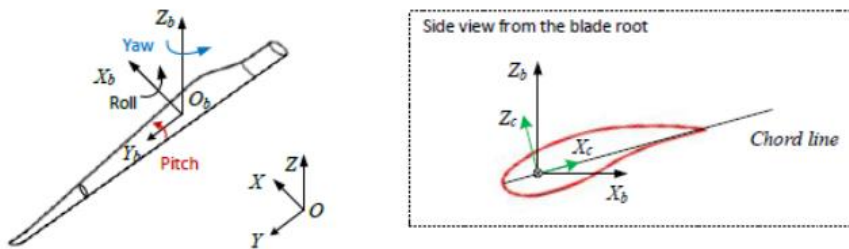


Figure 2.2: Definition of coordinate systems $O - XYZ$, $O - X_b Y_b Z_b$ and $O - X_c Y_c Z_c$ are respectively the global, blade-related and local blade element coordinate systems [40]

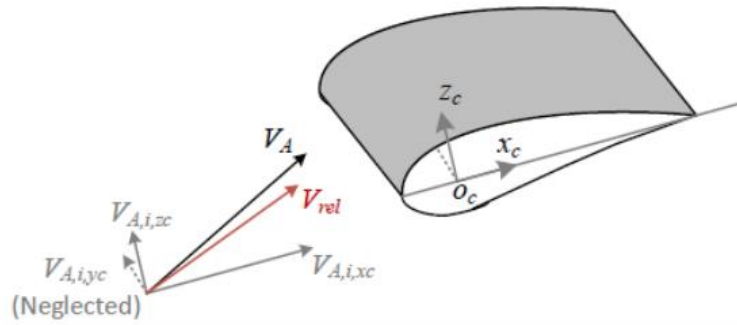


Figure 2.3: Illustration of cross-flow principle: $\mathbf{V}_{A,i} = [V_{A,ixc} \ V_{A,iyc} \ V_{A,izc}]^T$ [40]

The Beddoes-Leishman dynamic stall model is used. Gupta and Leishman[41] exploited it for application in wind turbine aerodynamics. Unsteady attached flow, unsteady separated flow, and dynamic vortex lift are distinguished in the Beddoes-Leishman dynamic stall model as shown in Figure 2.4. A circulatory and an impulsive loading compose the aerodynamic loading in the unsteady attached flow regime. The change rate of α and pitch moment makes the impulsive part. The attached flow results are affected by the flow separation on the low-pressure side of the airfoil, including leading edge and trailing edge separations. The final part of the model is the vortex buildup and shedding. The vortex lift contribution is considered as an excess circulation in the vicinity of the airfoil using the difference between the normal force coefficient C_N from the attached and separated flow. The total loading on the airfoil is the sum of the above components. Then the lift and drag forces on the blade element are computed using the obtained C_L and C_D . The total aerodynamic loads on the blade are the sum of these on all elements. [34]

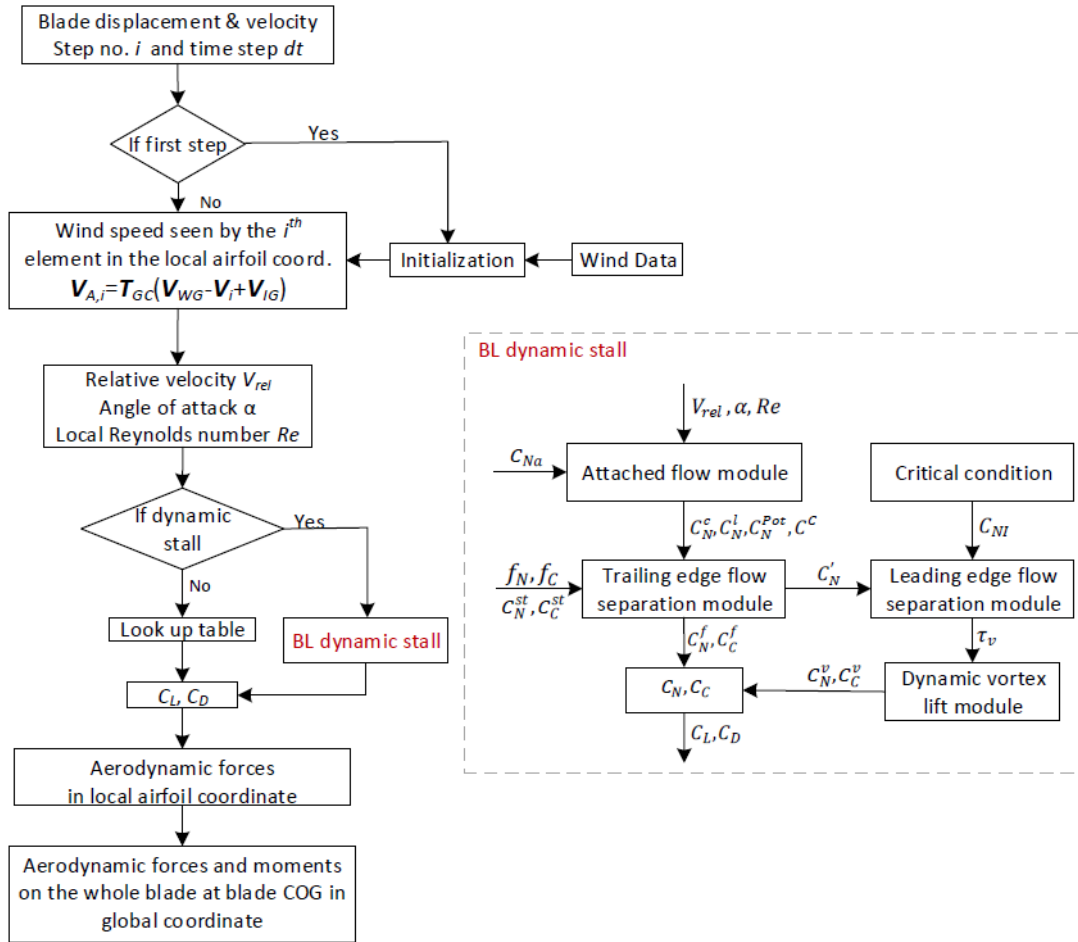
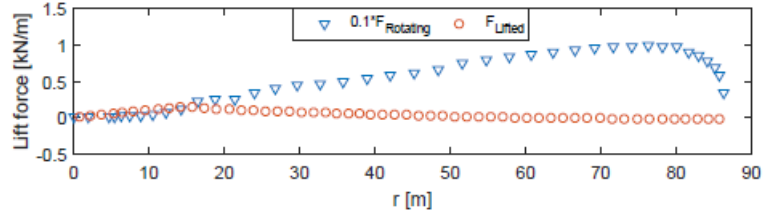


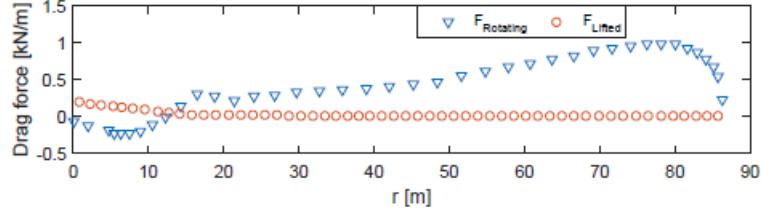
Figure 2.4: Flow chart for aerodynamic modeling

- Distribution of aerodynamic force on a lifted blade

The lift and drag force distribution on the blade during rotation and lifted condition are plotted in Figure 2.5. For the lifted blade, the main contribution of the aerodynamic loads comes from the middle and root part of the blade. Thus, the aerodynamic center of a lifted blade is located close to the blade root. Compared to the inflow wind velocity, the velocity of a lifted blade is insignificant.



(a) Lift force F_z



(b) Drag force F_x

Figure 2.5: Distribution of lift and drag forces on a blade under rotating condition and lifting condition: blade pitch angle 0; rotational speed for the rotating blade 8.029 rpm; constant wind 10m/s [34]

2.2.2 Wind loads on the jack-up hull

The wind loads are exerted on all the components of the jack-up vessel, the installation equipment, and the wind turbine components. The wind area above the hull baseline is replaced as a block with the equivalent area and wind coefficients. The wind loads on the parts of the legs between the free surface and the hull baseline are neglected. Since the motion of the jack-up vessel is mainly wave-induced during operations, this assumption is possible. The wind load is calculated as:

$$F_{x,wd} = \frac{1}{2} \rho_{air} C_s A V^2 \cos \alpha \quad (2.4)$$

$$F_{y,wd} = \frac{1}{2} \rho_{air} C_s A V^2 \sin \alpha \quad (2.5)$$

$$F_{z,wind} = 0 \quad (2.6)$$

where ρ_{air} is the density of air; α is the relative wind inflow angle [Figure 2.6]. V is relative wind speed, C_s is the overall shape coefficient. Here, $C_s = 1.1$. A is the area normal to the inflow wind:

$$A = A_{xn} |\cos \alpha| + A_{yn} |\sin \alpha| \quad (2.7)$$

where A_{xn} is the wind area of X_v axis, A_{yn} is the wind area of Y_v axis. The wind moments are:

$$M_{x,wd} = -z_c F_{y,wd} \quad (2.8)$$

$$M_{y,wd} = z_c F_{x,wd} \quad (2.9)$$

$$M_{z,wd} = x_c F_{y,wd} - y_c F_{x,wd} \quad (2.10)$$

where $[x_c \ y_c \ z_c]$ is the position vector for the center of the equivalent wind block [34].

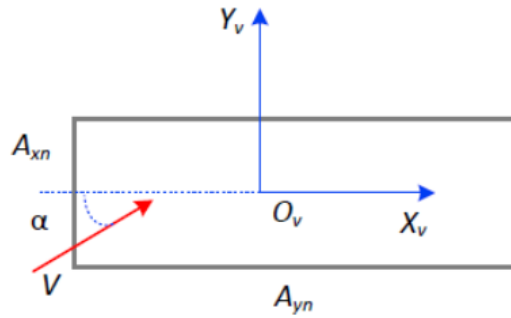


Figure 2.6: Illustration of wind area and relative wind inflow angle (top view)

2.3 Hydrodynamic loads

2.3.1 Wave loads on the jack-up legs

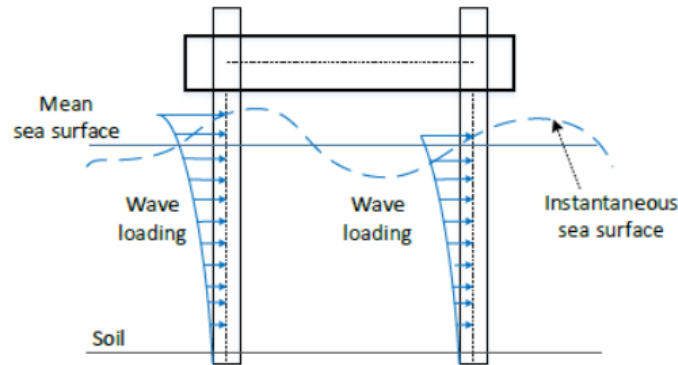


Figure 2.7: Wave loads on jack-up legs[40]

The hull of the jack-up crane vessel is kept elevated above the free surface in offshore wind turbine installation. The wave loads applied to the submerged legs can be evaluated by the integration of wave force. The strip theory based on the linear wave kinematics is used from the seabed to the free surface. [Figure 2.7].

Morison's formula Eq. (2.11) for relative motion is used to evaluate the instantons wave loads normal to the legs because the legs can be considered as slender body comparing wavelength.

$$\mathbf{F} = \int_{-h}^{\eta} [\rho A_{ext}(1 + C_A)\dot{\mathbf{u}}(z) - \rho A_{ext} C_A \ddot{\mathbf{r}}(z)] \quad (2.11)$$

$$+ \frac{1}{2} \rho D_{ext} C_D |\mathbf{u}(z) - \dot{\mathbf{r}}(z)| (\mathbf{u}(z) - \dot{\mathbf{r}}(z)) - \rho A_{int} \ddot{\mathbf{r}}(z) dz$$

where ρ is the density of water, D_{ext} is the outer diameter of the leg, A_{ext} and A_{int} are the external and internal cross-sectional areas of the leg, C_A and C_D are the non-dimensional 2D added mass and quadratic drag coefficients, \mathbf{u} , and $\dot{\mathbf{r}}$ are respectively the velocity vector of undistributed wave field and motion vector of the leg; h is the water depth and η is the instantaneous wave elevation. [37]

2.4 Jack-up soil-structure interaction

The soil reaction of the jack-up legs can be modeled as linear elastic springs and dampers without detailed spud cans modeling. If a significant wave height is lower than 2.5m – 3.0m, this simplification is acceptable [42] [43].

The loads acting on the spud cans are smaller than those required to activate the soil yield surface [44] [45]. The spud can location is the reference point in Figure 2.8. The soil reaction force can be expressed by the function of the spud can displacement.

$$\mathbf{F}_s = \mathbf{K}_s \mathbf{X}_{sc} + \mathbf{C}_s \dot{\mathbf{X}}_{sc} \quad (2.12)$$

where, $\mathbf{K}_s = [k_x \ k_y \ k_z \ k_\phi \ k_\theta \ k_\psi]$ is the soil stiffness vector in 6 DOFs without considering coupling effects.

The soil properties and the dimension and penetration depth of the spud cans affect the stiffness coefficient. Empirical formula[46, 47] or site-specific soil properties are used. \mathbf{C}_s is the soil damping coefficient. \mathbf{X}_{sc} is the displacement vector.

$$\mathbf{X}_{sc} = [x \ y \ z \ \phi \ \theta \ \psi] \quad (2.13)$$

where, x, y, z are the translation motion of the reference point. ϕ, θ , and ψ are the rotational motion of the leg at its lower end [34].

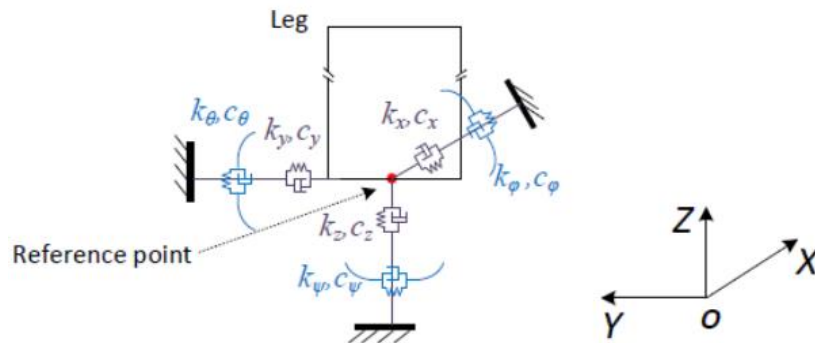


Figure 2.8: Modeling of soil resistance force on the spud can using linear springs and dampers [34]

2.5 Structural modeling

The blade can be regarded as a rigid body. The flexibility of the blade is negligible during installation [48]. Crane boom is modeled by beam elements. The boom wires control the boom inclination. The boom wires are modeled as a combination of bar elements. The crane deformation is mainly due to the flexibility of the boom and boom wires. The jack-up hull is modeled as a rigid body with 6 DOFs. Structural flexibility in the jack-up legs is

expressed using beam elements. The jack-up hull-leg connections are regarded as rigid connections. The spud cans are modeled as a point mass. Rayleigh damping model is used[49].

$$c = \alpha_1 m + \alpha_2 k \quad (2.14)$$

where, α_1 is mass damping coefficient and α_2 is stiffness damping coefficient[34].

2.6 Mechanical couplings

The non-compressive tugger line coupling forces are expressed as bi-linear spring forces.

$$T = \begin{cases} k\Delta L, & \text{if } \Delta L \geq 0 \\ 0, & \text{otherwise} \end{cases} \quad (2.15)$$

where T is the wire tension and ΔL is the wire elongation. k is the wire axial stiffness, which is given by:

$$\frac{1}{k} = \frac{L}{EA} + \frac{1}{k_0} \quad (2.16)$$

where A is the cross-sectional area of the wire, E is the modulus elasticity of the material of the wire and $1/k_0$ the connection flexibility [34].

2.7 Time-domain simulations

Steady-state time-domain simulations are performed. TurbSim[50] based on the IEC Kaimal Model defined in IEC 61400 was used to generate the 3D turbulent wind field. The normal wind profile is used as wind shear[51], where the mean wind speed U_z is calculated as a function of height z above the mean sea level, based on the power law principle, i.e.:

$$U(z) = U_{ref} \left(\frac{z}{z_{ref}} \right)^\alpha \quad (2.17)$$

where, U_{ref} is the reference mean wind speed at the reference height z_{ref} , while α is the power-law exponent. The value of α is set to 0.12 for the offshore wind field. The waves are simulated as long-crested irregular waves based on the Joint North Sea Wave Project (JONSWAP) spectrum i.e.:

$$S(\omega) = \frac{\alpha g^2}{\omega^5} \exp \left[-\beta \left(\frac{\omega_p}{\omega} \right)^4 \right] \gamma \left[\frac{\left(\frac{\omega}{\omega_p} - 1 \right)^2}{2\sigma^2} \right] \quad (2.18)$$

where, ω_p is the wave peak frequency; α is the spectral parameter; β is the form parameter, and r is the peakedness parameter[52].

2.8 Extreme value analysis by use of Gumbel distribution

The Gumbel distribution is used to estimate the distribution of the maximum(or the minimum) of many samples of various distributions. This distribution can be used to represent the distribution of the maximum level of a river in a particular year if there was

a list of maximum values for the past ten years. It is useful in predicting the chance that an extreme earthquake, flood, or other natural disasters will occur[53].

The formula of the Gumbel distribution is

$$F_G(x; a, b) = \exp(-e^{-(x-b)/a}), \quad -\infty < x < \infty \quad (2.19)$$

3 Numerical model

3.1 Model components specifications

3.1.1 Coordinate systems

Three coordinate systems are defined as shown in Figure 3.1; a global coordinate system $O - XYZ$, a vessel-related coordinate system $O_v - X_v Y_v Z_v$ and a blade related coordinate system $O_b - X_b Y_b Z_b$. The origin of the blade-related coordinate system $O_b - X_b Y_b Z_b$ locates on the COG of the blade. The origin of the vessel-related coordinate is located on the geometrical center of the elevated jack-up hull. The global coordinate system $O - XYZ$ has its origin located at the mean sea surface.

The incident wave angle is defined as the relative angle of wave direction and the positive X direction in the global coordinate system. The incident wind angle is defined the same way as the wave[34].

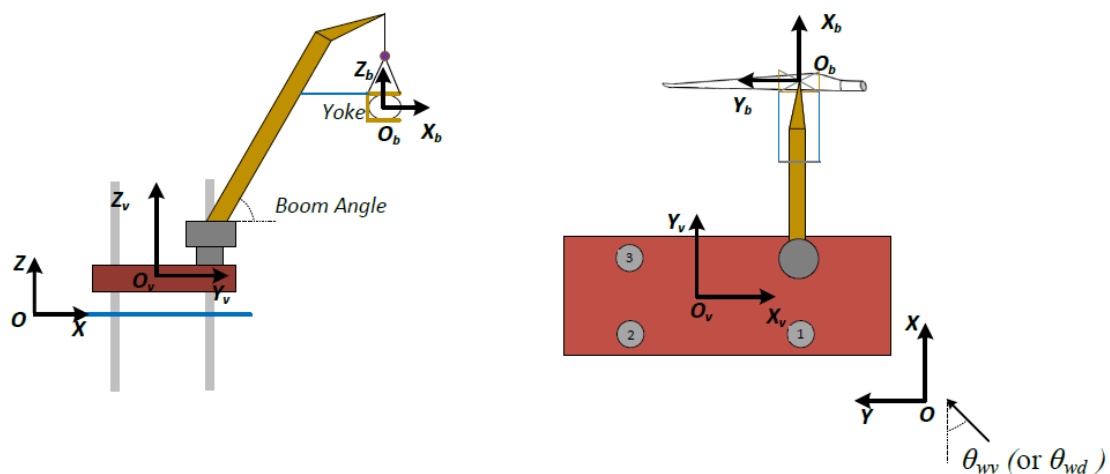


Figure 3.1: Definition of coordinate systems for the blade installation system[34]

3.1.2 Blade and lifting arrangements

The DTU 10MW wind turbine blade is used in the simulation. The blade COG is located 26.2m from its root, along the blade span. Yoke weighs 47 tons and seizes the blade around the blade COG. The yoke is lifted by the hook via four slings. Two horizontal tugger lines connect the yoke and the crane structure. Pretension is posed to the tugger lines to prevent slacklines.

Table 3.1: Main properties of the blade lifting system[34]

Parameter	Value	Unit
Hook mass	10	tons
Yoke mass	47	tons
Blade mass	41.67	tons
Blade length	86.37	m
Blade COG*	26.2	m
Installation height	119	m
Tugger line length	10	m

* The position of the blade COG is relative to the blade root and along the blade span.

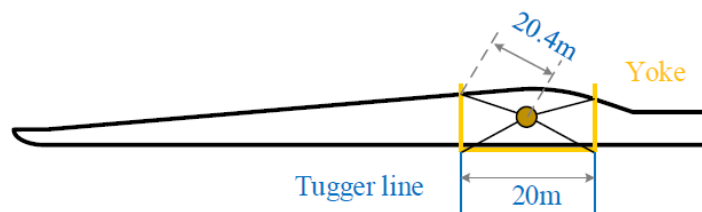


Figure 3.2: Illustration of the tugger line system

3.1.3 Jack-up vessel specification

A jack-up crane vessel is used in this simulation. It has four legs with its hull elevated above the mean sea surface during operations. The jack-up vessel specification is shown in Table 3.2.

Table 3.2: Main parameters of the jack-up vessel[37]

Parameters	Unit	Values
Hull length, breadth, and depth	[m]	132, 39, 9
Displacement during transportation	[m ³]	2.20 X 10 ⁴
Total elevated load	[t]	1.69 X 10 ⁴
Leg length and diameter	[m]	92.4, 4.5
Long. and trans. leg spacing	[m]	68.3, 30.6
Airgap	[m]	7.2
Leg below hull	[m]	49
Soil type		Dense sand
K_x, K_y and K_z *	[kN/m]	1.35 X 10 ⁶ , 1.35 X 10 ⁶ , 1.47 X 10 ⁶
K_θ, K_ϕ and K_ψ *	[kN/deg]	6.4 X 10 ⁵ , 6.4 X 10 ⁵ , 8.3 X 10 ⁵

* Equivalent linear spring stiffness of the soil in six DOFs

3.1.4 Crane specification

The crane shape is shown in Figure 3.3. The main parameters of the crane are listed in Table 3.3

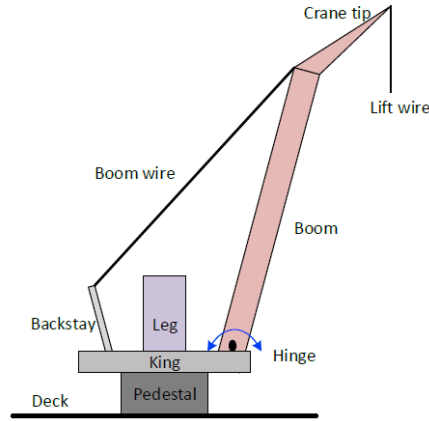


Figure 3.3: Illustration of a typical offshore pedestal crane [37]

Table 3.3: Main parameters of the crane

Boom length [m]	107.6
Crane boom angle [deg]	67.6
No. of equivalent boom wire [-]	2
Equivalent boom wire stiffness [kN/m]	9048
Equivalent boom wire damping [kNs/m]	90.5

3.2 Loading and coupling methods

3.2.1 Wind load

TurbSim is used for wind field generation. This program generates numerically simulated time series of wind-speed vectors in a two-dimensional vertical rectangular grid that is fixed in space[50]. Turbine input setting is shown in Table 3.4.

Table 3.4: TurbSim input setting

Vertical grid-point matrix dimension	32
Horizontal grid-point matrix dimension	50
Hub height [m]	119
Grid height [m]	190
Grid width [m]	300
Turbulence model	IECKAI (turbulent wind cases) None (constant wind cases)
Power law exponent	0.12 (turbulent wind cases) 0.0 (constant wind cases)
Surface roughness length [m]	0.0003

The wind field file has a form of independent file (wnd file). Aero code read the wind field file and the information of DTU 10MW wind turbine blade. The instantaneous blade motion in the global coordinate system is calculated by SIMO at each time step as shown in Figure 3.4. The instantaneous displacement is converted by the transformation matrix from the global coordinate to the local blade element coordinate. Then, the blade velocity and wind inflow velocity in the global coordinate system are transferred into the local blade element

coordinate system, to update the relative velocity seen by the local blade element and the angle of attack. The corresponding lift and drag are decided from a look-up table and used to estimate the lift and drag forces in the local blade element coordinate system. These aerodynamic forces are then transferred into the global coordinate system and are sent back to SIMO to calculate the blade displacement and velocity for the next time step. [34]

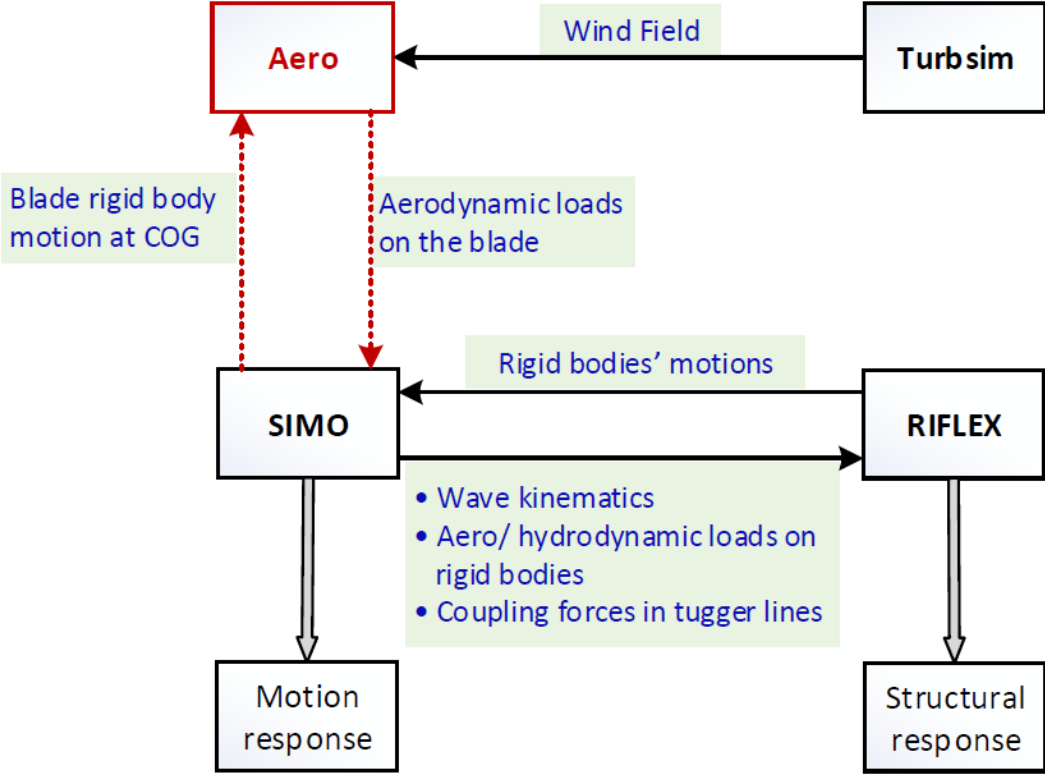


Figure 3.4: Overview of the coupled simulation method [34]

3.2.2 Hydrodynamic loads

The incident wave is simulated according to Jonswap spectrum. The wave period is 4 ~ 10 sec. The swell and current are not included in the simulation. The wave loads on the jack-up legs are calculated by RIFLEX. The jack-up legs are flexible bodies.

4 Results and discussion

4.1 Installation system characteristics

To understand the characteristics of the installation system, limited and simple external loads were applied, and the response of the system was examined. The responses of the jack-up vessel are practically nothing regardless of the external forces. Hence, only the results of the blade motion are included in this thesis.

4.1.1 No external load condition

No external load is applied to check initial conditions. x , y , z are the global position of the components. The blade position in a calm sea is shown in Table 4.1.

Table 4.1: The blade positions in no wind and no wave condition

	Displacement in x-direction (surge) [m]	Displacement in y-direction (sway) [m]	Displacement in z-direction (heave) [m]	Rotational angle about x-axis (roll) [deg]	Rotational angle about y-axis (pitch) [deg]	Rotational angle about z-axis (yaw) [deg]
Blade	61.388	-34.154	119.29	0.000627	9.021776	9.01494E-05

4.1.2 The blade position in the constant winds

The wind speeds are U_w 2, 5, and 10m/s, respectively. There is no wave. Four different wind directions are used. The blade pitch angle is 0 deg for all the cases.

Table 4.2: The blade position change due to the wind speed and the wind direction

Wind speed [m/s]	Wind direction [deg]	Displacement in x-direction (surge) [m]	Displacement in y-direction (sway) [m]	Displacement in z-direction (heave) [m]	Rotational angle about x-axis (roll) [deg]	Rotational angle about y-axis (pitch) [deg]	Rotational angle about z-axis (yaw) [deg]
2	0	61.38864	-34.135	119.29	0.059809	9.021359	0.008281
2	90	61.38861	-34.136	119.29	0.057815	9.021373	0.008005
2	180	61.38861	-34.1368	119.29	0.055864	9.021383	0.007736
2	270	61.38861	-34.136	119.29	0.057824	9.021374	0.008007
5	0	61.38774	-34.038	119.29	0.370237	9.021285	0.051272
5	90	61.38755	-34.026	119.29	0.407579	9.021518	0.056477
5	180	61.38788	-34.046	119.29	0.345608	9.021161	0.047859
5	270	61.38756	-34.027	119.29	0.40639	9.021498	0.05626
10	0	61.37122	-33.693	119.3	1.476077	9.049462	0.206549
10	90	61.37246	-33.709	119.3	1.4238	9.047111	0.198961
10	180	61.36877	-33.664	119.3	1.570608	9.053906	0.220113
10	270	61.37232	-33.708	119.3	1.429282	9.047403	0.199976

The blade position changes due to wind speed are not significant. The wind direction also does not cause significant changes. The translational displacements are less than 0.5m, and the rotational angles are less than 2 deg for all cases.

4.1.3 The blade position in regular wave loads

Regular waves come to the installation system. The wave periods are 2~15 sec. The incident wave amplitude is 1 m as shown in Figure 4.1. There is no wind.

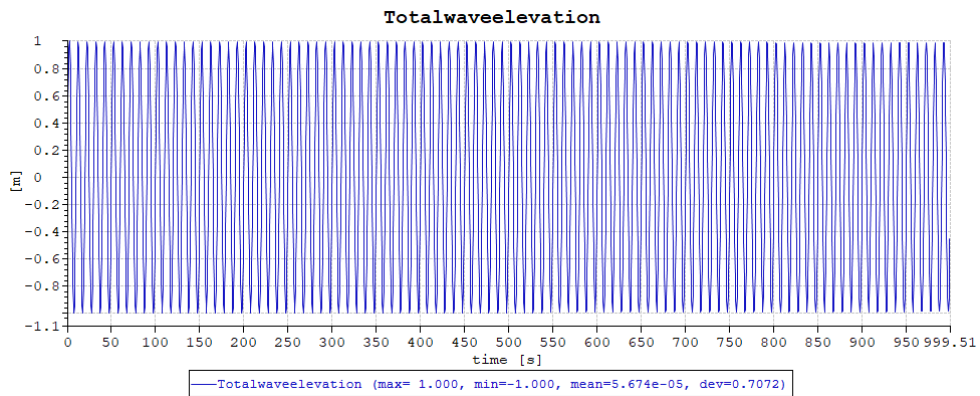
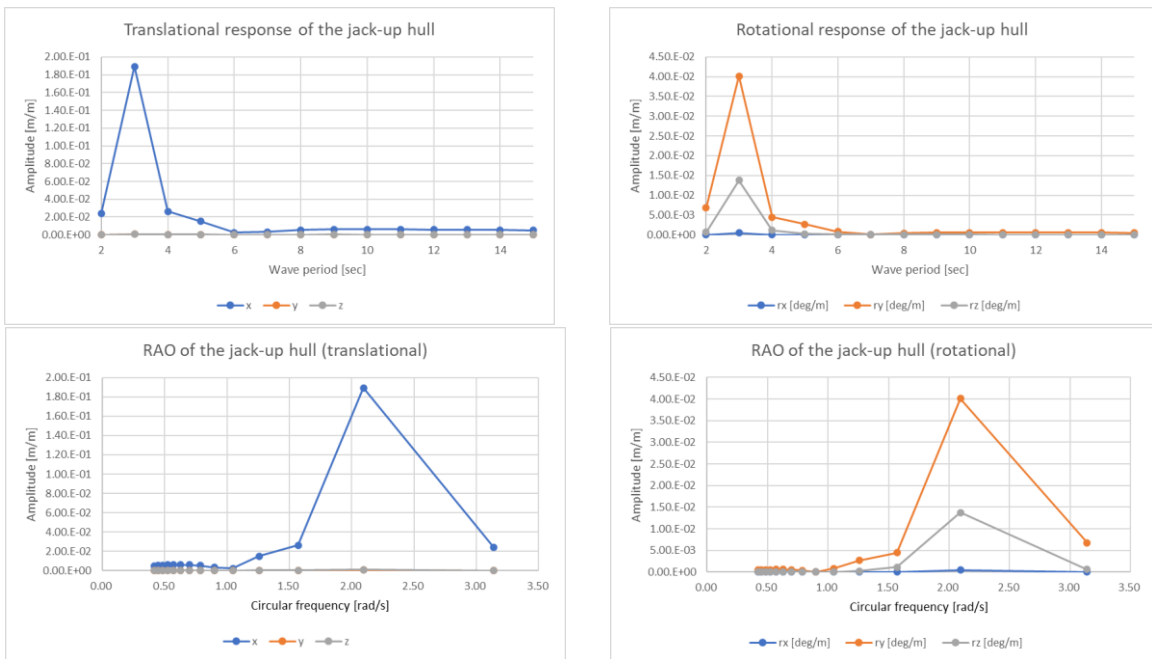
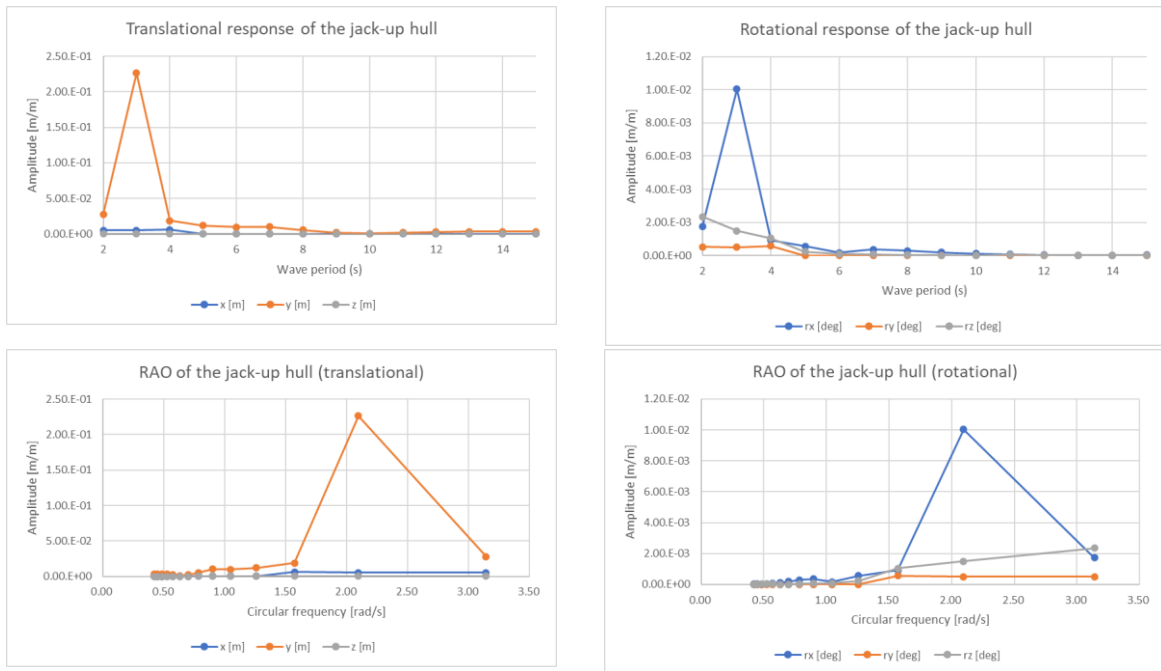


Figure 4.1: An example of the incident wave



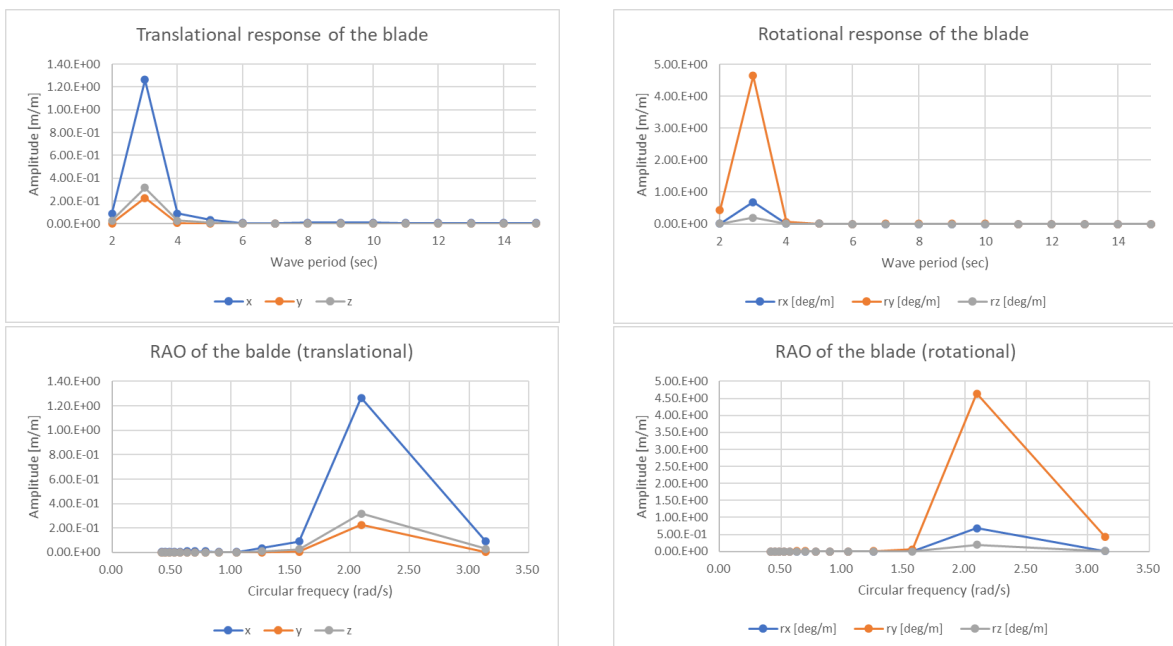
(a) Incident wave amplitude 1m, wave direction 0 deg



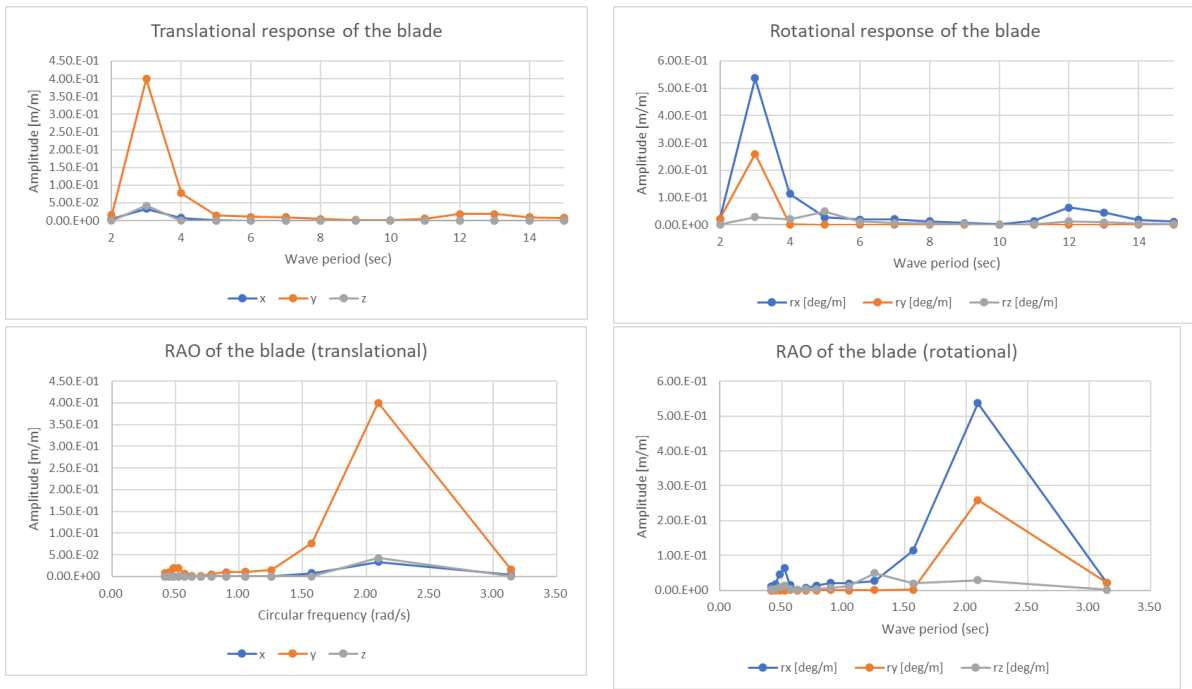
(b) Incident wave amplitude 1m, wave direction 90 deg

Figure 4.2: The responses of the jack-up hull for an incident wave with 1m amplitude

If the wave comes in 0 deg, i.e., x-axis direction, the dominant motion of the jack-up vessel is surge and pitch. If the wave comes in 90 deg, the jack-up vessel moves mainly in sway and roll as shown in Figure 4.2. The natural period of the jack-up vessel is about 3 sec. Since the jack-up vessel is supported by the jack-up legs and the jack-up legs are structural bodies, the natural period of the jack-up hull is smaller than the floating vessels.



(a) Incident wave amplitude 1m, wave direction 0 deg



(b) Incident wave amplitude 1m, wave direction 90 deg

Figure 4.3: The responses of the blade for an incident wave with 1m amplitude

The response of the blade shows a similar pattern to the jack-up hull. The maximum response occurs at 3 sec. This is because that the induced load by the wave is delivered to the blade.

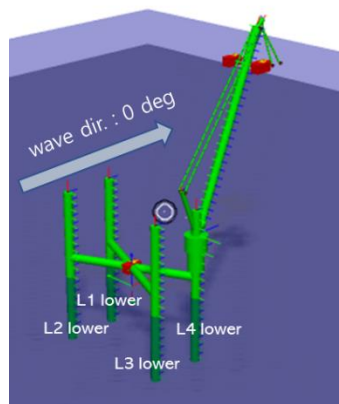
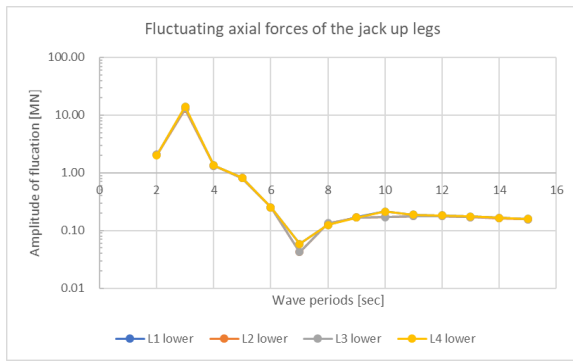
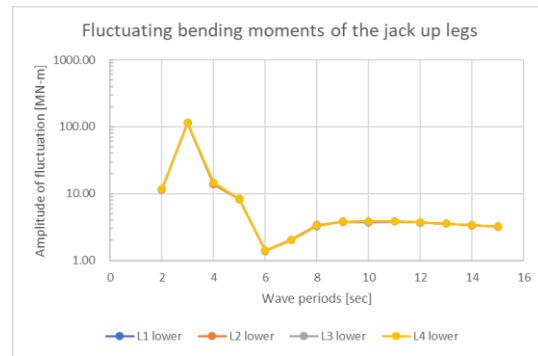


Figure 4.4: The name of the leg components



(a) The axial forces (log scale y-axis)



(b) The bending moments (log scale y-axis)

Figure 4.5: The fluctuating axial forces and the bending moments due to regular waves

The fluctuation of the axial force and the bending moments of the jack-up legs are investigated. The wave comes at 0 deg direction. The maximum fluctuation occurs in the lowest part of the jack-up legs. The spud cans are the only support points against the external loads. Hence, the axial force and the bending moments are concentrated there. There is not much difference in the axial forces/the bending moments among the legs. (L1, L2, L3, L4 legs) The maximum values occur when the wave period is 3 sec., the minimum occurs at 6 sec. period.

The wave period of the most significant blade motion is identical with the wave period of the largest fluctuation of the axial force and the bending motion of the jack-up leg. This means that the most severe blade motion is due to the characteristics of the jack-up vessel.

4.1.4 The effect of the initial blade pitch angles

The initial pitch angle of the blade affects the forces and moments on it.

Table 4.3: The forces and the moments on the blade due to the blade pitch angles (dynamic calculation)

Blade pitch angle [deg]	x-direction force [kN]	y-direction force [kN]	z-direction force [kN]	Moment about x-axis [kN -m]	Moment about y-axis [kN -m]	Moment about z-axis [kN -m]
45	19.8	0.0	21.9	1635.5	0.0	-1377.4
30	12.1	0.0	23.3	1698.6	0.0	-809.6
15	5.5	0.0	19.1	1355.2	0.0	-329.8
0	1.7	0.0	10.5	693.8	0.0	-67.6
-15	1.8	0.0	-0.3	-103.9	0.0	-93.8
-30	5.6	0.0	-10.3	-820.4	0.0	-399.9

Table 4.4: The translational and the rotational displacement of the blade due to the blade pitch angles (dynamic calculation)

Initial blade pitch angle [deg]	Displacement in x-direction (surge) [m]	Displacement in y-direction (sway) [m]	Displacement in z-direction (heave) [m]	Rotational angle about x-axis (roll) [deg]	Rotational angle about y-axis (pitch) in SIMA results [deg]	Rotational angle about z-axis (yaw) [deg]
45	61.36	-33.27	119.32	2.772	9.035	-0.311
30	61.32	-33.15	119.34	3.197	9.126	0.087
15	61.33	-33.30	119.33	2.749	9.121	0.280
0	61.37	-33.69	119.30	1.476	9.049	0.207
-15	61.39	-34.23	119.29	-0.260	9.013	-0.093
-30	61.37	-34.75	119.30	-1.944	9.059	-0.543

Table 4.5: The translational and the rotational displacement (static calculation)

Blade pitch angle [deg]	Displacement in x-direction (surge) [m]	Displacement in y-direction (sway) [m]	Displacement in z-direction (heave) [m]	Rotational angle about x-axis (roll) [deg]	Rotational angle about y-axis (pitch) [deg]	Rotational angle about z-axis (yaw) [deg]
All angles	61.39	-34.15	119.29	0.001	9.022	0.000

Table 4.6: The real blade pitch angle due to the initial blade pitch angle

Initial blade pitch angle [deg]	Rotational angle about the y-axis (pitch) in SIMA results [deg]	Net angle change about y-axis [deg]	Real blade pitch angle [deg]
45	9.035	0.014	45.014
30	9.126	0.105	30.105
15	9.121	0.100	15.100
0	9.049	0.028	0.028
-15	9.013	-0.009	-15.009
-30	9.059	0.038	-29.962

Regardless of the blade angles, the rotational angle about the y-axis of the blade is kept around 9 degrees as shown in Table 4.4. This is because the initial pitch angle of the blade is input by the DLL input file and the angle is not delivered to SIMA. SIMA just adds only the dynamic calculation effects to the static calculation results. The real angle of the blade is the sum of the initial angle of the DLL file input and the angle change of the dynamic effect. The real blade pitch angles are shown in Table 4.6. The change due to wind load is negligible.

The y-direction forces are always zero regardless of the pitch angle. However, the displacements in the y-direction are very large comparing those in the x-direction or the z-direction. This means that the blade is not constrained in the y-direction and locates in equilibrium. The blade is constrained with the tugger lines in the x-direction and the lift lines in the z-direction.

It is recommended that the blade pitch angle be maintained at -15 ~ 0 degrees during the blade installation because the forces and the moments are the minima at that range as shown in Table 4.3.

4.1.5 The effect of the turbulent wind and the irregular waves

The blade position and angle due to turbulent winds and irregular waves are investigated.

① Turbulent wind only case

There is no wave. The wind only exists. The wind angle is 0 deg.

Table 4.7: The blade position and angle due to the turbulent wind speed (winds only)

(a) Average of the blade position						
Wind speed [m/s]	Displacement in x-direction (surge) [m]	Displacement in y-direction (sway) [m]	Displacement in z-direction (heave) [m]	Rotational angle about x-axis (roll) [deg]	Rotational angle about y-axis (pitch) [deg]	Rotational angle about z-axis (yaw) [deg]
5	61.39	-34.03	119.29	0.38	9.02	0.05
10	61.37	-33.74	119.30	1.32	9.05	0.19

(b) Standard deviation of the blade position						
Wind speed [m/s]	Displacement in x-direction (surge) [m]	Displacement in y-direction (sway) [m]	Displacement in z-direction (heave) [m]	Rotational angle about x-axis (roll) [deg]	Rotational angle about y-axis (pitch) [deg]	Rotational angle about z-axis (yaw) [deg]
5	0.00	0.04	0.00	0.12	0.00	0.02
10	0.01	0.11	0.01	0.35	0.02	0.06

(C) Difference between the calm sea result(Table 4.1) and the average of the turbulent wind						
Wind speed [m/s]	Displacement in x-direction (surge) [m]	Displacement in y-direction (sway) [m]	Displacement in z-direction (heave) [m]	Rotational angle about x-axis (roll) [deg]	Rotational angle about y-axis (pitch) [deg]	Rotational angle about z-axis (yaw) [deg]
5	0.00	0.12	0.00	0.38	0.00	0.05
10	-0.01	0.41	0.01	1.32	0.02	0.19

The wind speed is larger, the position change is bigger.

② Irregular wave only case

- The effect of the significant wave height

There is no wind. The wave peak period is 9 sec. The blade position and angle due to the significant wave height are investigated.

Table 4.8: The blade motions due to the significant wave heights

(a) Average of the blade position						
Significant wave height [m]	Displacement in x-direction (surge) [m]	Displacement in y-direction (sway) [m]	Displacement in z-direction (heave) [m]	Rotational angle about x-axis (roll) [deg]	Rotational angle about y-axis (pitch) [deg]	Rotational angle about z-axis (yaw) [deg]
1	61.39	-34.15	119.29	0.00	9.02	0.00
2	61.39	-34.15	119.29	0.00	9.02	0.00
4	61.39	-34.15	119.29	0.00	9.02	0.00

(b) Standard deviation of the blade position						
Significant wave height [m]	Displacement in x-direction (surge) [m]	Displacement in y-direction (sway) [m]	Displacement in z-direction (heave) [m]	Rotational angle about x-axis (roll) [deg]	Rotational angle about y-axis (pitch) [deg]	Rotational angle about z-axis (yaw) [deg]
1	0.04	0.00	0.01	0.00	0.04	0.00
2	0.07	0.00	0.02	0.01	0.09	0.00
4	0.13	0.01	0.04	0.01	0.16	0.00

(c) Difference between the calm sea result(Table 4.1) and the average of the turbulent wind						
Significant wave height [m]	Displacement in x-direction (surge) [m]	Displacement in y-direction (sway) [m]	Displacement in z-direction (heave) [m]	Rotational angle about x-axis (roll) [deg]	Rotational angle about y-axis (pitch) [deg]	Rotational angle about z-axis (yaw) [deg]
1	0.00	0.00	0.00	0.00	0.00	0.00
2	0.00	0.00	0.00	0.00	0.00	0.00
4	0.00	0.00	0.00	0.00	0.00	0.00

The significant wave height does not affect the average of the blade position. However, it can affect the standard deviation of the blade position. As the wave height gets higher, the standard deviation of the blade position and angle increase.

- The effect of the wave peak periods

There is no wind. The significant wave height is 1 m. The blade position and angle due to the wave peak periods are investigated.

Table 4.9: The blade position and angle due to the wave peak periods

(a) Average of the blade position						
Wave peak periods [sec]	Displacement in x-direction (surge) [m]	Displacement in y-direction (sway) [m]	Displacement in z-direction (heave) [m]	Rotational angle about x-axis (roll) [deg]	Rotational angle about y-axis (pitch) [deg]	Rotational angle about z-axis (yaw) [deg]
4	61.39	-34.15	119.29	0.00	9.02	0.00
5	61.39	-34.15	119.29	0.00	9.02	0.00
6	61.39	-34.15	119.29	0.00	9.02	0.00
7	61.39	-34.15	119.29	0.00	9.02	0.00
8	61.39	-34.15	119.29	0.00	9.02	0.00
9	61.39	-34.15	119.29	0.00	9.02	0.00
10	61.39	-34.15	119.29	0.00	9.02	0.00
11	61.39	-34.15	119.29	0.00	9.02	0.00
12	61.39	-34.15	119.29	0.00	9.02	0.00

(b) Standard deviation of the blade position						
Wave peak periods [sec]	Displacement in x-direction (surge) [m]	Displacement in y-direction (sway) [m]	Displacement in z-direction (heave) [m]	Rotational angle about x-axis (roll) [deg]	Rotational angle about y-axis (pitch) [deg]	Rotational angle about z-axis (yaw) [deg]
4	0.15	0.01	0.05	0.02	0.19	0.00
5	0.11	0.01	0.04	0.01	0.13	0.00
6	0.08	0.01	0.03	0.01	0.10	0.00
7	0.06	0.00	0.02	0.01	0.07	0.00
8	0.05	0.00	0.02	0.00	0.06	0.00
9	0.04	0.00	0.01	0.00	0.04	0.00
10	0.03	0.00	0.01	0.00	0.04	0.00
11	0.03	0.00	0.01	0.00	0.03	0.00
12	0.02	0.00	0.01	0.00	0.03	0.00

The peak period does not affect the average of the blade position. However, it can affect the standard deviation of the blade position. The shorter wave period gives the more significant movement.

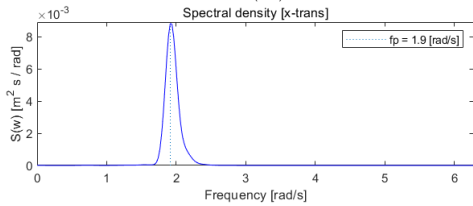
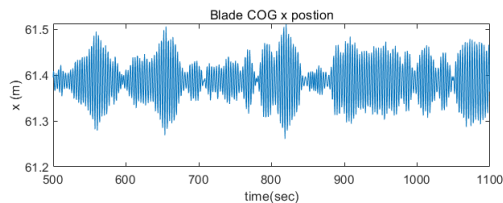
③ The combination of the turbulent winds and irregular waves

The environmental conditions are shown in Table 4.10. The time series and the spectral density plots of the blade and the jack-up hull are shown in Figure 4.6 and Figure 4.7, respectively. The surge, the heave, and the pitch motion of the blade have the peak frequencies at 1.9 rad/s. This is the natural frequency of the jack-up vessel. These motions are highly affected by the motion of the jack-up vessel. By the way, the sway, the roll, and the yaw motion have the peak frequency at 0 rad/s. This means that these motions are not affected by oscillating force with a specific period. It can be guessed that these motions are affected by turbulent wind. If they are affected by the wave, they must have the same peak frequencies with the wave.

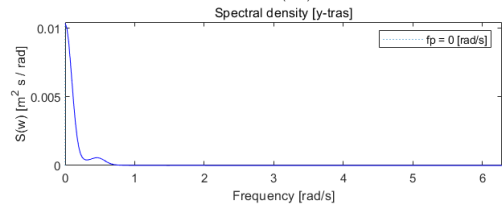
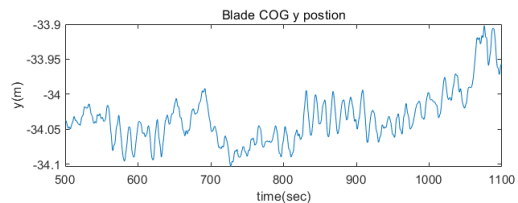
Table 4.10: The environmental conditions (the turbulent wind and irregular wave combinations)

Wave height [m]	Wave direction [deg]	Wave period [sec.]	Wave spectrum
0.5, 1.0, 2.0	0	5, 7, 9, 11	Jonswap

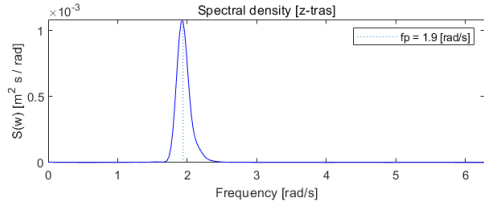
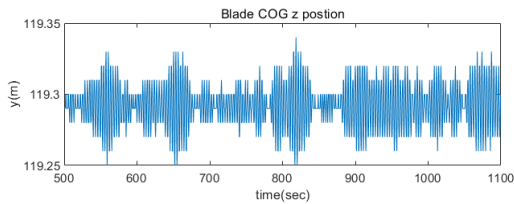
Wind speed [m/s]	wind direction [deg]	Turbulence model	Power law exponent	Turbulent intensity [%]
5.0, 1.0	0	Kaimal	0.12	15



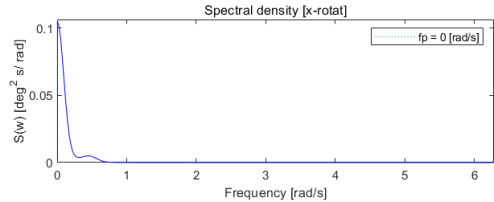
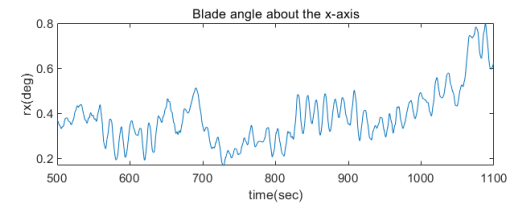
(a) Displacement in x-direction (surge)



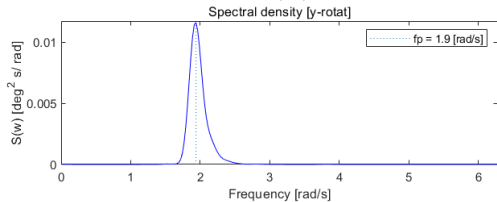
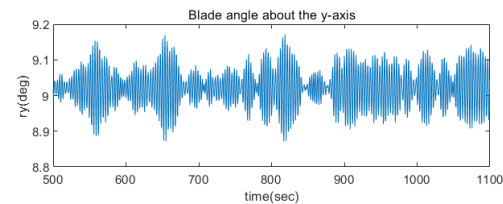
(b) Displacement in y-direction (sway)



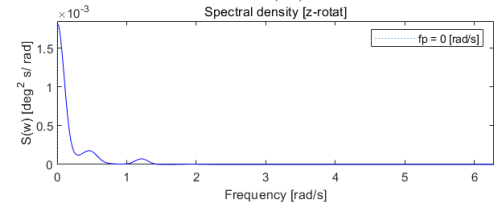
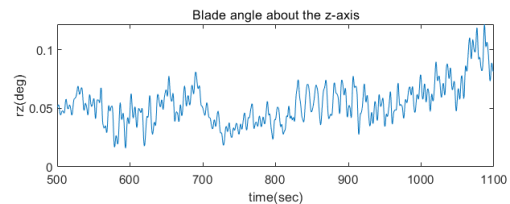
(c) Displacement in z-direction (heave)



(d) Rotational angle about the x-axis (roll)

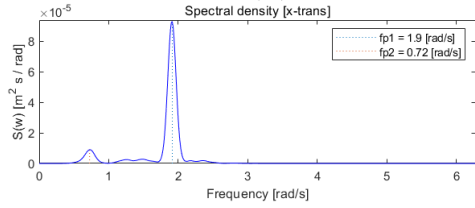
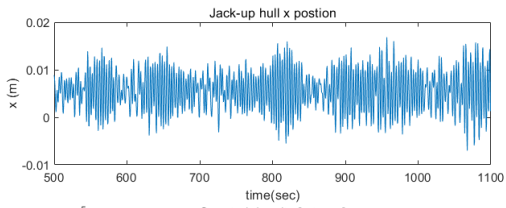


(e) Rotational angle about the y-axis (pitch)

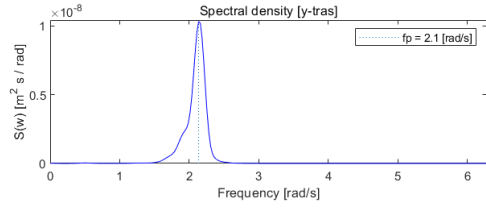
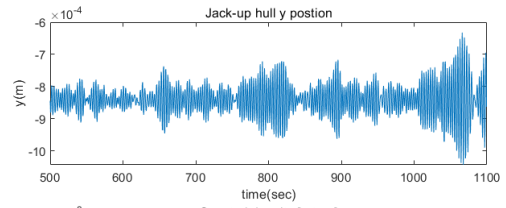


(f) Rotational angle about the z-axis (yaw)

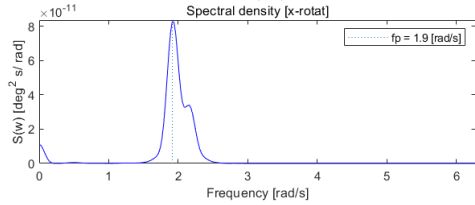
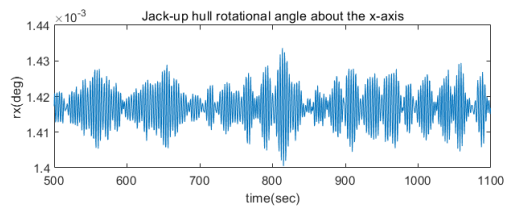
Figure 4.6: Time series and spectral density plots of the blade motion ($H_s = 1.0\text{m}$, $T_p = 9\text{ sec}$, $U_w = 5\text{m/s}$)



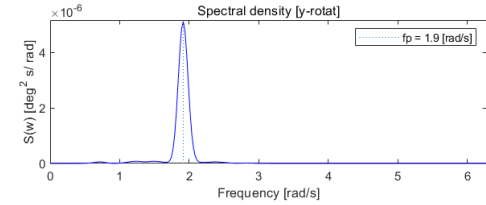
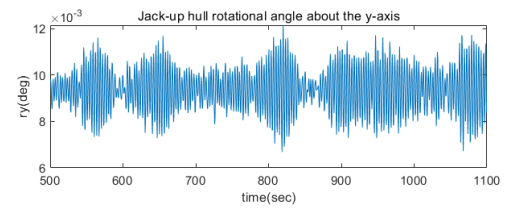
(a) Displacement in x-direction (surge)



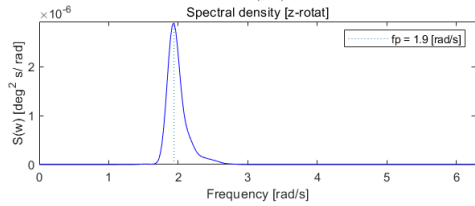
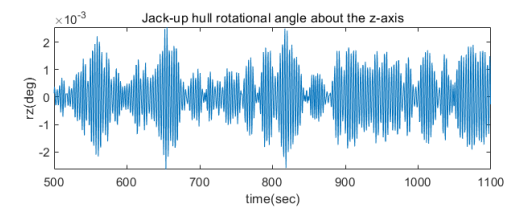
(b) Displacement in y-direction (sway)



(c) Rotational angle about the x-axis (roll)



(d) Rotational angle about the y-axis (pitch)



(e) Rotational angle about the z-axis (yaw)

Figure 4.7: Time series and spectral density plots of the jack-up hull motion ($H_s = 1.0\text{m}$, $T_p = 9\text{ sec}$, $U_w = 5\text{m/s}$)

Table 4.11: The blade motion due to the turbulent winds and irregular waves combinations

(a) Displacement in x-direction (surge)

Average						Standard deviation					
		Tp [sec.]						Tp [sec.]			
Hs [m]	Uw [m/s]	5	7	9	11	Hs [m]	Uw [m/s]	5	7	9	11
0.5	5.0	61.39	61.39	61.39	61.39	0.5	5.0	0.06	0.04	0.02	0.02
1.0	5.0	61.39	61.39	61.39	61.39	1.0	5.0	0.12	0.07	0.04	0.03
1.0	10.0	61.37	61.37	61.37	61.37	1.0	10.0	0.12	0.07	0.04	0.03
2.0	10.0	61.37	61.37	61.37	61.37	2.0	10.0	0.24	0.14	0.09	0.07

(b) Displacement in y-direction (sway)

Average						Standard deviation					
		Tp [sec.]						Tp [sec.]			
Hs [m]	Uw [m/s]	5	7	9	11	Hs [m]	Uw [m/s]	5	7	9	11
0.5	5.0	-34.03	-34.03	-34.03	-34.03	0.5	5.0	0.04	0.04	0.04	0.04
1.0	5.0	-34.03	-34.03	-34.03	-34.03	1.0	5.0	0.04	0.04	0.04	0.04
1.0	10.0	-33.74	-33.74	-33.74	-33.74	1.0	10.0	0.11	0.11	0.11	0.11
2.0	10.0	-33.74	-33.74	-33.74	-33.74	2.0	10.0	0.11	0.11	0.11	0.11

(c) Displacement in z-direction (heave)

Average						Standard deviation					
		Tp [sec.]						Tp [sec.]			
Hs [m]	Uw [m/s]	5	7	9	11	Hs [m]	Uw [m/s]	5	7	9	11
0.5	5.0	119.29	119.29	119.29	119.29	0.5	5.0	0.02	0.01	0.01	0.01
1.0	5.0	119.29	119.29	119.29	119.29	1.0	5.0	0.04	0.03	0.02	0.01
1.0	10.0	119.30	119.30	119.30	119.30	1.0	10.0	0.04	0.03	0.02	0.01
2.0	10.0	119.30	119.30	119.30	119.30	2.0	10.0	0.08	0.05	0.03	0.02

(d) Rotational angle about the x-axis (roll)

Average						Standard deviation					
		Tp [sec.]						Tp [sec.]			
Hs [m]	Uw [m/s]	5	7	9	11	Hs [m]	Uw [m/s]	5	7	9	11
0.5	5.0	0.38	0.38	0.38	0.38	0.5	5.0	0.12	0.12	0.12	0.12
1.0	5.0	0.38	0.38	0.38	0.38	1.0	5.0	0.12	0.12	0.12	0.12
1.0	10.0	1.32	1.32	1.32	1.32	1.0	10.0	0.35	0.35	0.35	0.35
2.0	10.0	1.32	1.32	1.32	1.32	2.0	10.0	0.35	0.36	0.35	0.35

(e) Rotational angle about the y-axis (pitch)

Average						Standard deviation					
		Tp [sec.]						Tp [sec.]			
Hs [m]	Uw [m/s]	5	7	9	11	Hs [m]	Uw [m/s]	5	7	9	11
0.5	5.0	9.02	9.02	9.02	9.02	0.5	5.0	0.08	0.04	0.03	0.02
1.0	5.0	9.02	9.02	9.02	9.02	1.0	5.0	0.16	0.09	0.05	0.04
1.0	10.0	9.05	9.05	9.05	9.05	1.0	10.0	0.16	0.09	0.06	0.04
2.0	10.0	9.06	9.05	9.05	9.05	2.0	10.0	0.34	0.18	0.11	0.08

(f) Rotational angle about the z-axis (yaw)

Average						Standard deviation					
		Tp [sec.]						Tp [sec.]			
Hs [m]	Uw [m/s]	5	7	9	11	Hs [m]	Uw [m/s]	5	7	9	11
0.5	5.0	0.05	0.05	0.05	0.05	0.5	5.0	0.02	0.02	0.02	0.02
1.0	5.0	0.05	0.05	0.05	0.05	1.0	5.0	0.02	0.02	0.02	0.02
1.0	10.0	0.19	0.19	0.19	0.19	1.0	10.0	0.06	0.06	0.06	0.06
2.0	10.0	0.19	0.19	0.19	0.19	2.0	10.0	0.07	0.06	0.06	0.06

The average x-position of the blade is affected by the wind speed. However, the standard deviation of the x-position of the blade is affected by the wave peak period and the significant wave height as shown in Table 4.11(a). The average y-position of the blade and the standard deviation is affected by the wind speed only as shown in Table 4.11(b). However, the standard deviation of the y-position of the blade is affected by both the wave peak period and the wave height respectively as shown in Table 4.8(b) and Table 4.9(b). The change of the average z-position of the blade is negligible. Its standard deviation gets larger when the wave period gets smaller, the wave height gets larger. The effect of the wind speed on the standard deviation is negligible as shown in Table 4.11(c). The rotational angle about the x-axis of the blade is affected dominantly by the wind speed as shown in Table 4.11(d). The standard deviation of the rotational angle about the y-axis of the blade is affected by the wave height and the wave period, respectively as shown in Table 4.11(e). The rotational angle about the z-axis of the blade is affected dominantly by the wind speed as shown in Table 4.11(f).

The largest fluctuation occurs in the x-direction displacement and the rotational angle about the x-axis when the wind speed is the fastest, the wave height is the largest, and the wave peak period is the shortest. The influential factors on each motion are distributed in Table 4.12. These characteristics of the blade position and angle should be considered for the blade installation.

Table 4.12: The influence of the environmental factors on each motion

		Displacement in x-direction (surge)	Displacement in y-direction (sway)	Displacement in z-direction (heave)	Rotational angle about x-axis (roll)	Rotational angle about y-axis (pitch)	Rotational angle about z-axis (yaw)
Wind speed	average	○	⊙	X	⊙	X	⊙
	std. dev	X	⊙	X	⊙	X	⊙
Wave period	average	X	X	X	X	X	X
	std. dev	○	X	○	X	○	X
Wave height	average	X	X	X	X	X	X
	std. dev	○	X	○	X	○	X

※ Symbols: ⊙ highly affected, ○ weekly affected, X negligible

The wave force is delivered to the blade via the jack-up. Hence, it can affect the x-directional and z-directional forces only. However, the displacement due to the wave force is small because the jack-up is supported by its legs. The jack-up vessel is practically fixed in small environmental forces.

The wind affects the position change in the x-direction, the y-direction, and the rotational angles about the x-axis and the z-axis. The wind blows at the x-direction. Naturally, wind affects the x-axis motion. The blade is a slender body and laid along the y-axis. The section shape varies along the blade length. This causes different local forces. The blade is very light comparing its dimension. Hence, small local forces can make big moments on the blade. The blade is relatively less restricted along the y-axis. The tugger lines prevent the x-directional displacement by the tension. The gravity and the lift wire tension prevent the z-directional displacement.

4.1.6 Simulations with different wind and wave seeds

20 simulations with identical sea environments with different seeds are generated. The significant wave height(H_s) is 2m. The wave peak period(T_p) is 9 sec. The turbulent wind blows at 0 deg. The wind speed(U_w) is 10 m/s. Each simulation has its wave seed and wind seed.

① The seeds of the turbulent wind and the irregular wave

The first random seed number can be from -2147483648 to 2147483647 in the Turbsim input file. The seed numbers for the simulation are determined randomly with even distribution. The wave seed numbers are selected arbitrarily. All the seeds numbers are shown in Table 4.13.

Table 4.13: The seeds of the wind and wave of simulations

Run number	Wind seeds	Wave seeds
1	1380469326	100
2	744903028	101
3	-1931013759	102
4	-1801367361	103
5	1711922163	104
6	-1659124769	200
7	-1261119636	201
8	1899248659	202
9	1538270013	203
10	1089447476	204
11	-139118402	300
12	-77431392	301
13	-1035971066	302
14	590771239	303
15	132450265	304
16	-1220293325	400
17	-1324300614	401
18	-963395014	402
19	-104419964	403
20	2088778182	404

② The statistical analysis of the position and angle of the blade

The blade position and angle are statistically analyzed. The averages and the standard deviations of the simulation are shown in Table 4.14. The average numbers in Table 4.14 are expressed according to the global coordinate. The net values can be evaluated by subtracting the initial values which are presented in Table 4.1.

Table 4.14: Statistical result of 6 D.O.F. motions of the blade in the 20 simulations with different seeds ($H_s = 2.0\text{m}$, $T_p = 9\text{sec}$, $U_w = 10\text{m/s}$)

(a) Displacement in x-direction (surge) [m]					(b) Displacement in y-direction (sway) [m]				
Run number	Average	Std. dev.	max	min	Run number	Average	Std. dev.	max	min
1	61.37	0.08	61.65	61.11	1	-33.69	0.10	-33.36	-33.95
2	61.37	0.07	61.58	61.16	2	-33.67	0.12	-33.33	-33.99
3	61.37	0.07	61.56	61.16	3	-33.72	0.11	-33.41	-34.03
4	61.37	0.09	61.63	61.11	4	-33.73	0.12	-33.32	-33.96
5	61.36	0.08	61.65	61.11	5	-33.61	0.13	-33.28	-33.90
6	61.37	0.08	61.60	61.15	6	-33.68	0.10	-33.43	-34.00
7	61.36	0.08	61.61	61.08	7	-33.63	0.13	-33.19	-33.89
8	61.37	0.07	61.59	61.14	8	-33.72	0.13	-33.30	-34.06
9	61.37	0.08	61.57	61.15	9	-33.70	0.11	-33.41	-33.97
10	61.37	0.09	61.64	61.14	10	-33.73	0.11	-33.44	-34.04
11	61.36	0.07	61.59	61.14	11	-33.64	0.16	-33.17	-34.00
12	61.37	0.06	61.56	61.19	12	-33.66	0.12	-33.28	-33.95
13	61.37	0.08	61.66	61.11	13	-33.70	0.13	-33.37	-34.05
14	61.37	0.09	61.60	61.14	14	-33.67	0.13	-33.27	-33.95
15	61.37	0.07	61.57	61.21	15	-33.69	0.13	-33.24	-33.98
16	61.37	0.08	61.58	61.17	16	-33.71	0.12	-33.41	-33.98
17	61.37	0.07	61.58	61.16	17	-33.71	0.13	-33.29	-33.97
18	61.36	0.07	61.60	61.15	18	-33.62	0.13	-33.27	-33.92
19	61.37	0.09	61.66	61.11	19	-33.68	0.10	-33.42	-33.98
20	61.37	0.07	61.56	61.16	20	-33.69	0.16	-33.04	-33.99

(c) Displacement in y-direction (heave) [m]					(d) Rotational angle about x-axis (roll) [deg]				
Run number	Average	Std. dev.	max	min	Run number	Average	Std. dev.	max	min
1	119.30	0.03	119.40	119.21	1	1.49	0.31	2.50	0.72
2	119.30	0.03	119.38	119.23	2	1.54	0.37	2.61	0.55
3	119.30	0.02	119.38	119.24	3	1.39	0.36	2.36	0.46
4	119.30	0.03	119.39	119.21	4	1.36	0.38	2.59	0.63
5	119.31	0.03	119.40	119.21	5	1.75	0.41	2.82	0.87
6	119.30	0.03	119.38	119.22	6	1.52	0.32	2.32	0.56
7	119.31	0.03	119.41	119.22	7	1.69	0.39	2.82	0.90
8	119.30	0.03	119.39	119.23	8	1.39	0.40	2.72	0.37
9	119.30	0.03	119.39	119.23	9	1.45	0.33	2.36	0.66
10	119.30	0.03	119.39	119.21	10	1.35	0.33	2.18	0.39
11	119.31	0.03	119.40	119.22	11	1.65	0.49	3.10	0.52
12	119.30	0.02	119.37	119.23	12	1.58	0.38	2.77	0.66
13	119.30	0.03	119.39	119.20	13	1.44	0.39	2.45	0.37
14	119.30	0.03	119.39	119.22	14	1.56	0.40	2.85	0.66
15	119.30	0.02	119.36	119.23	15	1.47	0.42	2.88	0.57
16	119.30	0.03	119.38	119.23	16	1.43	0.37	2.34	0.58
17	119.30	0.03	119.38	119.23	17	1.42	0.40	2.66	0.66
18	119.31	0.03	119.38	119.22	18	1.72	0.42	2.79	0.81
19	119.30	0.03	119.39	119.20	19	1.51	0.32	2.29	0.71
20	119.30	0.03	119.38	119.23	20	1.49	0.49	3.47	0.60

(e) Rotational angle about the y-axis (pitch) [deg]

Run number	Average	Std. dev.	max	min
1	9.05	0.10	9.39	8.69
2	9.06	0.09	9.34	8.77
3	9.05	0.09	9.32	8.80
4	9.05	0.11	9.36	8.69
5	9.07	0.10	9.37	8.70
6	9.05	0.10	9.30	8.76
7	9.06	0.10	9.42	8.75
8	9.05	0.09	9.33	8.77
9	9.05	0.10	9.35	8.79
10	9.05	0.11	9.35	8.69
11	9.06	0.09	9.40	8.74
12	9.06	0.08	9.29	8.77
13	9.05	0.09	9.36	8.68
14	9.06	0.11	9.36	8.72
15	9.05	0.09	9.27	8.80
16	9.05	0.10	9.31	8.76
17	9.05	0.09	9.33	8.75
18	9.07	0.09	9.32	8.76
19	9.05	0.11	9.33	8.69
20	9.06	0.09	9.33	8.78

(f) Rotational angle about the z-axis (yaw) [deg]

Run number	Average	Std. dev.	max	min
1	0.21	0.05	0.38	0.07
2	0.22	0.06	0.40	0.05
3	0.20	0.06	0.39	0.04
4	0.19	0.06	0.43	0.04
5	0.25	0.07	0.43	0.08
6	0.21	0.05	0.39	0.07
7	0.24	0.07	0.48	0.07
8	0.20	0.06	0.43	-0.02
9	0.20	0.06	0.38	0.06
10	0.19	0.05	0.35	0.04
11	0.23	0.08	0.51	0.05
12	0.22	0.06	0.47	0.06
13	0.20	0.07	0.39	0.03
14	0.22	0.06	0.42	0.06
15	0.21	0.07	0.44	0.05
16	0.20	0.06	0.39	0.04
17	0.20	0.07	0.41	0.06
18	0.25	0.07	0.44	0.09
19	0.21	0.06	0.37	0.07
20	0.21	0.08	0.54	0.04

The average and the standard deviation do not have much difference among the simulations. The seeds do not affect these values.

③ Spectral density analysis of the blade displacement and the axial force of the lift wire

Spectral density plots of the blade position and angle are plotted by use of WAFO[54]. WAFO is a Matlab toolbox created by Lund University. It is used for statistical analysis and simulation of random waves and random loads. The plots of the 20 simulations are shown from Figure 7.1 to Figure 7.20 in Appendix 1. In addition to the 6 D.O.F motions of the blade, the incident wave elevation and the axial force of the lift wire are also analyzed. The lift wire holds the blade as shown in Figure 4.8. The axial force in the lift wire is investigated.

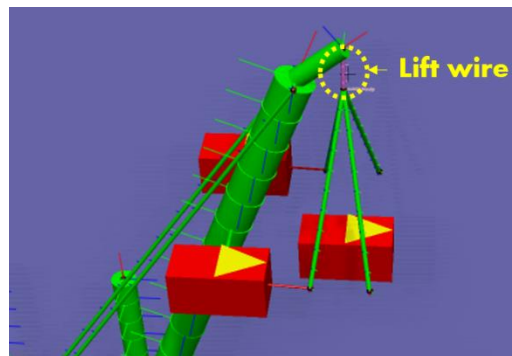


Figure 4.8: Lift Wire

The peak period of the wave is 9 sec. Hence, the peak frequency is about 0.70 rad/s. The natural period of the jack-up vessel is about 3 sec. according to sec. 4.1.3. So, the natural frequency of the jack-up vessel is about 2.09 rad/s.

Surge, heave, and pitch motion have peak frequencies of 1.9 rad/s in most simulations. Sway, roll, and yaw motion have peak frequencies of 0 rad/s in most simulations. All of them are far from the wave peak frequency, which ranges from 0.65 to 0.79 rad/s. This means that the blade motion is hardly affected by the wave. The peak frequencies of the surge, heave, and pitch are very close to the natural frequency of the jack-up vessel. That is, these motions are highly affected by the natural frequency of the jack-up vessel. Sway, roll, and yaw motions have peak frequencies of 0 rad/s. This means that these motions are not affected by specific oscillation motion. It is assumed that these motions are affected by turbulent winds. The axial force of the lift wire has a close peak frequency to that of the jack-up vessel. It also means that the lift wire is affected mainly by the natural frequency of the jack-up vessel. In conclusion, it should be avoided to install the blade under the oscillation close to the natural frequency of the jack-up vessel.

Table 4.15: Peak frequency of the blade motion, the wave elevation, and the axial force of the lift wire of the irregular waves and turbulent wind environment [rad/s]

	(a)	(b)	(c)	(d)	(e)	(f)	(g)	(f)
run #1	1.9	0	1.9	0	1.9	0, 1.2	0.69	1.8
run #2	1.9	0	1.9	0	1.9	0	0.69	1.8
run #3	1.9	0	1.9	0	1.9	0	0.74	1.8
run #4	1.9	0	1.9	0	1.9	0	0.74	1.8
run #5	1.9	0	1.9	0	1.9	0	0.79	1.8
run #6	1.9	0	1.9	0	1.9	0	0.75, 0.64, 0.88, 1	1.8
run #7	1.9	0	1.9	0	1.9, 2.1	0, 1.2	0.78, 0.69, 0.98	2.1
run #8	1.9	0	1.9	0	1.9	0	0.74	1.8
run #9	1.9	0	1.9	0	1.9	0, 0.47, 1.2	0.79	1.8
run #10	1.9	0	1.9	0	1.9	0	0.79, 0.97	1.8
run #11	1.9	0	1.9	0	1.9	0, 1.2	0.69	1.8
run #12	1.9	0	1.9	0	1.9, 2.1	0, 1.2	0.74	2.1
run #13	1.9	0	1.9	0	1.9	0	0.68, 0.81, 1	1.8
run #14	1.9	0	1.9	0	1.9, 2.1	0	0.74	1.8
run #15	1.9	0	1.9	0	1.9	0	0.69	1.8
run #16	1.9	0	1.9	0	1.9	0	0.69	1.8
run #17	1.9	0	1.9	0	2	0	0.74	1.8
run #18	1.9	0	1.9	0	1.9	0	0.65	1.8
run #19	1.9	0	1.9	0	1.9, 2.1	0, 1.2	0.69	1.8
run #20	1.9	0	1.9	0	1.9	0	0.74	1.8

* (a) Displacement in x-direction (surge), (b) Displacement in y-direction (sway), (c) Displacement in z-direction (heave), (d) Rotational angle about x-axis (roll), (e) Rotational angle about y-axis (pitch), (f) Rotational angle about z-axis (yaw), (g) Wave elevation, (h) Lift wire axial force

④ The statistical analysis of the axial force of the lift wire

The axial forces of the lift wire are shown in Table 4.16. The average axial force is 981 kN in no wind, no wave condition. It becomes about 970 kN in the given environment. A lift force of 10 kN is created. The standard deviation is about 10kN in the given environment. However, the standard deviation of the calm sea is 18kN. It should be zero because there is no external force practically. There are two possible guesses. The first guess is that it is a numerical error of the simulation. Since the dynamic force is very small compared with the static force, the fluctuation of the dynamic force is within the numerical error boundary. The second one is that the blade is suppressed in the 'run' conditions. The blade receives wind and the drag is applied to the blade. The tension of the tugger lines may seize the blade. The tugger line force is investigated for several simulations as shown in Table 4.17. This means that the tugger line does not seize the blade. In conclusion, the dynamic force is so small compared to the static force that the change of the dynamic force is negligible.

Table 4.16: Axial force of the lift wire of the irregular waves and turbulent wind environment ($H_s = 2.0\text{m}$, $T_p = 9\text{sec}$, $U_w = 10\text{m/s}$)

Run number	Average [kN]	Std. dev. [kN]
1	971	11
2	971	9
3	972	9
4	972	12
5	970	11
6	971	7
7	970	10
8	972	10
9	972	10
10	972	12
11	971	10
12	971	8
13	972	10
14	971	11
15	972	9
16	972	10
17	972	9
18	970	9
19	971	11
20	972	9
Static condition with no wind, no wave	981	-
Dynamic condition with no wind, small wave ($H_s = 0.01\text{m}$)	981	18

Table 4.17: The axial force of the tugger line

Run number	Average [kN]	Std. dev. [kN]	max [kN]	min [kN]
12	0	0	0	0
13	0	0	0	0
14	0	0	0	0
15	0	0	0	0
16	0	0	0	0
17	0	0	0	0
18	0	0	0	0
19	0	0	0	0
20	0	0	0	0

⑤ Distribution of the maximum and the minimum values of the blade position and angle

The Gumbel distribution is used to analyze the maximum and the minimum of the blade position and angle by use of the WAFO plotgumb function[54]. The maximum and the minimum values of the translational motion are expressed by the global coordinate. To facilitate the extreme analysis, the maximum and the minimum values are corrected by the values of the steady-state values in no external force. The maximum and the minimum values in Table 4.14 are subtracted by the calm sea values in Table 4.1. They are shown in Table 4.18.

Table 4.18: The maximum and the minimum values of the blade position and angle

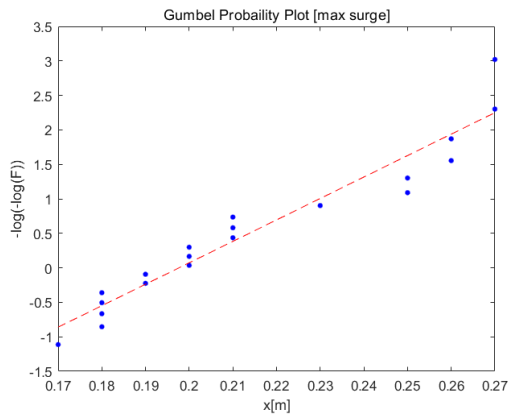
(a) Displacement in x-direction (surge) [m]			(b) Displacement in y-direction (sway) [m]			(c) Displacement in y-direction (heave) [m]		
Run number	max	min	Run number	max	min	Run number	max	min
1	0.26	-0.28	1	0.79	0.21	1	0.11	-0.08
2	0.19	-0.23	2	0.83	0.17	2	0.09	-0.06
3	0.17	-0.23	3	0.75	0.13	3	0.09	-0.05
4	0.25	-0.28	4	0.84	0.19	4	0.10	-0.08
5	0.26	-0.28	5	0.88	0.25	5	0.11	-0.08
6	0.21	-0.24	6	0.72	0.15	6	0.09	-0.07
7	0.23	-0.31	7	0.96	0.26	7	0.12	-0.07
8	0.20	-0.25	8	0.85	0.09	8	0.10	-0.06
9	0.18	-0.24	9	0.75	0.18	9	0.10	-0.06
10	0.25	-0.25	10	0.71	0.12	10	0.10	-0.08
11	0.20	-0.25	11	0.99	0.16	11	0.11	-0.07
12	0.18	-0.20	12	0.87	0.20	12	0.08	-0.06
13	0.27	-0.28	13	0.78	0.11	13	0.10	-0.09
14	0.21	-0.25	14	0.88	0.21	14	0.10	-0.07
15	0.18	-0.18	15	0.92	0.17	15	0.07	-0.06
16	0.19	-0.22	16	0.74	0.17	16	0.09	-0.06
17	0.20	-0.23	17	0.87	0.18	17	0.09	-0.06
18	0.21	-0.24	18	0.89	0.23	18	0.09	-0.07
19	0.27	-0.28	19	0.74	0.18	19	0.10	-0.09
20	0.18	-0.23	20	1.12	0.16	20	0.09	-0.06

(d) Rotational angle about x-axis (roll) [deg]			(e) Rotational angle about the y-axis (pitch) [deg]			(f) Rotational angle about the z-axis (yaw) [deg]		
Run number	max	min	Run number	max	min	Run number	max	min
1	2.50	0.72	1	0.37	-0.33	1	0.38	0.07
2	2.61	0.55	2	0.32	-0.25	2	0.40	0.05
3	2.36	0.46	3	0.30	-0.23	3	0.39	0.04
4	2.59	0.63	4	0.34	-0.33	4	0.43	0.04
5	2.82	0.87	5	0.35	-0.32	5	0.43	0.08
6	2.32	0.56	6	0.28	-0.26	6	0.39	0.07
7	2.82	0.90	7	0.40	-0.27	7	0.48	0.07
8	2.72	0.37	8	0.31	-0.25	8	0.43	-0.02
9	2.36	0.66	9	0.33	-0.23	9	0.38	0.06
10	2.18	0.39	10	0.33	-0.33	10	0.35	0.04
11	3.10	0.52	11	0.38	-0.28	11	0.51	0.05
12	2.77	0.65	12	0.27	-0.25	12	0.47	0.06
13	2.45	0.36	13	0.33	-0.34	13	0.39	0.03
14	2.84	0.65	14	0.34	-0.30	14	0.42	0.06
15	2.88	0.57	15	0.25	-0.23	15	0.44	0.05
16	2.34	0.57	16	0.29	-0.26	16	0.39	0.04
17	2.66	0.66	17	0.30	-0.27	17	0.41	0.06
18	2.79	0.81	18	0.30	-0.26	18	0.44	0.09
19	2.29	0.71	19	0.30	-0.33	19	0.37	0.07
20	3.47	0.60	20	0.31	-0.24	20	0.54	0.04

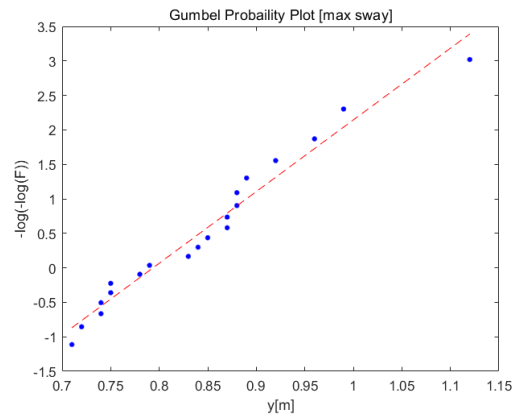
The plots are shown in Figure 4.9 and the coefficients a, b are shown in Table 4.19.

Table 4.19: Coefficients of the Gumbel distribution of the maximum of the 6 D.O.F motions of the blade

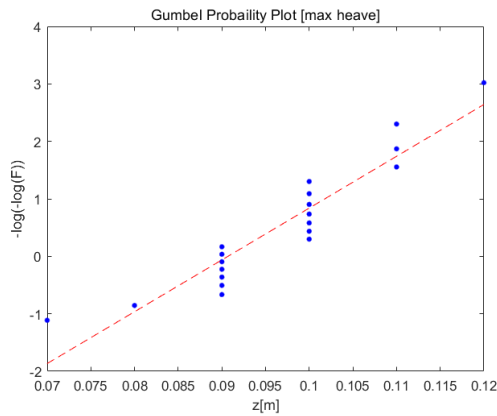
	a	b
(a) Displacement in x-direction (surge)	0.0322	0.1977
(b) Displacement in y-direction (sway)	0.0962	0.7936
(c) Displacement in y-direction (heave)	0.0111	0.0907
(d) Rotational angle about x-axis (roll)	0.2919	2.4907
(e) Rotational angle about the y-axis (pitch)	0.0344	0.3020
(f) Rotational angle about the z-axis (yaw)	0.0448	0.3985



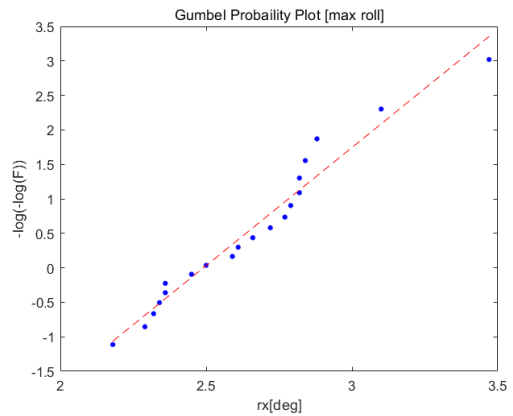
(a) Maximum displacement in the x-direction (surge)



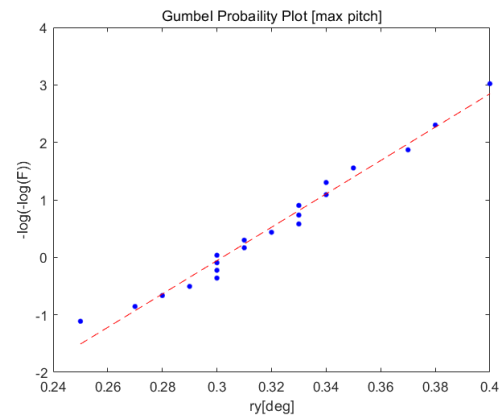
(b) Maximum displacement in the y-direction (sway)



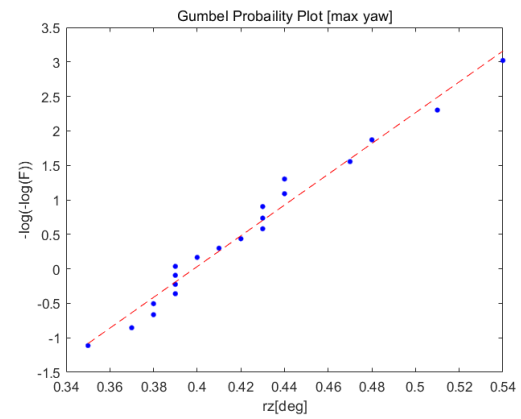
(c) Maximum displacement in the z-direction (heave)



(d) Maximum rotational angle about the x-axis (roll)



(e) Maximum rotational angle about the y-axis (pitch)



(f) Maximum rotational angle about the z-axis (yaw)

Figure 4.9: The Gumbel distribution plots of the maximum and the minimum of the 6 D.O.F motions of the blade

4.1.7 Comparison of the blade installation simulation results of the jack-up vessel and the semi vessel (collaboration research)

Identical simulations are done for a semi-submergible vessel with the identical sea environment conditions of the sec. 4.1.6. as collaboration research. The turbulent wind speed is 10 m/s, the wind heading direction is 0 deg. The significant wave height is 2.0 m/s. The peak period of the wave is 9 sec. The wave heading direction is 0 deg. The wave seed and the wind seed are identical with the jack-up vessel case as shown in Table 4.13.

The standard deviations of the position and angle of the blade installed by the semi are much larger than those of the jack-up vessel. The maximum values of the blade displacement of the semi are larger than those of the jack-up vessel as shown in Table 4.22. The jack vessel can provide a more stable installation than the semi.

Table 4.20: The blade positions of the semi in no wind and no wave condition

	Displacement in x-direction (surge) [m]	Displacement in y-direction (sway) [m]	Displacement in z-direction (heave) [m]	Rotational angle about x-axis (roll) [deg]	Rotational angle about y-axis (pitch) [deg]	Rotational angle about z-axis (yaw) [deg]
Blade in the semi	62.064	-66.000	119.35	-4.52e-07	9.0125	-6.5519e-08

Table 4.21: Statistical values of the blade position and angle in the 20 simulations with different seeds ($H_s = 2.0\text{m}$, $T_p = 9\text{sec}$, $U_w = 10\text{m/s}$) [semi-submergible]

(a) Displacement in x-direction (surge)				(b) Displacement in y-direction (sway)			
Average	Std. dev.	max	min	Average	Std. dev.	max	min
62.34	0.39	63.15	61.58	-65.26	0.19	-64.78	-65.65
62.11	0.18	62.44	61.66	-65.01	0.19	-64.62	-65.48
62.31	0.27	62.92	61.57	-65.35	0.13	-65.04	-65.60
62.15	0.40	63.20	61.33	-65.00	0.15	-64.59	-65.34
62.30	0.27	62.94	61.58	-65.25	0.26	-64.82	-65.75
62.20	0.22	62.79	61.80	-65.12	0.16	-64.77	-65.46
62.17	0.27	62.70	61.59	-65.29	0.15	-64.94	-65.64
62.24	0.39	63.27	61.40	-65.22	0.18	-64.86	-65.57
62.24	0.25	62.99	61.60	-65.32	0.22	-64.92	-65.84
62.19	0.21	62.73	61.77	-65.41	0.15	-65.13	-65.72
62.24	0.33	63.26	61.60	-65.39	0.15	-65.06	-65.71
62.15	0.27	62.95	61.56	-65.18	0.12	-64.93	-65.48
62.11	0.16	62.48	61.74	-65.30	0.23	-64.78	-65.72
62.28	0.32	62.91	61.48	-65.19	0.15	-64.86	-65.55
62.24	0.24	62.82	61.74	-65.34	0.20	-64.91	-65.69
62.23	0.24	62.81	61.77	-65.22	0.13	-64.99	-65.52
62.22	0.34	63.03	61.64	-65.28	0.16	-64.98	-65.71
62.21	0.33	62.89	61.51	-65.32	0.14	-64.98	-65.53
62.20	0.23	62.75	61.64	-65.38	0.15	-64.85	-65.62
62.13	0.19	62.49	61.65	-65.23	0.22	-64.88	-65.65

(c) Displacement in y-direction (heave)

Average	Std. dev.	max	min
119.36	0.19	119.74	118.98
119.40	0.09	119.60	119.19
119.36	0.13	119.68	119.07
119.39	0.18	119.81	118.94
119.37	0.14	119.75	119.00
119.38	0.11	119.64	119.05
119.37	0.12	119.64	119.11
119.37	0.18	119.71	118.91
119.37	0.13	119.71	118.98
119.36	0.11	119.62	119.10
119.37	0.15	119.71	118.89
119.37	0.12	119.64	118.91
119.38	0.08	119.53	119.21
119.37	0.18	119.77	118.97
119.37	0.13	119.63	119.06
119.37	0.13	119.64	119.08
119.37	0.16	119.69	118.98
119.36	0.16	119.10	119.00
119.37	0.13	119.67	119.06
119.38	0.09	119.59	119.15

(d) Rotational angle about x-axis (roll)

Average	Std. dev.	max	min
2.21	0.48	3.43	1.18
3.13	0.59	4.46	1.88
1.99	0.27	2.67	1.39
3.17	0.45	4.40	2.20
2.33	0.40	2.98	1.56
2.71	0.50	3.87	1.73
2.20	0.43	3.47	1.17
2.38	0.49	3.39	1.31
2.12	0.60	3.17	0.85
1.81	0.40	2.53	1.00
1.84	0.33	2.37	1.05
2.56	0.36	3.07	1.85
2.20	0.67	1.68	1.14
2.49	0.43	3.59	1.64
2.04	0.48	3.06	1.30
2.43	0.33	3.04	1.52
2.22	0.48	2.98	0.86
2.08	0.33	2.81	1.48
1.93	0.33	2.86	1.39
2.36	0.57	3.36	1.58

(e) Rotational angle about the y-axis (pitch)

Average	Std. dev.	max	min
9.12	0.11	9.36	8.88
9.18	0.08	9.41	8.95
9.09	0.08	9.30	8.93
9.20	0.11	9.49	8.96
9.12	0.09	9.34	8.95
9.14	0.08	9.33	8.93
9.10	0.07	9.25	8.96
9.12	0.11	9.38	8.93
9.10	0.08	9.33	8.92
9.07	0.06	9.20	8.92
9.08	0.08	9.32	8.91
9.13	0.08	9.44	8.96
9.10	0.07	9.37	8.98
9.13	0.11	9.49	8.94
9.10	0.08	9.25	8.88
9.12	0.09	9.32	8.95
9.11	0.09	9.28	8.91
9.10	0.08	9.27	8.94
9.08	0.08	9.29	8.93
9.11	0.06	9.27	8.99

(f) Rotational angle about the z-axis (yaw)

Average	Std. dev.	max	min
0.35	0.11	0.61	0.07
0.46	0.10	0.66	0.24
0.31	0.08	0.48	0.13
0.47	0.10	0.67	0.24
0.37	0.09	0.56	0.18
0.41	0.08	0.63	0.25
0.33	0.09	0.56	0.12
0.37	0.11	0.64	0.11
0.32	0.11	0.55	0.01
0.27	0.08	0.45	0.01
0.28	0.09	0.48	0.00
0.38	0.08	0.56	0.20
0.31	0.12	0.60	0.12
0.38	0.09	0.63	0.19
0.31	0.10	0.58	0.14
0.36	0.08	0.55	0.14
0.33	0.11	0.57	0.12
0.31	0.08	0.56	0.15
0.30	0.07	0.45	0.16
0.35	0.09	0.54	0.16

Table 4.22: The maximum values of the blade position and angle of the semi (The values are corrected by the static results in the calm sea)

Run number	(a)	(b)	(c)	(d)	(e)	(f)
1	1.09	1.224	0.39	3.43	0.35	0.61
2	0.37	1.38	0.25	4.46	0.4	0.66
3	0.856	0.958	0.33	2.67	0.29	0.48
4	1.131	1.409	0.46	4.40	0.48	0.67
5	0.878	1.185	0.4	2.98	0.33	0.56
6	0.727	1.233	0.29	3.87	0.32	0.63
7	0.63	1.06	0.29	3.47	0.24	0.56
8	1.207	1.144	0.36	3.39	0.37	0.64
9	0.922	1.077	0.36	3.17	0.32	0.55
10	0.662	0.874	0.27	2.53	0.19	0.45
11	1.19	0.939	0.36	2.37	0.32	0.48
12	0.888	1.07	0.29	3.07	0.43	0.56
13	0.41	1.225	0.18	1.68	0.36	0.60
14	0.84	1.143	0.42	3.59	0.48	0.63
15	0.756	1.091	0.28	3.06	0.24	0.58
16	0.744	1.014	0.29	3.04	0.31	0.55
17	0.964	1.021	0.34	2.98	0.27	0.57
18	0.826	1.017	0.35	2.81	0.26	0.56
19	0.684	1.15	0.32	2.86	0.28	0.45
20	0.422	1.124	0.34	3.36	0.26	0.54

* (a) Displacement in x-direction (surge), (b) Displacement in y-direction (sway), (c) Displacement in z-direction (heave), (d) Rotational angle about x-axis (roll), (e) Rotational angle about y-axis (pitch), (f) Rotational angle about z-axis (yaw),

The peak frequencies of the blade position and angle when it is installed by the semi are shown in Table 4.23. Most motions are dominated by the wave. Surge, heave, pitch, and yaw motions show very close peak frequency with the wave peak frequency. This is different from the jack-up vessel. The surge, heave, and pitch of the jack-up vessel are highly affected by the natural peak frequency of the jack-up vessel. The yaw motion of the blade of the semi is affected by the wave frequency. However, That of the jack-up is not. Its peak frequency is 0. This is because the semi is free with the yaw motion. Sway and roll motion show the peak frequency of 0 rad/s. This result is the same as the jack-up vessel case.

Table 4.23: The spectral density peak frequency of the position and angle of the blade installed by a semi-submersible vessel

	(a)	(b)	(c)	(d)	(e)	(f)	(g)
sim #01	0.71	0	0.69	0	0.69	0.74	0.69
sim #02	0.71	0	0.69	0	0.66	0	0.69
sim #03	0.74	0.18, 0.27	0.71	0	0.69	0.74, 1.2	0.74
sim #04	0.74	0	0.71	0	0.25, 0.69	0.76	0.74
sim #05	0.74	0.27	0.69	0	0.66	0	0.79
sim #06	0.031, 0.25, 0.76	0	0.25, 0.64, 0.75	0	0.25, 0.64, 0.75	0.79	0.64, 0.75, 0.88, 1
sim #07	0.76	0	0.74	0	0.26, 0.69	0.79	0.69, 0.78, 0.98
sim #08	0.74	0.28	0.71	0	0.69	0.79	0.74
sim #09	0.74	0	0.69	0	0.69	0.83	0.79
sim #10	0.26, 0.77	0	0.27, 0.72	0	0.25, 0.71	0.79	0.79, 0.97
sim #11	0.71	0	0.69	0	0.69	0.76	0.69
sim #12	0.74	0	0.69	0	0.25, 0.69	0.79	0.74
sim #13	0.7	0	0.68, 0.79	0	0.66	0.81	0.68, 0.81, 1
sim #14	0.74	0	0.71	0	0.69	0.76	0.74
sim #15	0.71	0.26	0.27, 0.69	0	0.031, 0.68, 0.25	0.79	0.69
sim #16	0.71	0	0.71	0	0.69	0.71	0.69
sim #17	0.76	0.049, 0.26, 0.55	0.25, 0.74	0	0.25, 0.71	0.79	0.74
sim #18	0.74	0.27, 0.47, 0.64	0.69	0	0.65	0.79	0.65
sim #19	0.74	0	0.69	0	0.69	0.74	0.69
sim #20	0.76	0	0.74	0	0.69	0.79	0.74

* (a) Displacement in x-direction (surge), (b) Displacement in y-direction (sway), (c) Displacement in z-direction (heave), (d) Rotational angle about x-axis (roll), (e) Rotational angle about y-axis (pitch), (f) Rotational angle about z-axis (yaw), (g) Wave elevation

5 Conclusions

5.1 The summary of the discussion about results

The blade motion during the single blade installation of the offshore wind turbine is investigated in this thesis. The motions of the blade are simulated by SIMA. The wind and wave loads are applied as external forces. The results and discussion of the simulation are summarized below.

- The constant wind is applied. The wind speeds are 2~10m/s, the wind directions are 0, 90, 180, 270 deg. There is no wave. The maximum translation displacement is less than 0.5m. The maximum rotated angle is less than 2 deg.
- Regular waves are applied to the jack-up vessel. The wave amplitude is 1m. The wave periods are 2 ~ 15 sec. The blade motion is exceptionally large when the wave period is 3 sec. It is estimated that the natural period of the jack-up vessel is around 3 sec. The fluctuation of the axial forces and the bending moments are also largest when the wave period is 3 sec. This means that the blade motion is significantly affected by the natural period of the jack-up vessel.
- The applied forces and the moments on the blade according to the initial blade angles are examined. They are smallest when the blade pitch angle is -15 ~ 0 deg. The y-axis direction force and the moment about the y-axis are always zero regardless of the blade pitch angle. It is guessed that there is no constraint in those directions and the blade is in equilibrium conditions in those directions.
- Wind speed can affect both the average position of the blade and the standard deviation of the blade position. Wave can affect the standard deviation of the blade position only.
- According to the spectral density function analysis, the natural frequency of the jack-up vessel gives the dominant effect on the blade motion. The surge, heave, and pitch motion of the blade have peak frequency at the natural frequency of the jack-up vessel. The peak frequencies of the sway, roll and yaw motions are zero. They are not affected by repeated load. The axial force of the lift wire of the blade is also highly affected by the natural frequency of the jack-up vessel.
- According to comparison with a semi-submersible, the wave has an important role in the blade motion. The surge, heave, pitch, and yaw motions of the blade have the same peak frequency as the peak frequency of the wave. The peak frequency of the sway and the roll motions is zero. This is the same with the jack-up vessel.

5.2 Future work suggestion

- The installation by the jack-up vessel with longer legs needs to be analyzed. As the wind turbine operation water depth gets deeper, the motion response of the jack-up vessel in the deeper water is necessary.
- The operation limit of the environmental loads needs to be analyzed.

6 Reference

- [1] Wikipedia. *Wind turbine*. Available from: https://en.wikipedia.org/wiki/Wind_turbine.
- [2] Wikipedia. *Cost of electricity by source*. Available from: https://en.wikipedia.org/wiki/Cost_of_electricity_by_source.
- [3] Krogsgaard Madsen, *Offshore Wind Power*. 2010: Wayback Machine BTM Consult.
- [4] *Wind power*, in *New York Times*.
- [5] Wikipedia. *Offshore wind power*. Available from: https://en.wikipedia.org/wiki/Offshore_wind_power.
- [6] Global wind energy council, *Global offshore wind report 2020*. 2020.
- [7] 4C Offshore. *Hornsea project one - fully commissioned offshore wind farm - united kingdom.*; Available from: www.4c offshore.com.
- [8] *Orsted clears taiwan hurdle*, in *Renewable Enegy News*. 2017.
- [9] DNV-GL, *Energy transition outlook 2020 excutive summary*. 2020, DNV-GL.
- [10] IEA, *IEA 2013*. 2013.
- [11] Zhen Gao. *Marine operations related installation of offshore wind turbine blades*. in *WESC 2019*. 2019.
- [12] S. Butterfield W. Musial J. Jonkman, G. Scott., *Definition of a 5-mw reference wind turbine for offshore system development*. 2009.
- [13] Christian Bak, *The DTU 10-mw reference wind turbine*.
- [14] Jennifer Rinker et. al Evan Gaertner, *Definition of the iea 15-megawatt offshore reference wind*. 2020.
- [15] Wikipedia. *List of offshore wind farms*. Available from: https://en.wikipedia.org/wiki/List_of_offshore_wind_farms.
- [16] Byron Byrne Dan Kallehave, Christian Thilsted, and Kristian Mikkelsen, *Optimization of monopiles for offshore wind turbines*. physical and engineering sciences, 2015. 373(2035).
- [17] José-Santos López-Gutiérrez M. Dolores Esteban, Vicente Negro, *Gravity-based foundations in the offshore wind sector*. Journal of marine science and engineering, 2019.
- [18] E. Y. K. Ng Kok Hon Chew, Kang Tai, Michael Muskulus, Daniel Zwick, *Offshore wind turbine jacket substructure: A comparison study between four-legged and three-legged designs*. Journal of Ocean and Wind Energy, 2014. 1.
- [19] IBERDROLA. Available from: <https://www.iberdrola.com/sustainability/offshore-wind-turbines-foundations>.
- [20] Kurt E. Thomsen, *OFFSHORE WIND*. second ed. 2014.
- [21] Wikipedia. *Floating wind turbine*. Available from: https://en.wikipedia.org/wiki/Floating_wind_turbine.
- [22] Global Wind Channel, *How to build an offshore wind farm*.
- [23] Zhengru Ren, *Advanced Control Algorithms to support Automated Offshore Wind Turbine Installation*, in *Marine Technology department*. 2019, NTNU: Trondheim.
- [24] Zhiyu Jain et al., *A parametric study on the final blade installation process for monopile wind turbines under rough environmental conditions*. Engineering Structures, 2018(172(2018)): p. 1042-1056.
- [25] Sea Jacks. *Offshore wind solutions*. Available from: <https://www.seajacks.com/offshore-wind-solutions/>.
- [26] OffshoreWIND, *Jan de nul orders super-sized floating installation vessel.*, in *Offshore Energy*.
- [27] Sea Jacks. *Sea jack scylla*. Available from: <https://www.seajacks.com/self-propelled-jack-up-vessels/seajacks-scylla/>.

- [28] Fred. Olsen Windcarrier. *Fred. Olsen Windcarrier*. Available from: <https://windcarrier.com/fleet>.
- [29] Ulstein. *Ulstein Jack Up*. Available from: <https://ulstein.com/ship-design/jack-up>.
- [30] SAIPEM. *SAIPEM 7000*. Available from: <https://www.saipem.com/en/identity-and-vision/assets/saipem-7000>.
- [31] Jan De Nul. *Heavy lift vessels*. Available from: <https://www.jandenu.com/fleet/heavy-lift-vessels>.
- [32] Seaway Heavy Lifting. *Oleg strashnov*. Available from: https://www.seawayheavylifting.com.cy/uploads/media/SHL084_Equipment_Factsheet_DEF_WT_LOW.pdf.
- [33] Ulstein. *Securing your future in offshore wind*. 2019; Available from: <https://ulstein.com/news/2019/securing-your-future-in-offshore-wind>.
- [34] Yuna Zhao, *Numerical Modeling and Dynamic Analysis of Offshore Wind Turbine Blade Installation*. 2019, NTNU.
- [35] SINTEF Ocean, *SIMO-Theory Manual Version 4.10*. 2017, Trondheim: SINTEF Ocean.
- [36] SINTEF Ocean, *RIFLEX - Theory Manual 4.10.1*. . 2017, Trondheim: SINTEF Ocean.
- [37] P. C. Sandvik Z. Gao T. Moan Y. Zhao, Z. Cheng and E. V. Buren, *Numerical modeling and analysis of the dynamic motion response of an offshore wind turbine blade during installation by a jack-up crane vessel*. Ocean Engineering, 2018. 165: p. 353-364.
- [38] S. Horner, *Fluid dynamic drag: Practical information on aerodynamic drag and hydrodynamic resistance*. Hoerner Fluid Dyn. 1965, NJ: Midland Park.
- [39] H. V. Borst. S. F. Hoerner, *Fluid-dynamic lift: practical information on aerodynamic and hydrodynamic lift*. 1985, Vancouver, WA: Hoerner Fluid Dynamics.
- [40] Z. Cheng P. C. Sandvik Z. Gao Y. Zhao, T. Moan., *An integrated dynamic analysis method for simulating installation of a single blade for offshore wind turbines*. Ocean Engineering, 2018. 152: p. 72-88.
- [41] S. Gupta and J. G. Leishman, *Dynamic stall modelling of the s809 aerofoil and comparison with experiments*. Wind Energy, 2006. 9(6): p. 521-547.
- [42] Sung-chul Shin Dang Ahn, Soo-young Kim, Hicham Kharoufi, Hyun-cheol Kim, *Comparative evaluation of different offshore wind turbine installation vessels for Korean west-south wind farm*. International Journal of Naval Architecture and Ocean Engineering, 2017. 9(1): p. 45-54.
- [43] Kurt J. Paterson P. R. Thies, F. D'Amico and G. Harrison, *Offshore wind installation vessels - a comparative assessment for uk offshore rounds 1 and 2*. Ocean Engineering, 2018. 148: p. 637-649.
- [44] M. M. Christopher, *Physical and numerical modelling of offshore foundations under combined loads*. 1994, University of Oxford.
- [45] Z. Cheng and T. Moan Z. Gao Y. Zhao, *Effect of foundation modeling on the dynamic motion response of an offshore wind turbine blade during installation by a jack-up crane vessel*, in *International Offshore Wind Technical Conference(IOWC)*. 2018: San Francisco.
- [46] SNAME, *Guidelines for Site Specific Assessment of Mobile Jack-Up Units*. 2008.
- [47] International Organization for Standardization, *Petroleum and natural gas industries- site specific assessment of mobile offshore units part 1: Jack-ups*. 2009, ISO.
- [48] L. Bergami and F. Zahle S. Guntur M. Gaunaa, *First-order aerodynamic and aeroelastic behavior of a single-blade installation setup*. Journal of Physics: Conference Series,, 2014. 524(1): p. 012073.
- [49] L. Rayleigh, *Theory of Sound (two volumes)*. 1877, New York: Dover Publications.
- [50] B. J. Jonkman, *Turbsim user's guide: Version 1.50*. 2019.
- [51] IEC, *International standard 61400-1, wind turbines, part 1: Design requirements*. 2005: IEC.

- [52] DNV, *DNV-RP-C205 Environmental conditions and environmental loads*. 2007, DET NORSKE VERITAS: Oslo, Norway.
- [53] Wikipedia. *Gumbel distribution*. Available from:
https://en.wikipedia.org/wiki/Gumbel_distribution.
- [54] Lund University, *WAFO*. 2018.

7 Appendices

Appendix 1: The time series plots and the spectral density plots of the 20 simulations of the blade motion in section 4.1.6

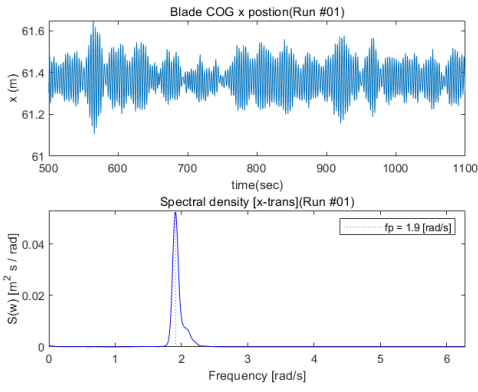
The turbulent wind blows at 0 deg. Wind speed is 10m/s. Irregular wave goes at 0 deg. The wave peak period is 9 sec. The significant wave height is 2.0m.

The time series plots and the spectral density plots of the blade motions are provided. The start time is 500 sec for every time series plot because 0~500 sec. is used for the transient state.

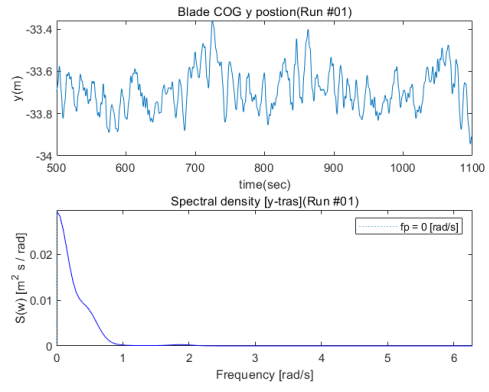
Appendix 2: MATLAB script

MATLAB scripts for the spectral density analysis and the Gumbel distribution are provided.

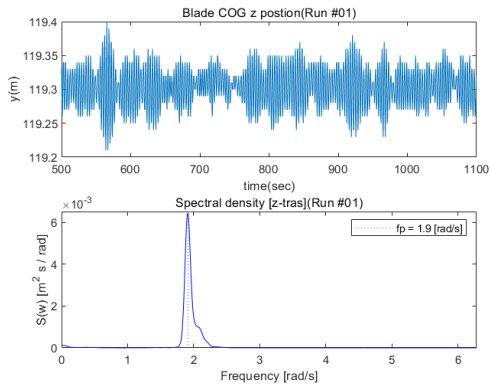
Appendix 1: The time series plots and the spectral density plots of the 20 simulations of the blade motion in section 4.1.6



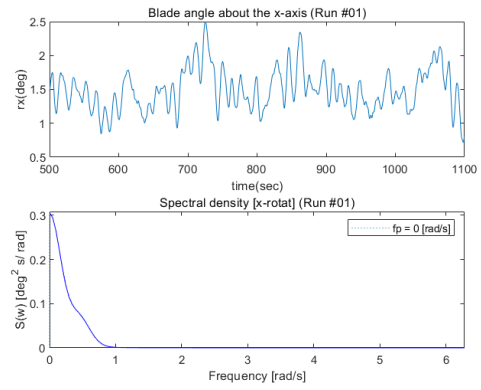
(a) Displacement in the x-direction



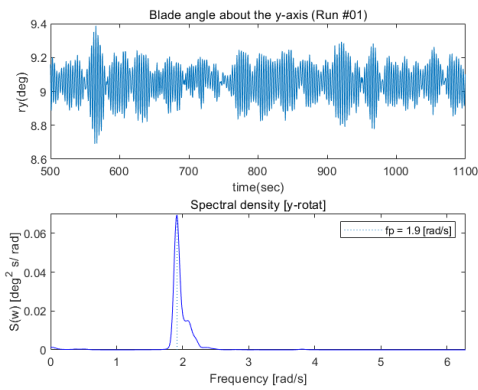
(b) Displacement in the y-direction



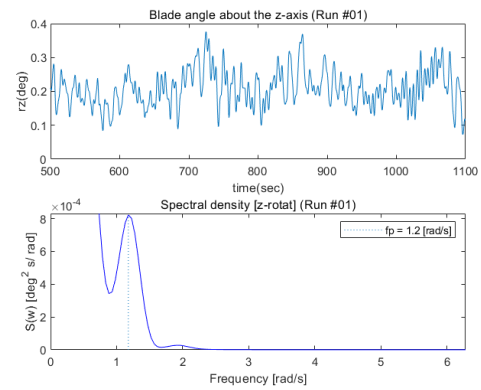
(c) Displacement in the z-direction



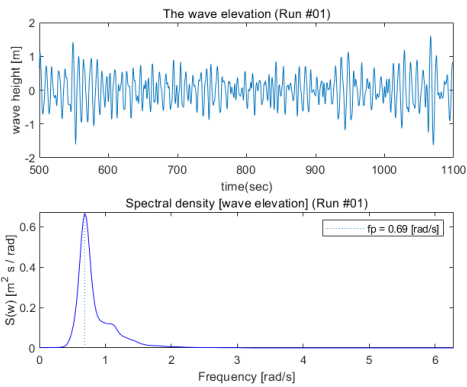
(d) Rotational angle about the x-axis



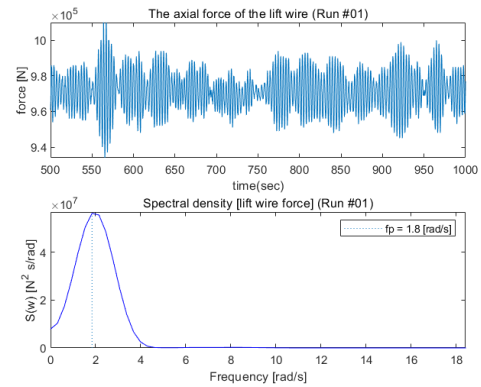
(e) Rotational angle about the y-axis



(f) Rotational angle about the z-axis

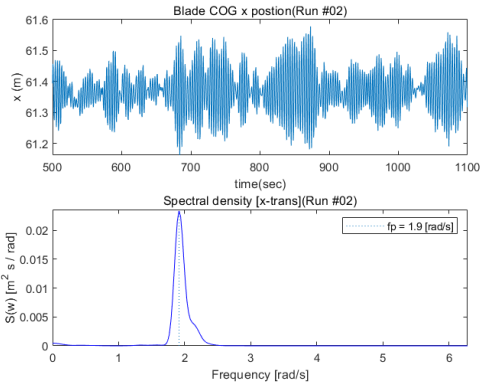


(g) Wave elevation

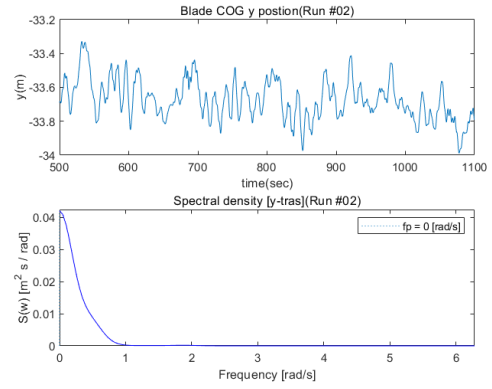


(h) Lift wire axial force

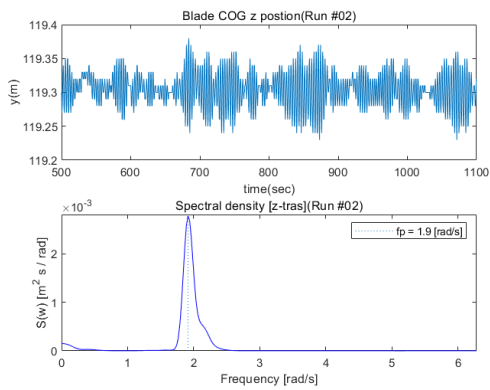
Figure 7.1: Time series and spectral density plots of run #1



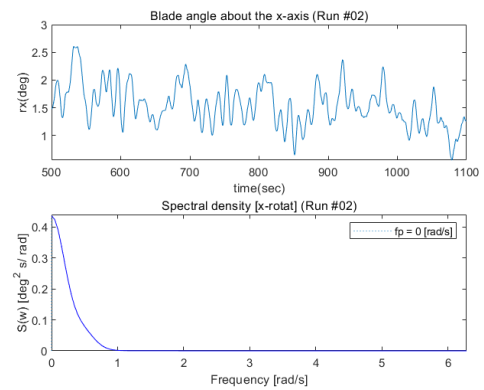
(a) Displacement in the x-direction



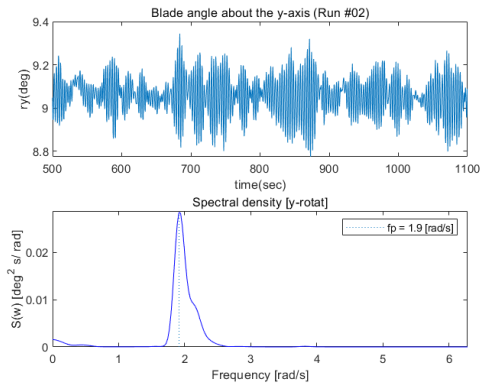
(b) Displacement in the y-direction



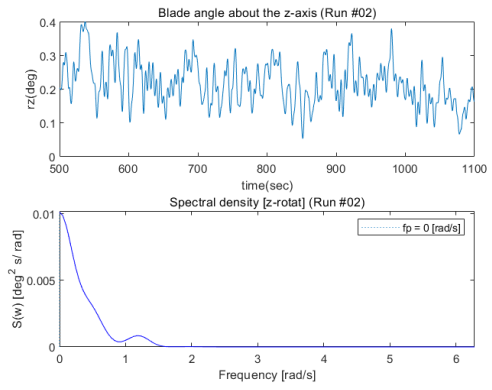
(c) Displacement in the z-direction



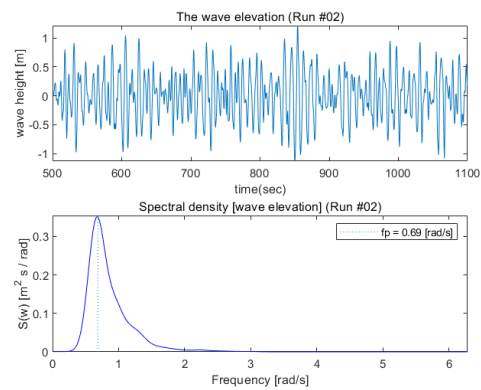
(d) Rotational angle about the x-axis



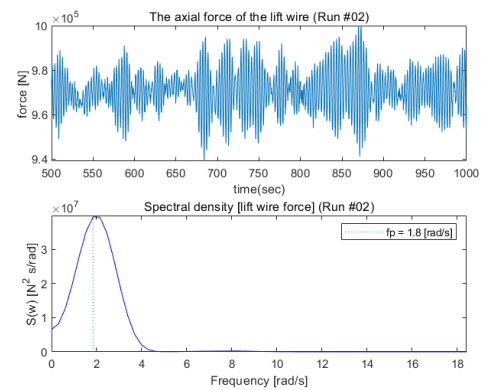
(e) Rotational angle about the y-axis



(f) Rotational angle about the z-axis

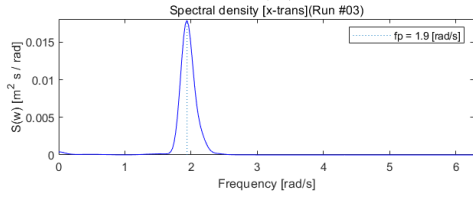
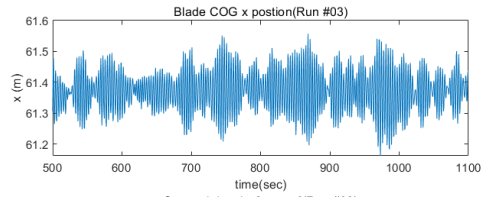


(g) Wave elevation

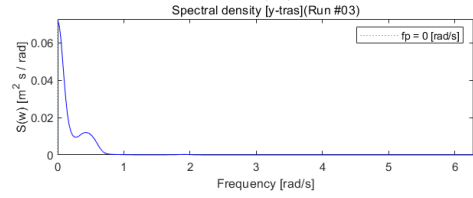
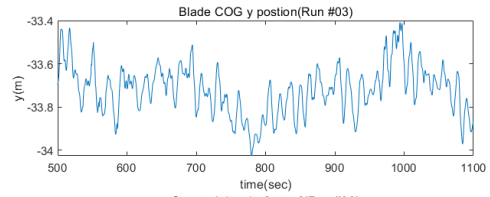


(h) Lift wire axial force

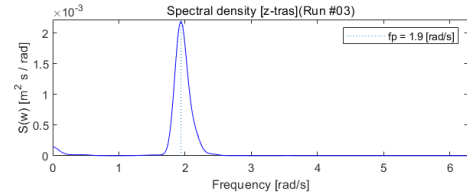
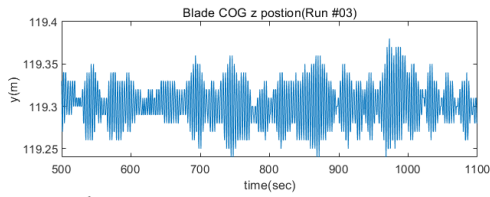
Figure 7.2: Time series and spectral density plots of run #2



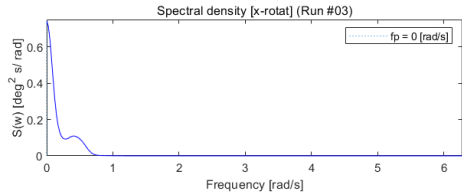
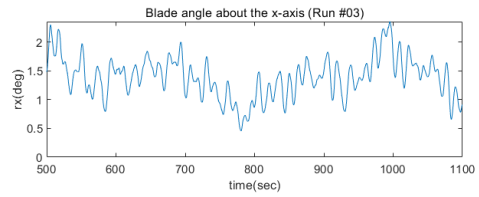
(a) Displacement in the x-direction



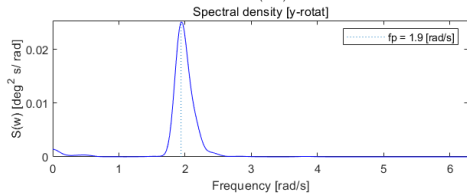
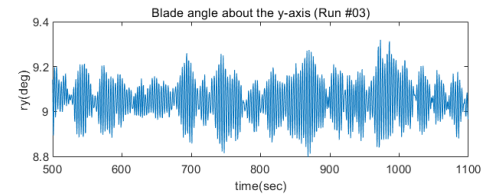
(b) Displacement in the y-direction



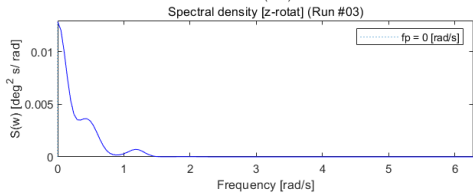
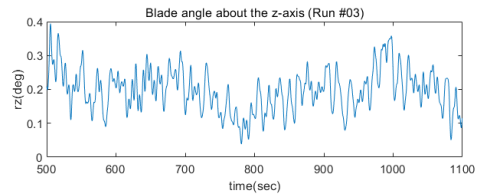
(c) Displacement in the z-direction



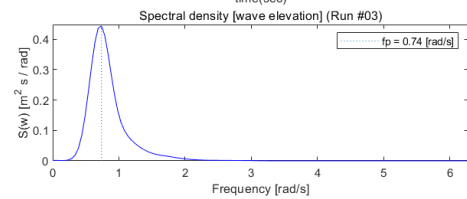
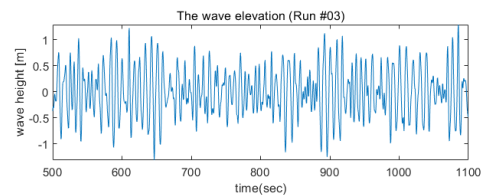
(d) Rotational angle about the x-axis



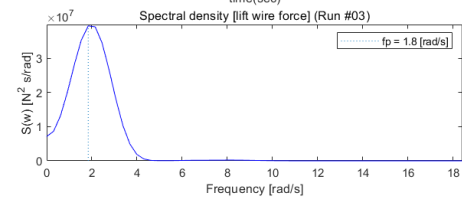
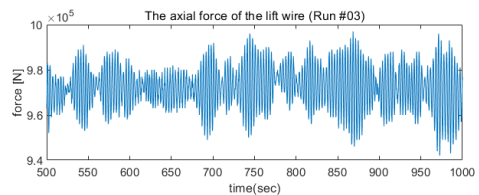
(e) Rotational angle about the y-axis



(f) Rotational angle about the z-axis

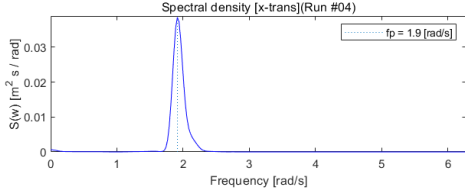
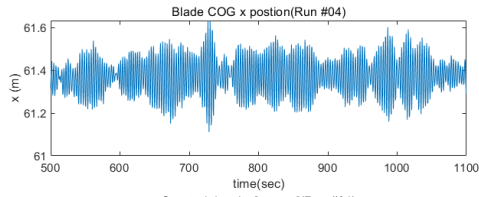


(g) Wave elevation

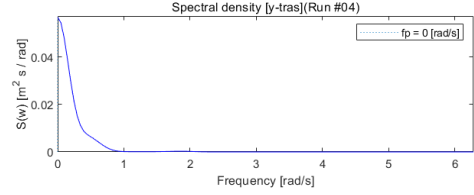
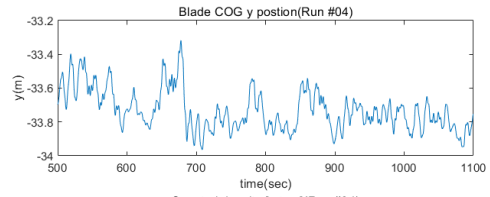


(h) Lift wire axial force

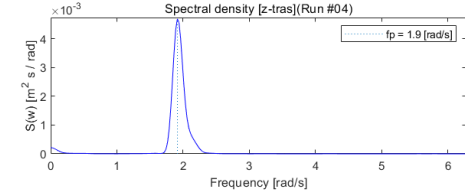
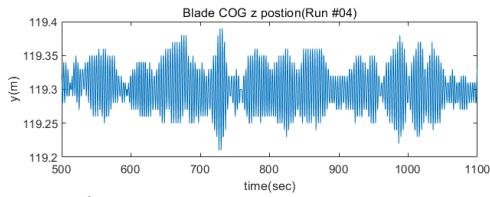
Figure 7.3: Time series and spectral density plots of run #3



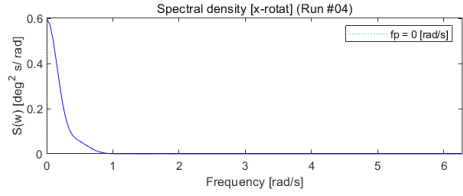
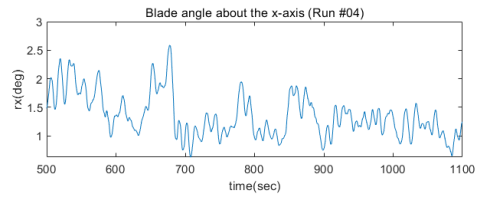
(a) Displacement in the x-direction



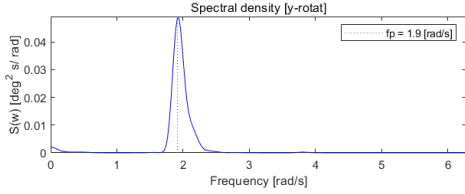
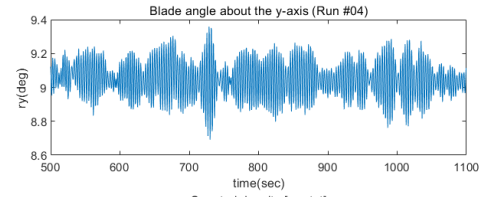
(b) Displacement in the y-direction



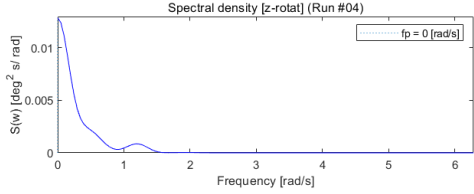
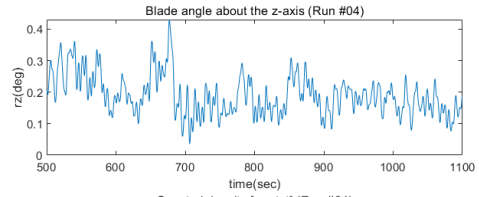
(c) Displacement in the z-direction



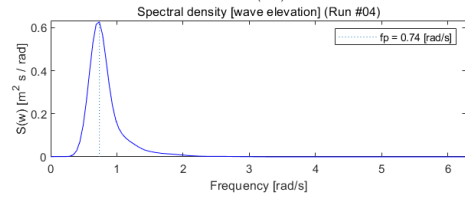
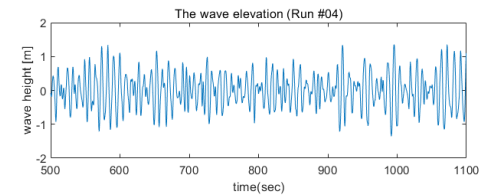
(d) Rotational angle about the x-axis



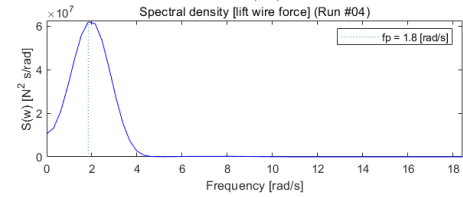
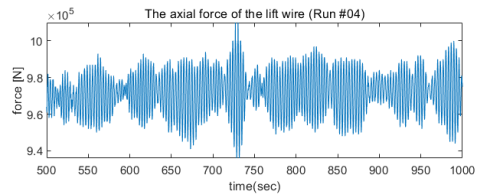
(e) Rotational angle about the y-axis



(f) Rotational angle about the z-axis

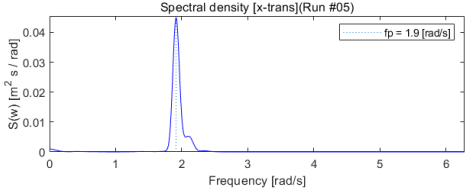
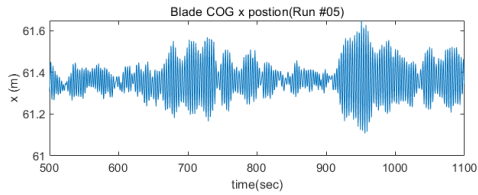


(g) Wave elevation

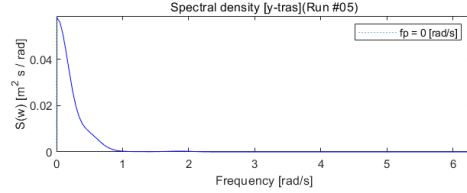
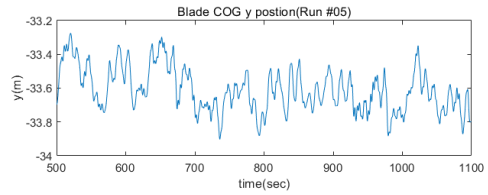


(h) Lift wire axial force

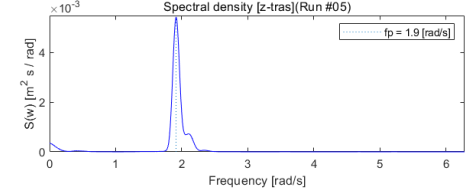
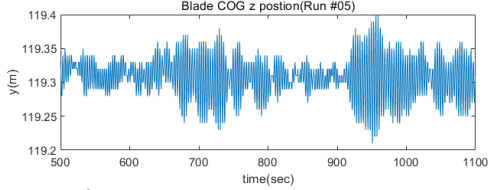
Figure 7.4: Time series and spectral density plots of run #4



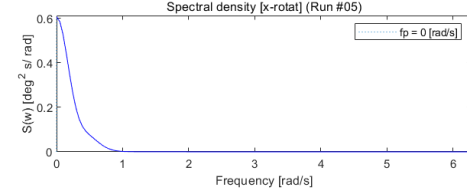
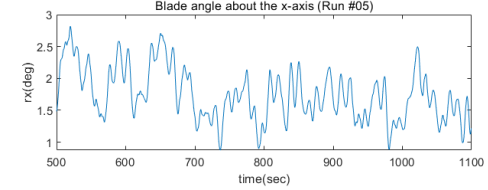
(a) Displacement in the x-direction



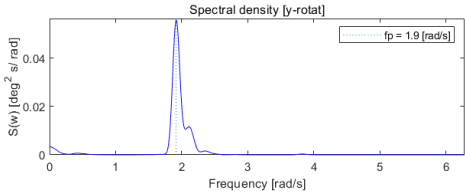
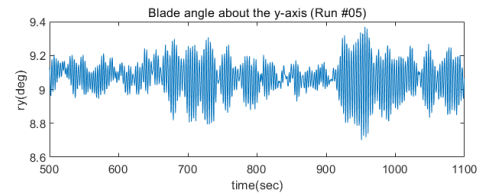
(b) Displacement in the y-direction



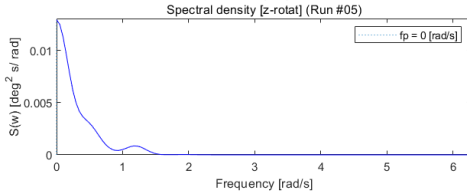
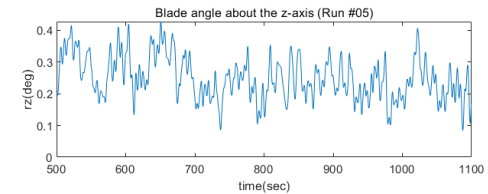
(c) Displacement in the z-direction



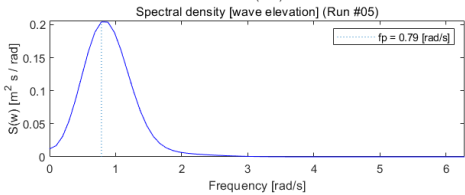
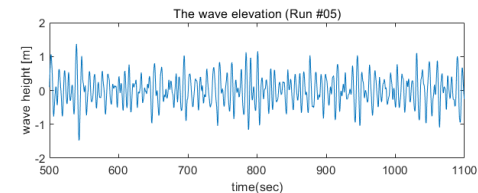
(d) Rotational angle about the x-axis



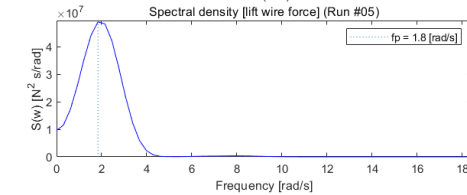
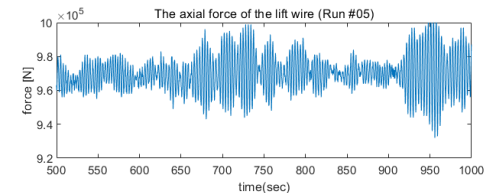
(e) Rotational angle about the y-axis



(f) Rotational angle about the z-axis

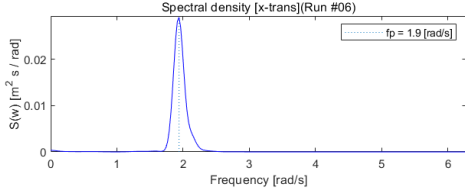
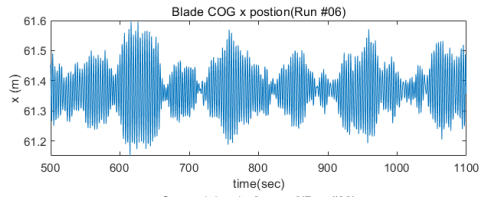


(g) Wave elevation

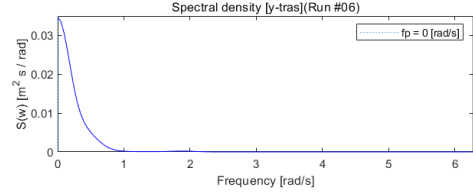
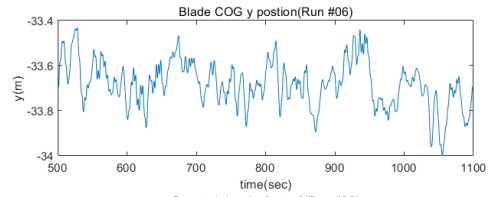


(h) Lift wire axial force

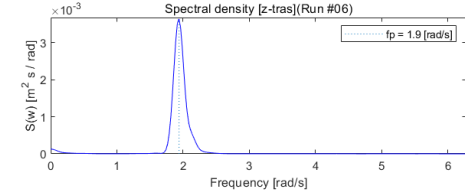
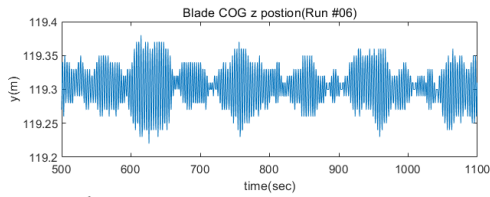
Figure 7.5: Time series and spectral density plots of run #5



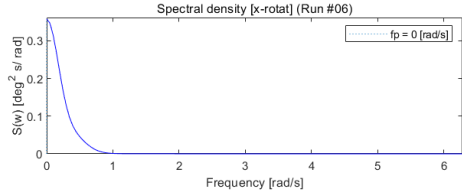
(a) Displacement in the x-direction



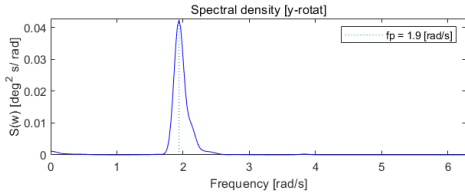
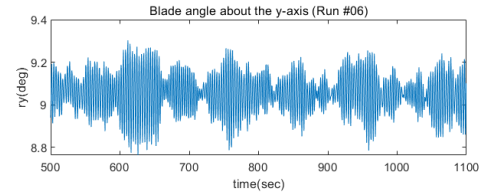
(b) Displacement in the y-direction



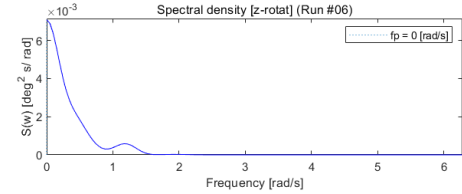
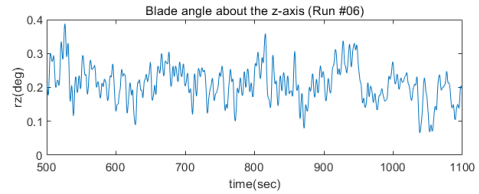
(c) Displacement in the z-direction



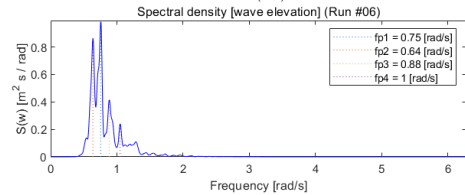
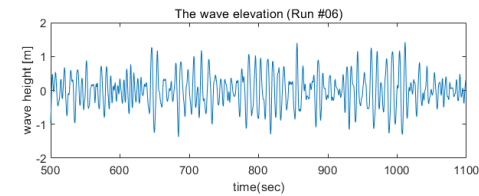
(d) Rotational angle about the x-axis



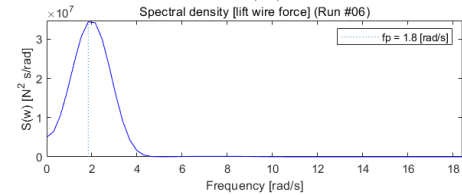
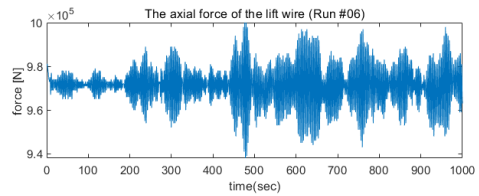
(e) Rotational angle about the y-axis



(f) Rotational angle about the z-axis

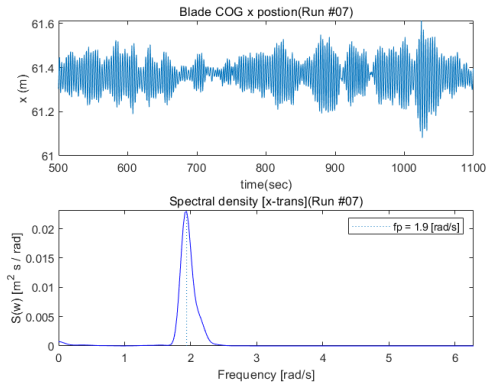


(g) Wave elevation

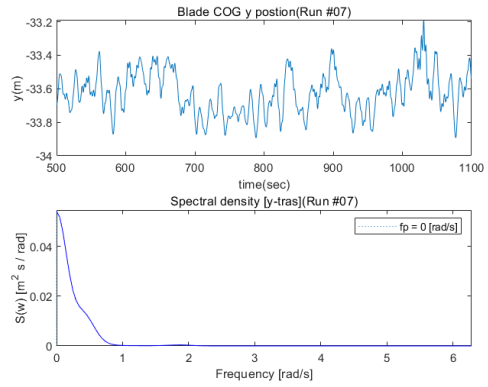


(h) Lift wire axial force

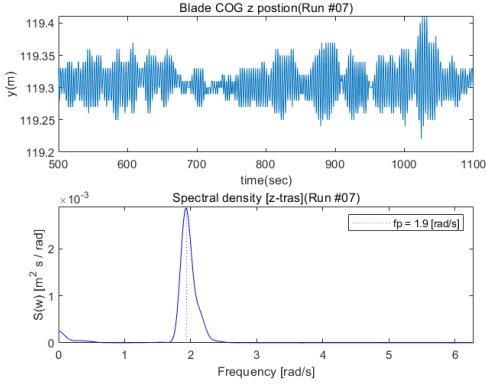
Figure 7.6: Time series and spectral density plots of run #6



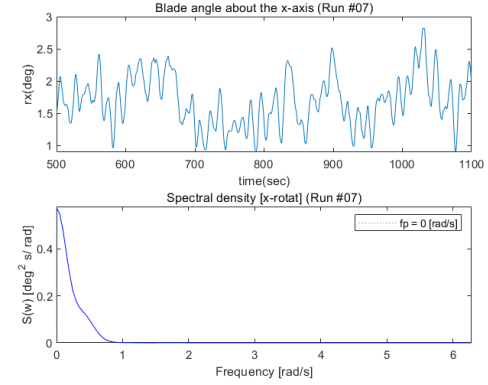
(a) Displacement in the x-direction



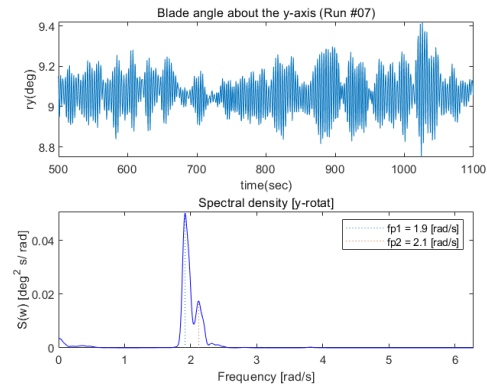
(b) Displacement in the y-direction



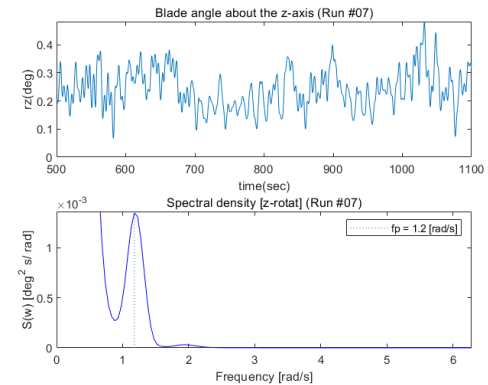
(c) Displacement in the z-direction



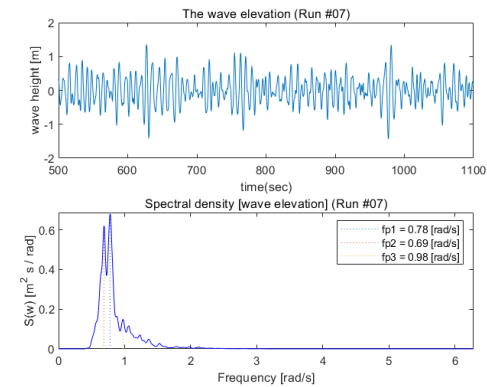
(d) Rotational angle about the x-axis



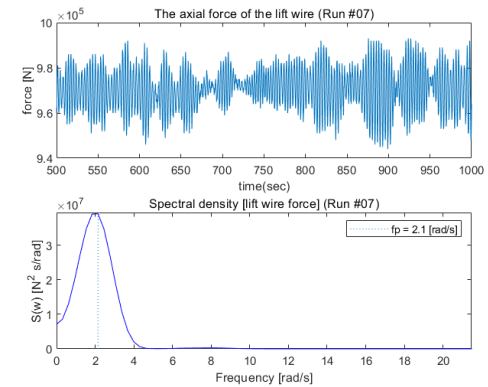
(e) Rotational angle about the y-axis



(f) Rotational angle about the z-axis

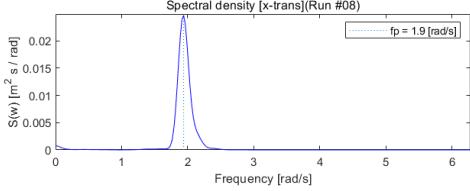
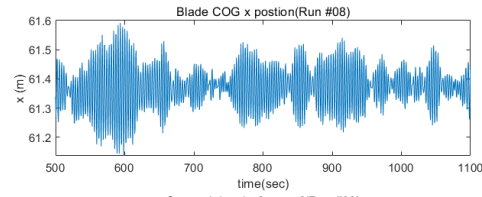


(g) Wave elevation

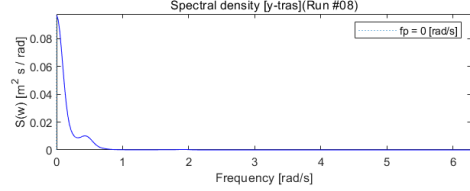
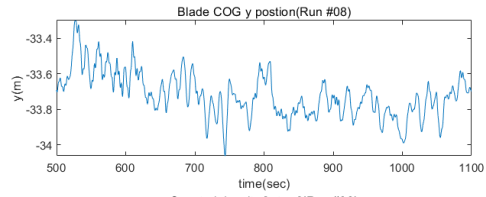


(h) Lift wire axial force

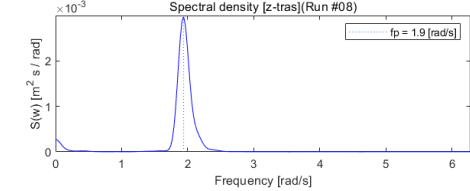
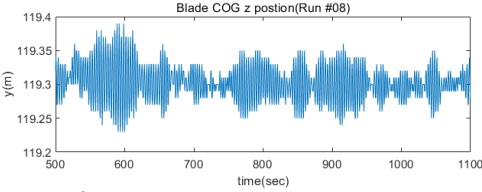
Figure 7.7: Time series and spectral density plots of run #7



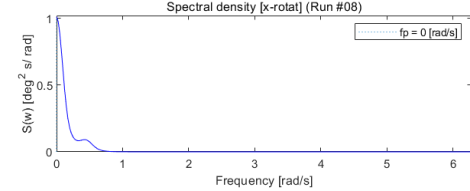
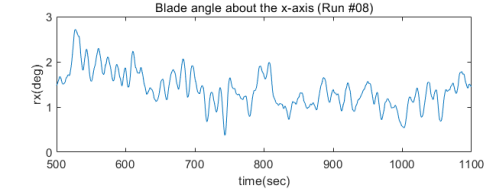
(a) Displacement in the x-direction



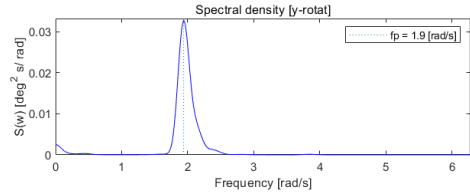
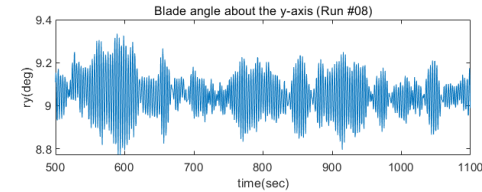
(b) Displacement in the y-direction



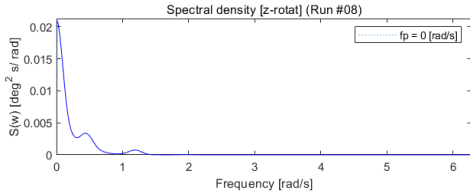
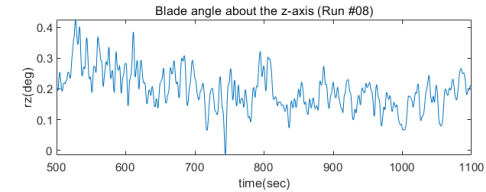
(c) Displacement in the z-direction



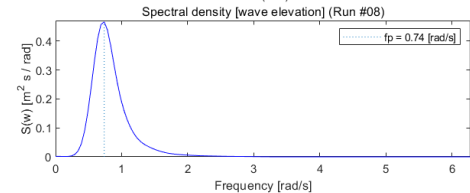
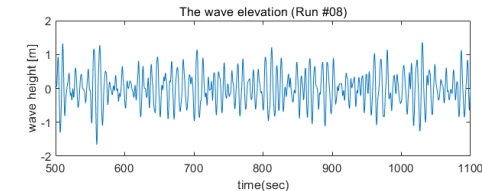
(d) Rotational angle about the x-axis



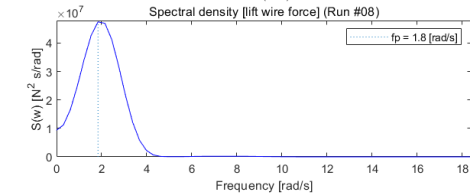
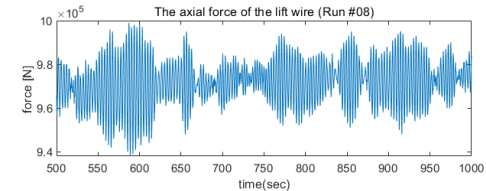
(e) Rotational angle about the y-axis



(f) Rotational angle about the z-axis

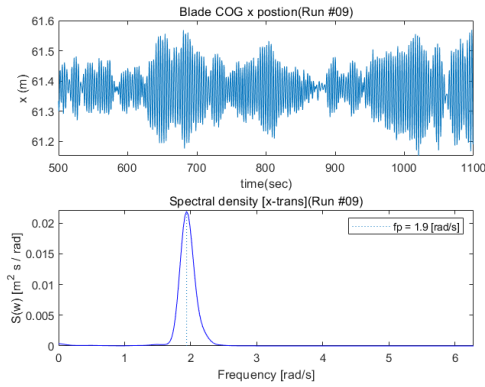


(g) Wave elevation

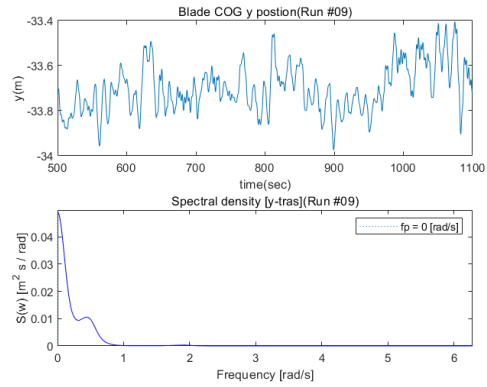


(h) Lift wire axial force

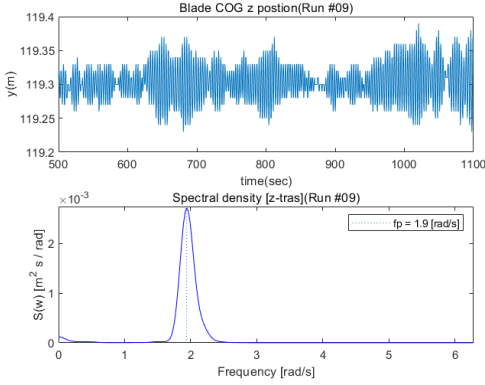
Figure 7.8: Time series and spectral density plots of run #8



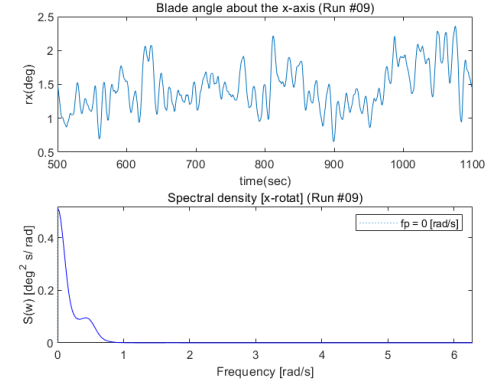
(a) Displacement in the x-direction



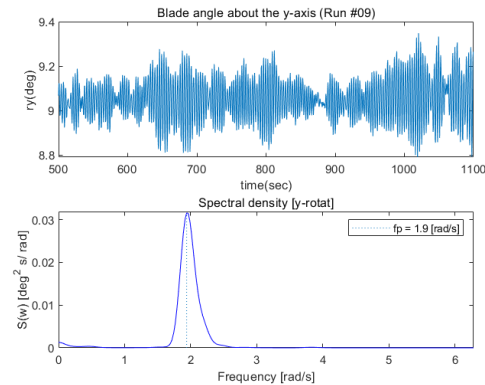
(b) Displacement in the y-direction



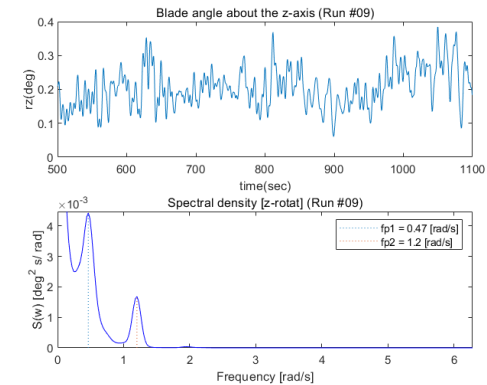
(c) Displacement in the z-direction



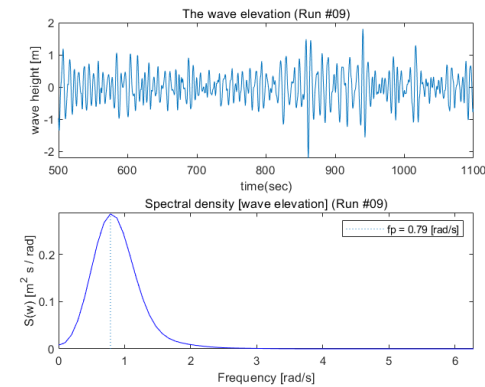
(d) Rotational angle about the x-axis



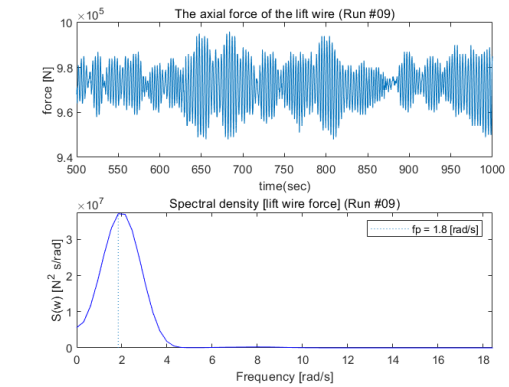
(e) Rotational angle about the y-axis



(f) Rotational angle about the z-axis

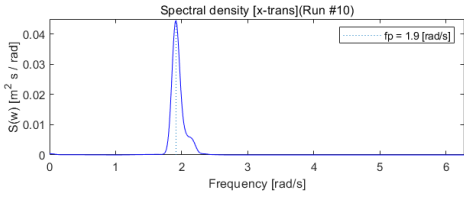
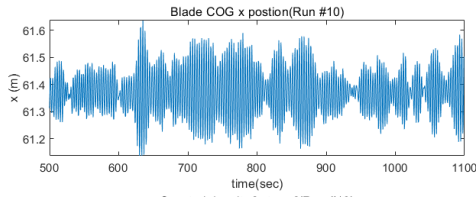


(g) Wave elevation

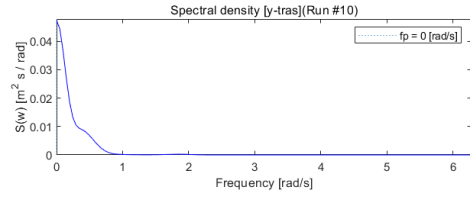
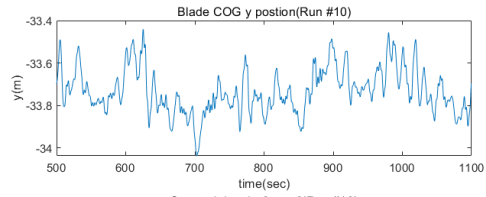


(h) Lift wire axial force

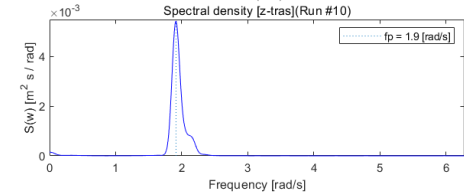
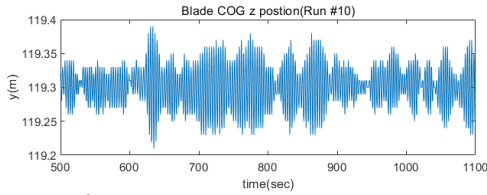
Figure 7.9: Time series and spectral density plots of run #9



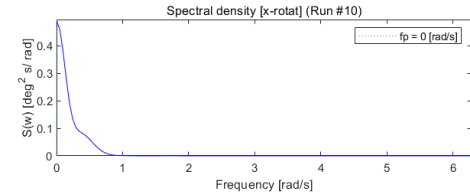
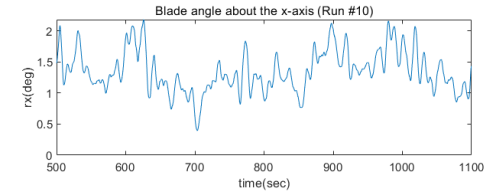
(a) Displacement in the x-direction



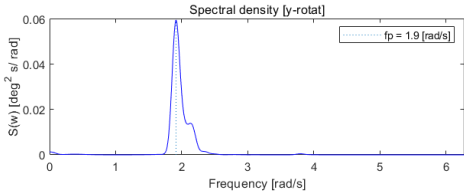
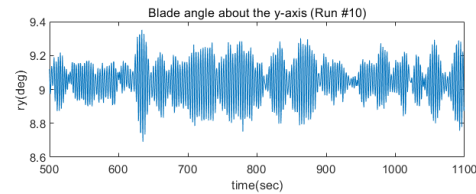
(b) Displacement in the y-direction



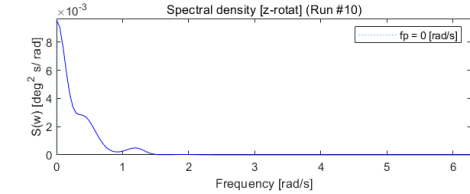
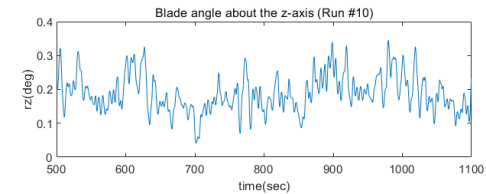
(c) Displacement in the z-direction



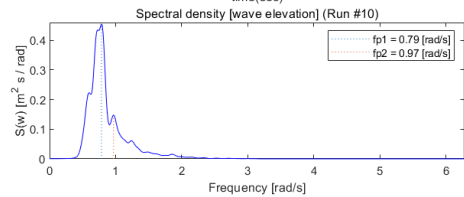
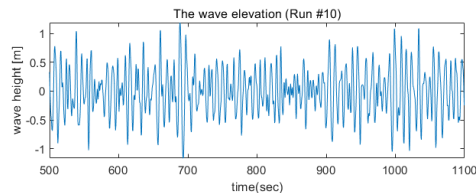
(d) Rotational angle about the x-axis



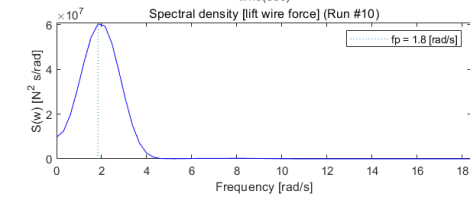
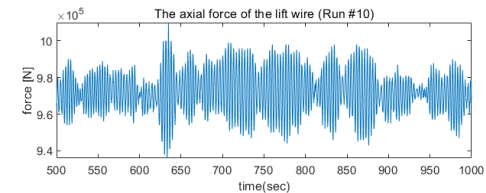
(e) Rotational angle about the y-axis



(f) Rotational angle about the z-axis

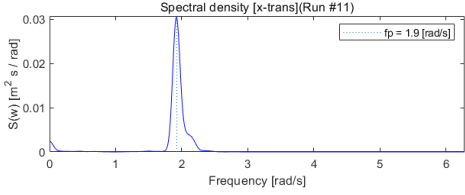
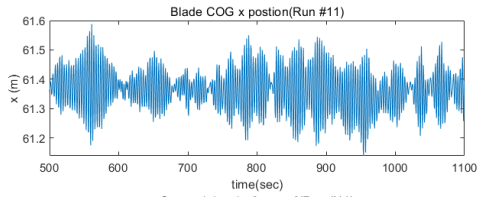


(g) Wave elevation

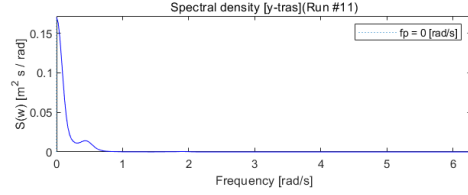
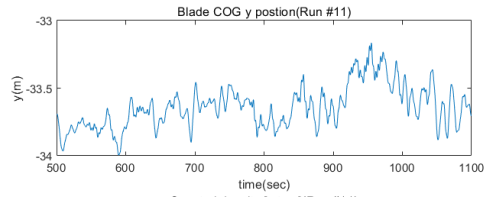


(h) Lift wire axial force

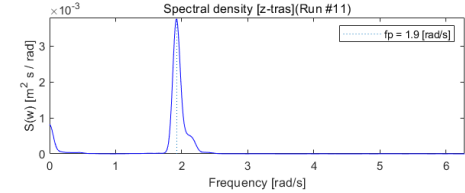
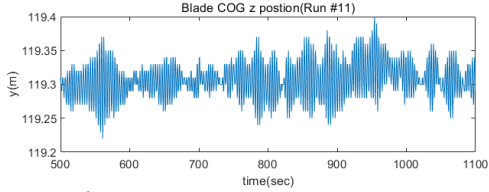
Figure 7.10: Time series and spectral density plots of run #10



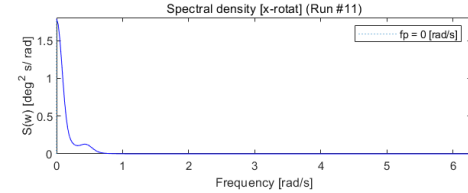
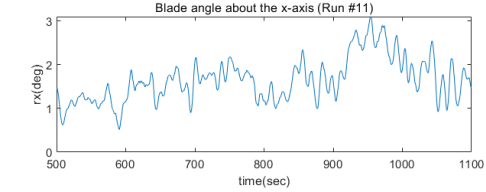
(a) Displacement in the x-direction



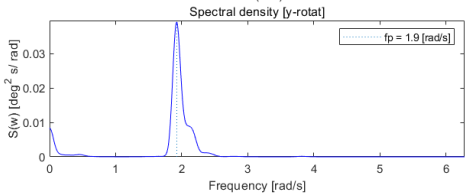
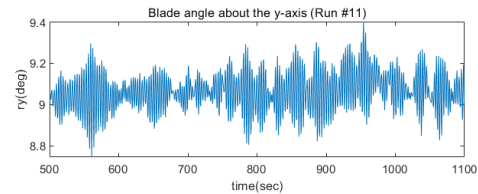
(b) Displacement in the y-direction



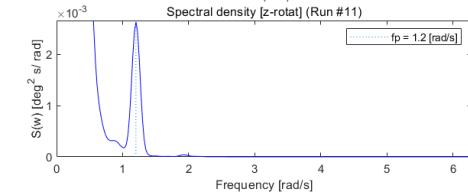
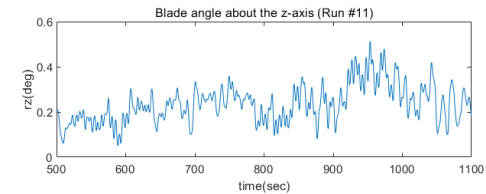
(c) Displacement in the z-direction



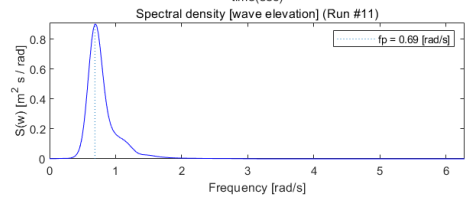
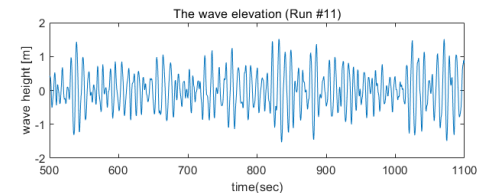
(d) Rotational angle about the x-axis



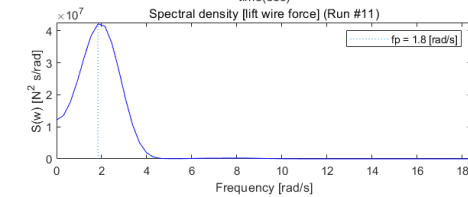
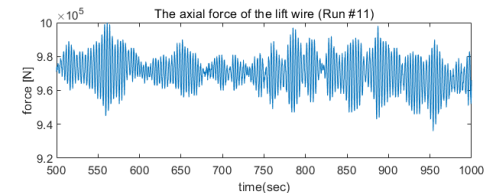
(e) Rotational angle about the y-axis



(f) Rotational angle about the z-axis

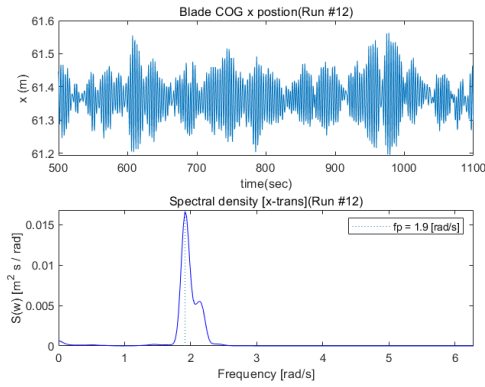


(g) Wave elevation

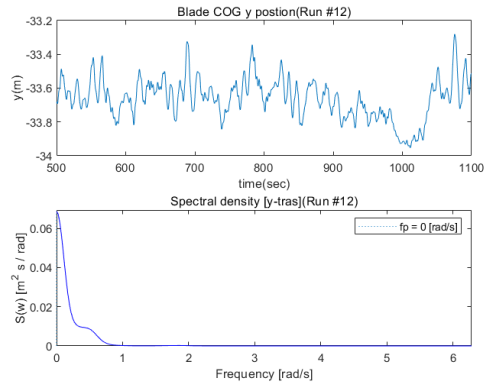


(h) Lift wire axial force

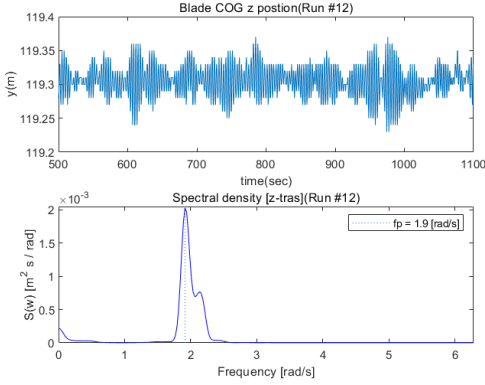
Figure 7.11: Time series and spectral density plots of run #11



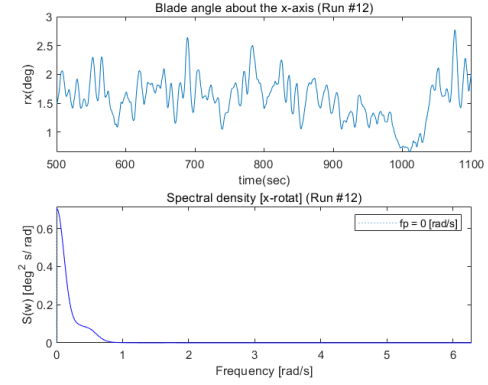
(a) Displacement in the x-direction



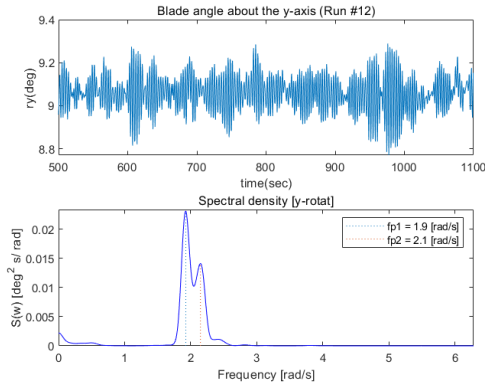
(b) Displacement in the y-direction



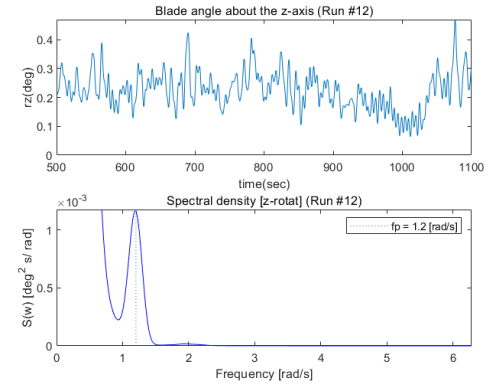
(c) Displacement in the z-direction



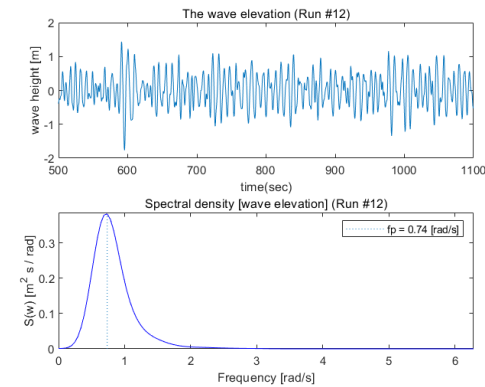
(d) Rotational angle about the x-axis



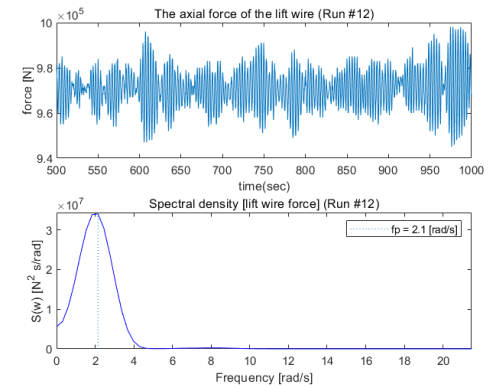
(e) Rotational angle about the y-axis



(f) Rotational angle about the z-axis

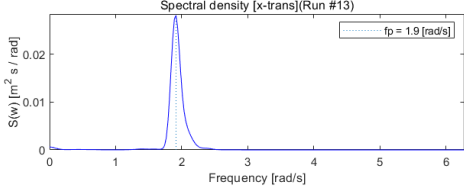
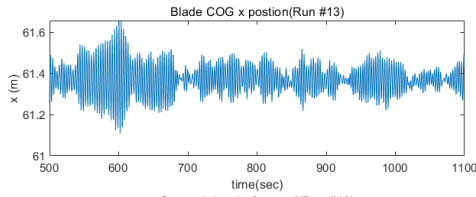


(g) Wave elevation

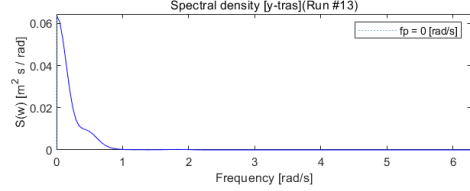
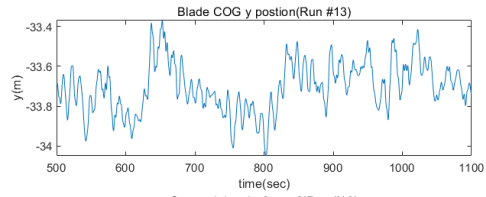


(h) Lift wire axial force

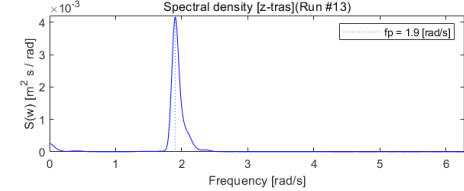
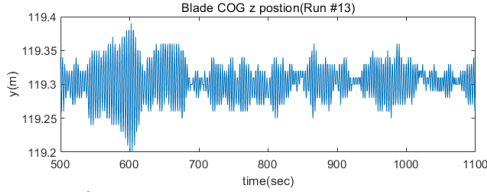
Figure 7.12: Time series and spectral density plots of run #12



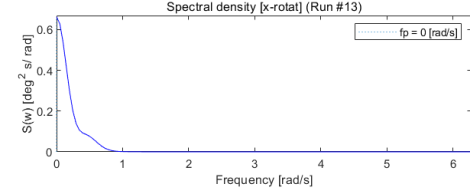
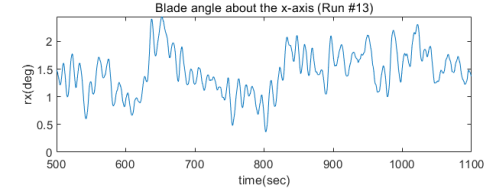
(a) Displacement in the x-direction



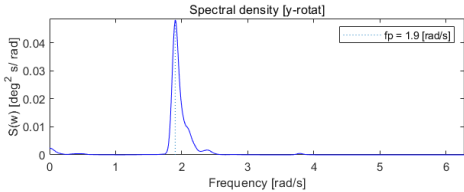
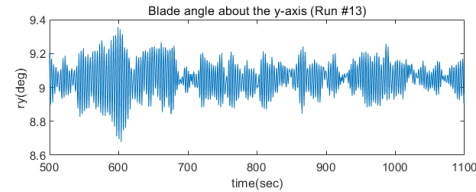
(b) Displacement in the y-direction



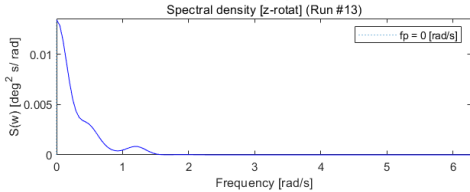
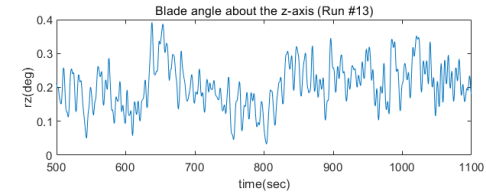
(c) Displacement in the z-direction



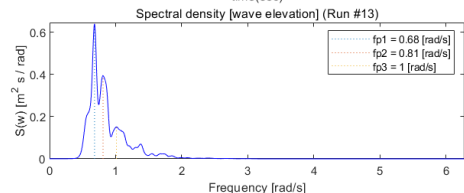
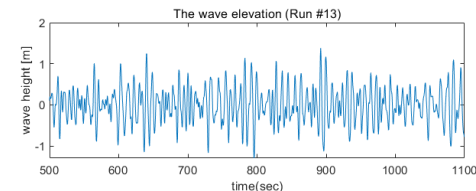
(d) Rotational angle about the x-axis



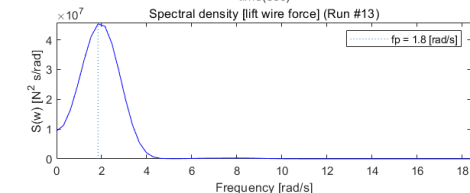
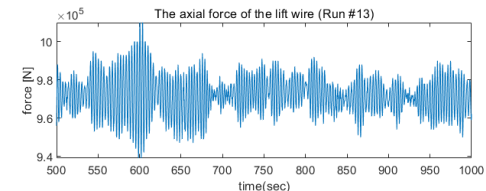
(e) Rotational angle about the y-axis



(f) Rotational angle about the z-axis

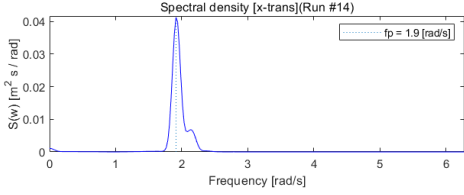
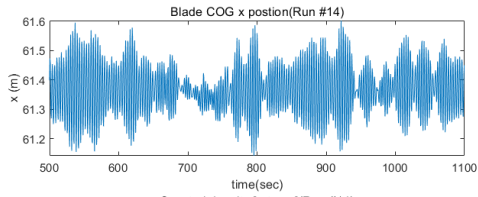


(g) Wave elevation

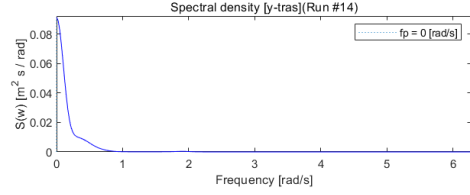
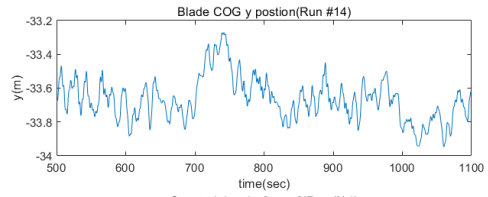


(h) Lift wire axial force

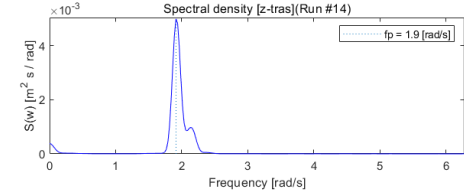
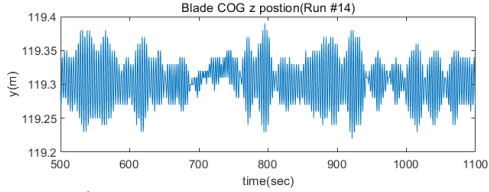
Figure 7.13: Time series and spectral density plots of run #13



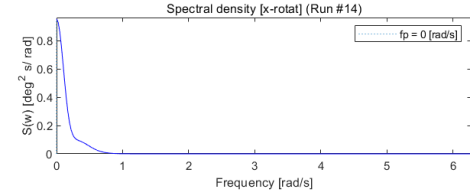
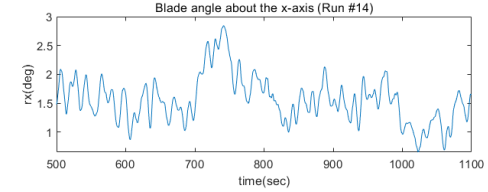
(a) Displacement in the x-direction



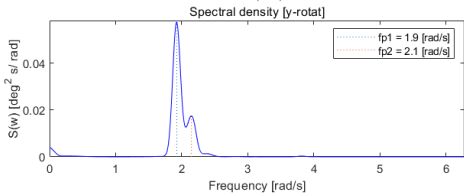
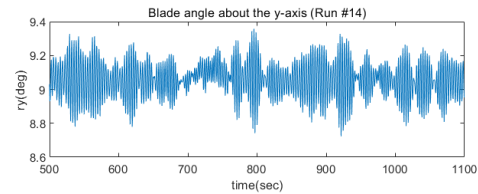
(b) Displacement in the y-direction



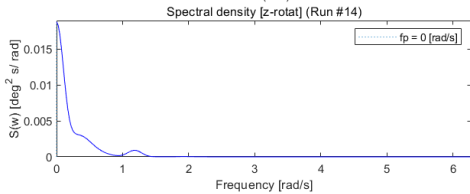
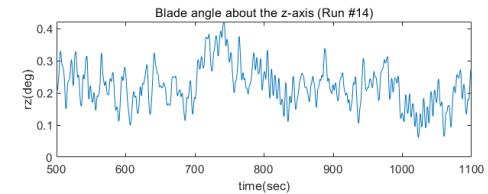
(c) Displacement in the z-direction



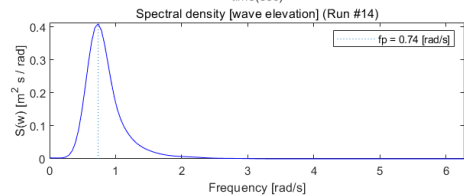
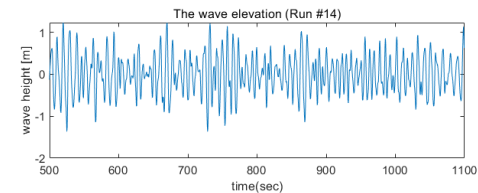
(d) Rotational angle about the x-axis



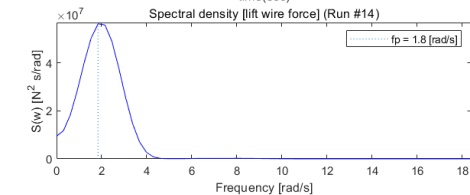
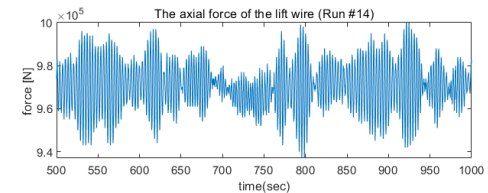
(e) Rotational angle about the y-axis



(f) Rotational angle about the z-axis

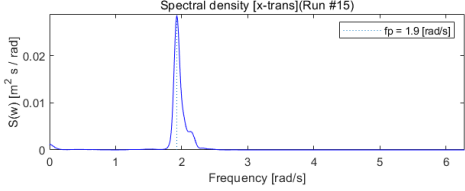
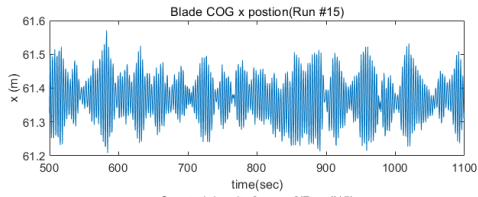


(g) Wave elevation

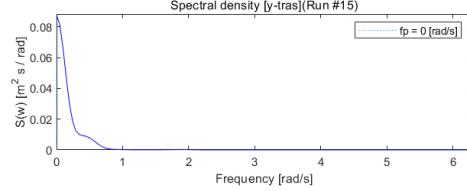
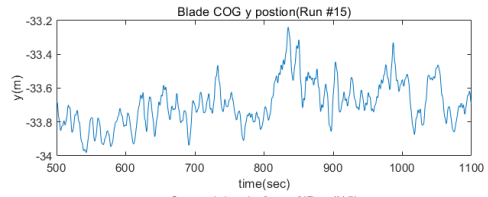


(h) Lift wire axial force

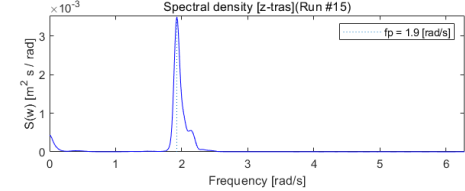
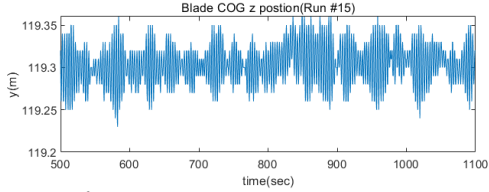
Figure 7.14: Time series and spectral density plots of run #14



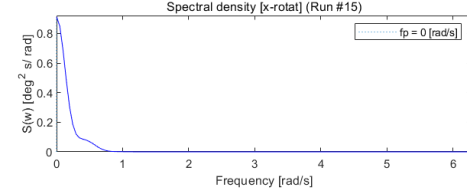
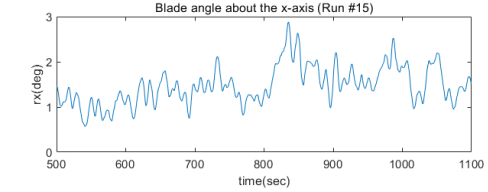
(a) Displacement in the x-direction



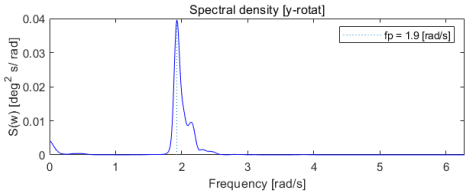
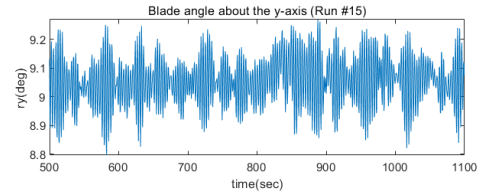
(b) Displacement in the y-direction



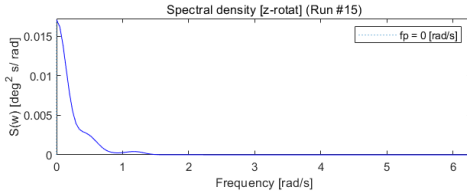
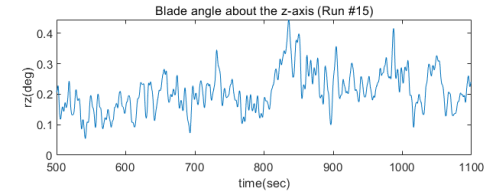
(c) Displacement in the z-direction



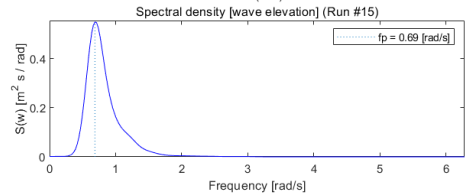
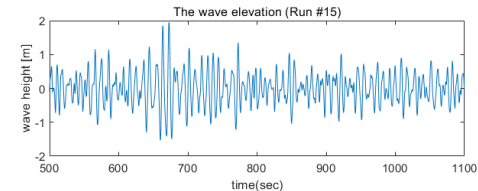
(d) Rotational angle about the x-axis



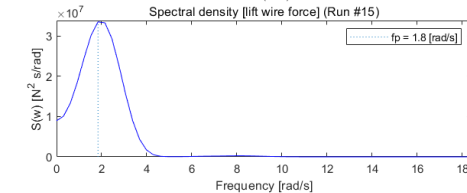
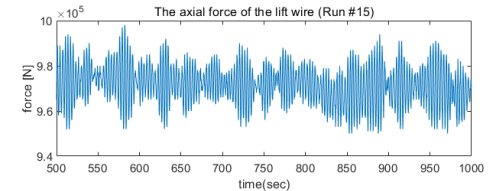
(e) Rotational angle about the y-axis



(f) Rotational angle about the z-axis

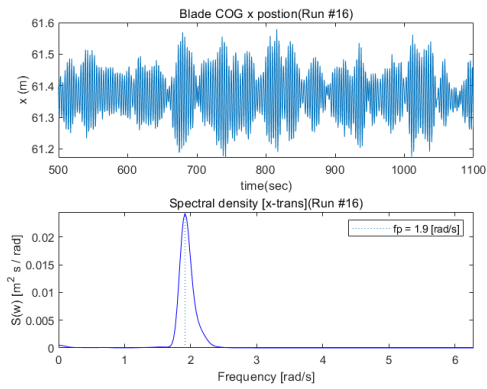


(g) Wave elevation

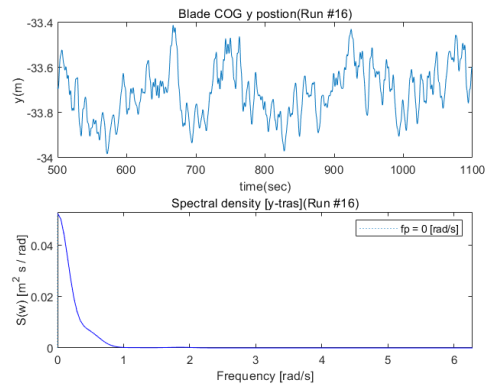


(h) Lift wire axial force

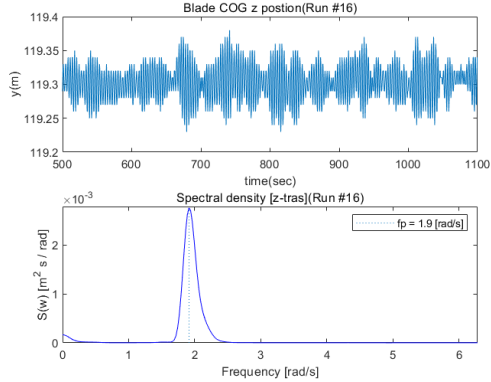
Figure 7.15: Time series and spectral density plots of run #15



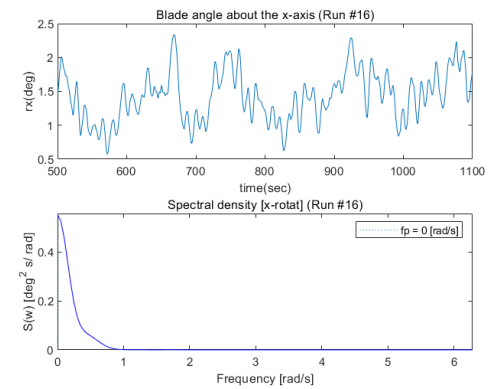
(a) Displacement in the x-direction



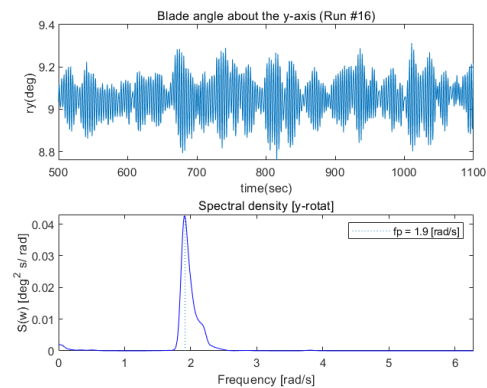
(b) Displacement in the y-direction



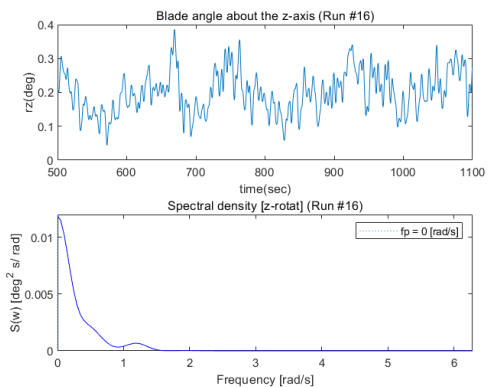
(c) Displacement in the z-direction



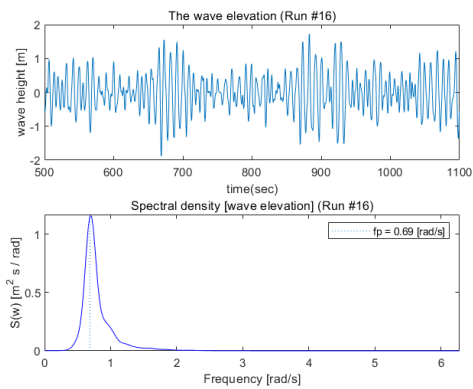
(d) Rotational angle about the x-axis



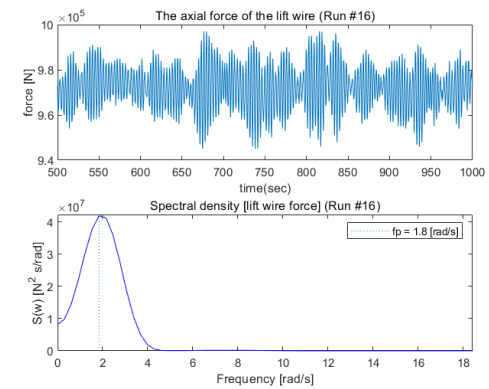
(e) Rotational angle about the y-axis



(f) Rotational angle about the z-axis

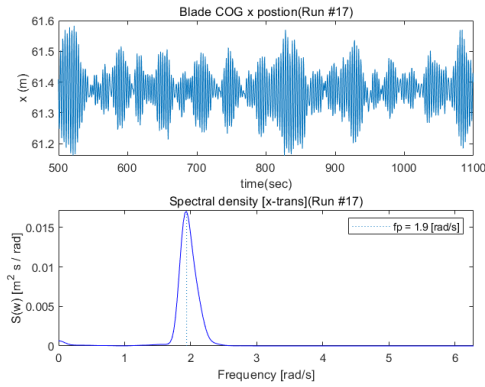


(g) Wave elevation

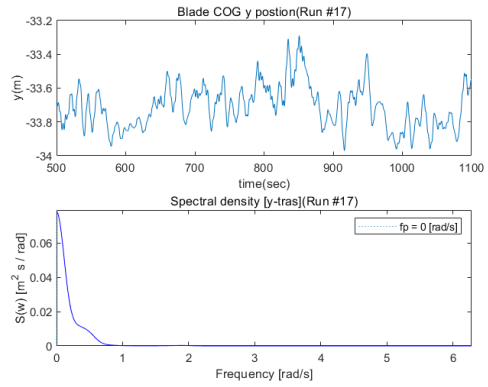


(h) Lift wire axial force

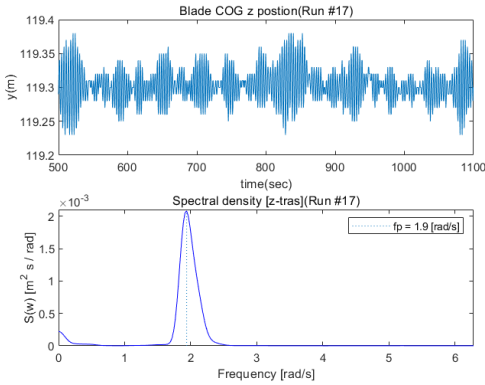
Figure 7.16: Time series and spectral density plots of run #16



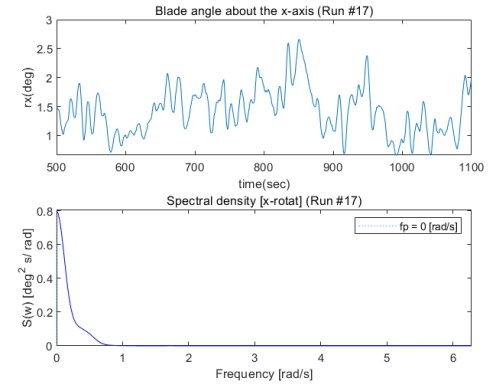
(a) Displacement in the x-direction



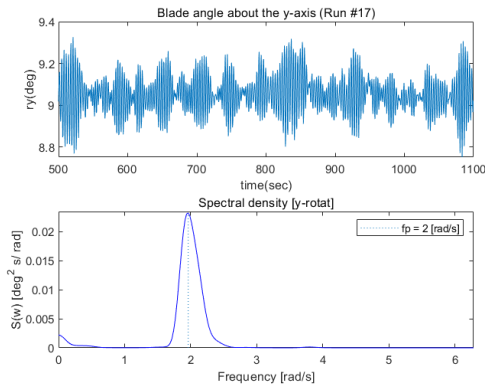
(b) Displacement in the y-direction



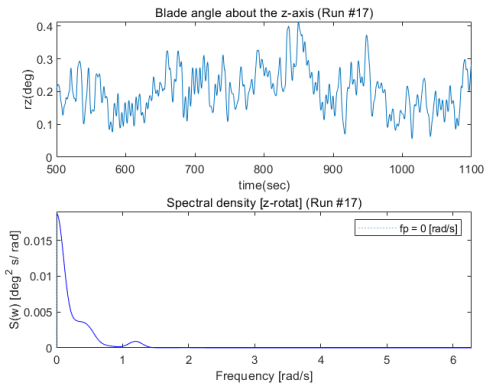
(c) Displacement in the z-direction



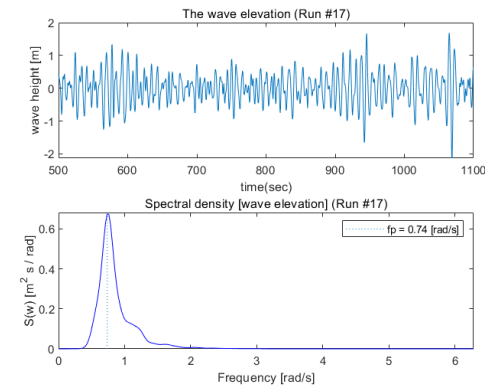
(d) Rotational angle about the x-axis



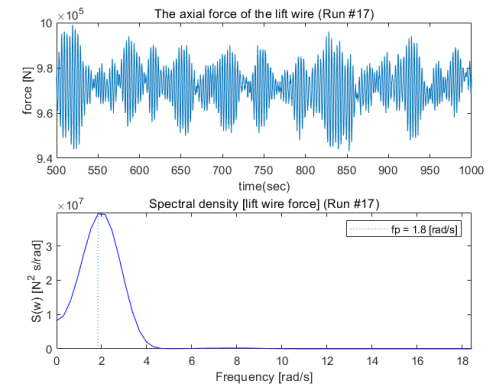
(e) Rotational angle about the y-axis



(f) Rotational angle about the z-axis

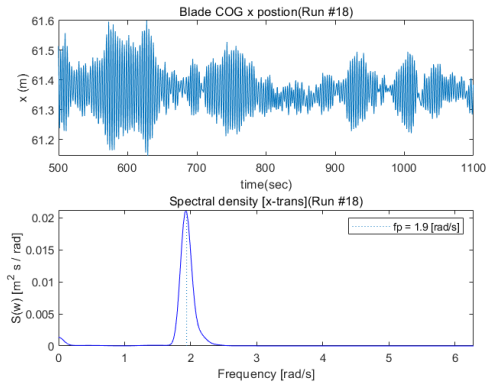


(g) Wave elevation

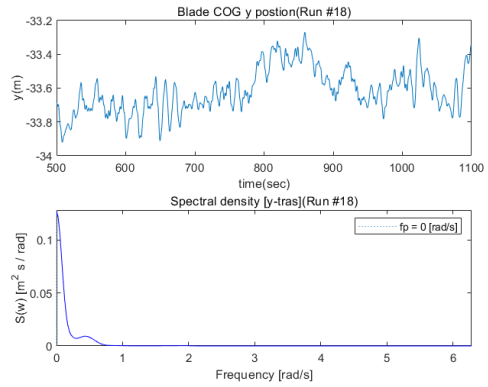


(h) Lift wire axial force

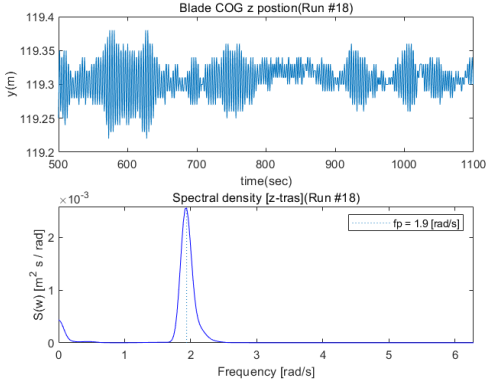
Figure 7.17: Time series and spectral density plots of run #17



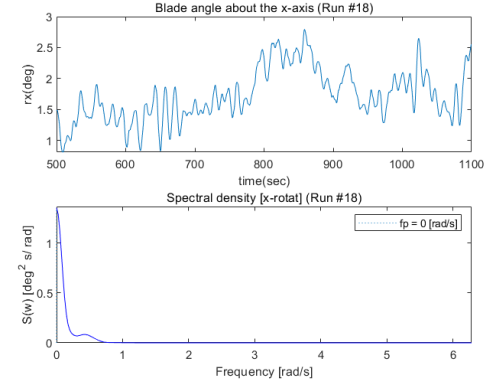
(a) Displacement in the x-direction



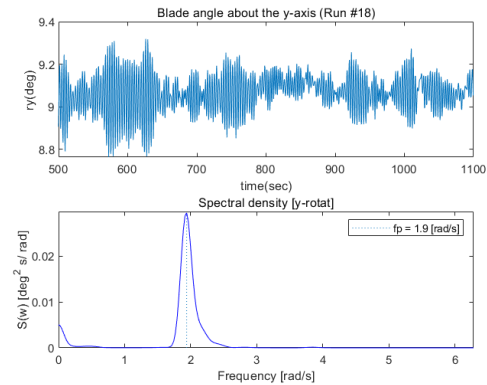
(b) Displacement in the y-direction



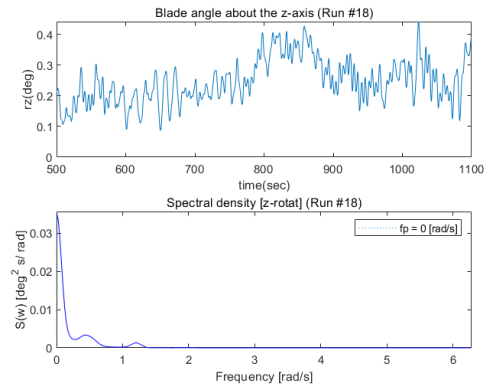
(c) Displacement in the z-direction



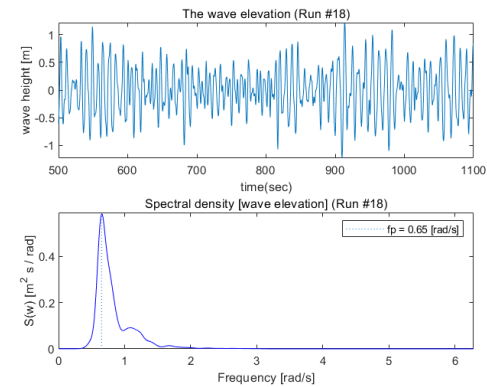
(d) Rotational angle about the x-axis



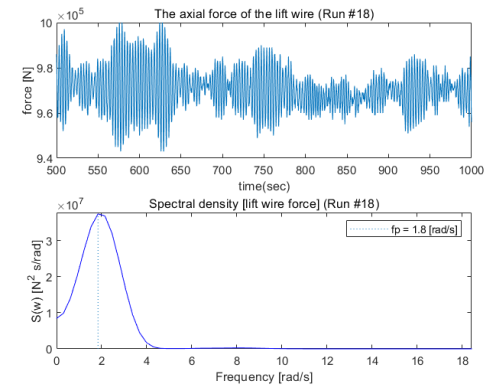
(e) Rotational angle about the y-axis



(f) Rotational angle about the z-axis

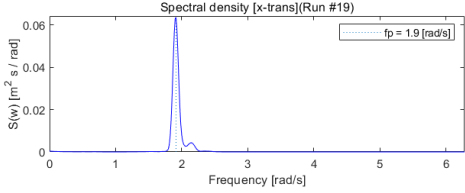
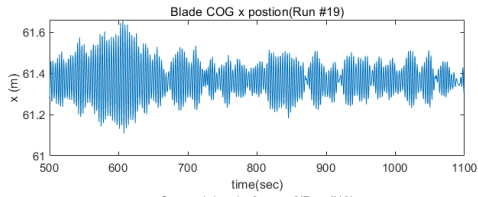


(g) Wave elevation

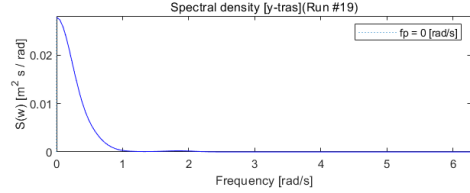
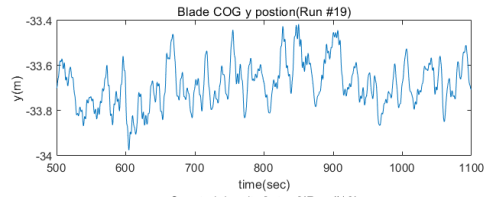


(h) Lift wire axial force

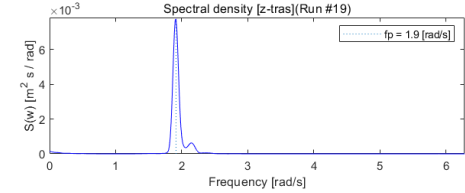
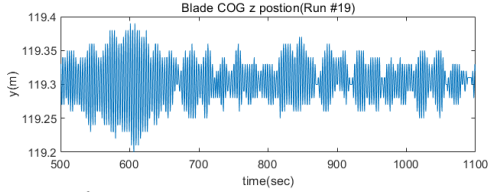
Figure 7.18: Time series and spectral density plots of run #18



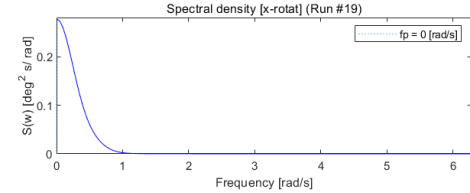
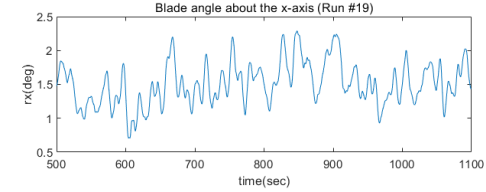
(a) Displacement in the x-direction



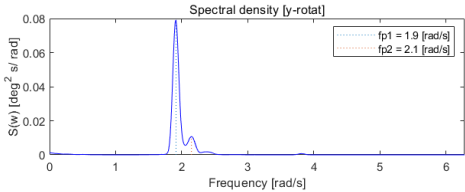
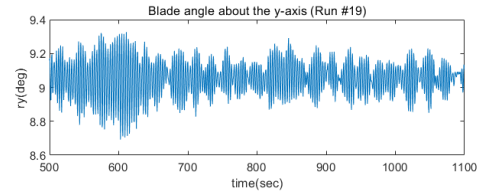
(b) Displacement in the y-direction



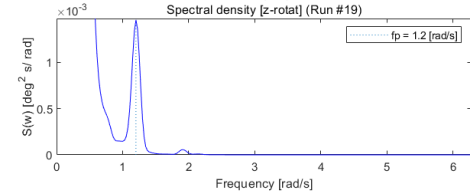
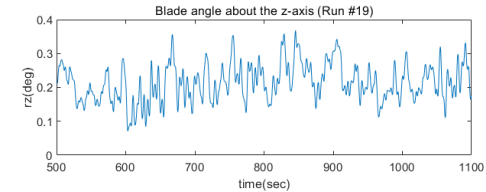
(c) Displacement in the z-direction



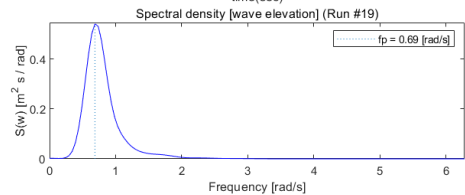
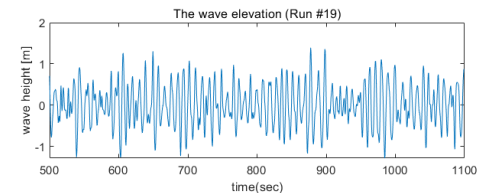
(d) Rotational angle about the x-axis



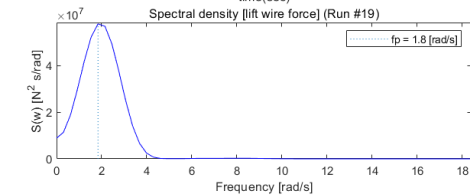
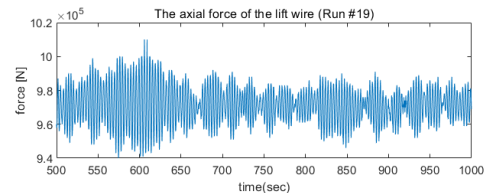
(e) Rotational angle about the y-axis



(f) Rotational angle about the z-axis

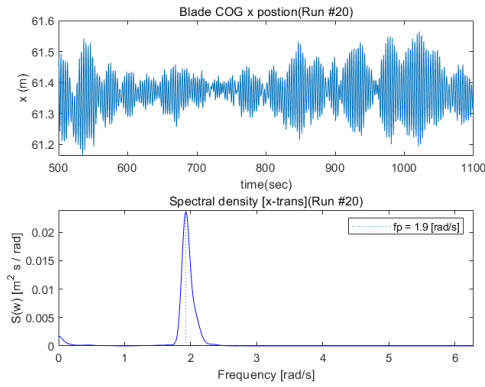


(g) Wave elevation

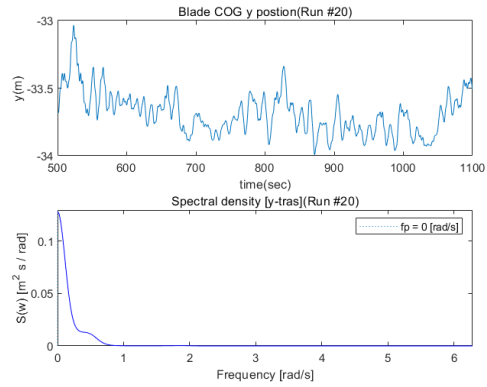


(h) Lift wire axial force

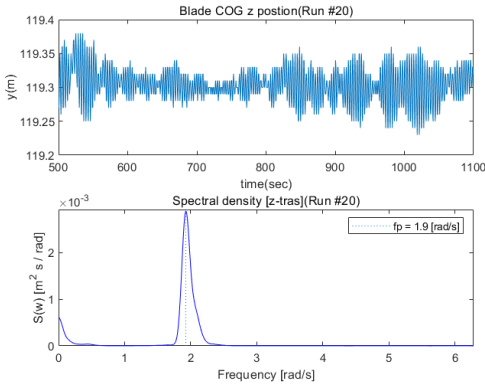
Figure 7.19: Time series and spectral density plots of run #19



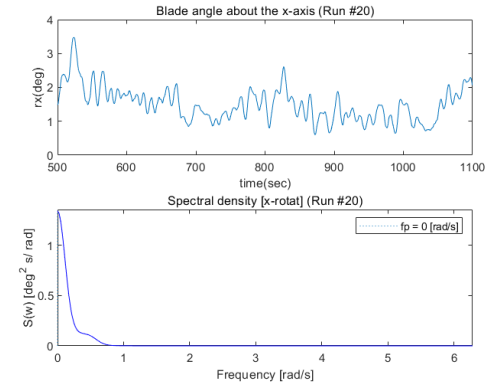
(a) Displacement in the x-direction



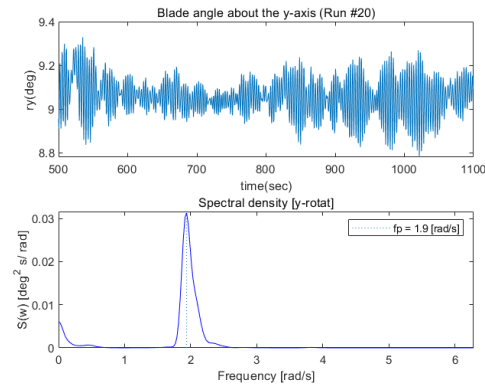
(b) Displacement in the y-direction



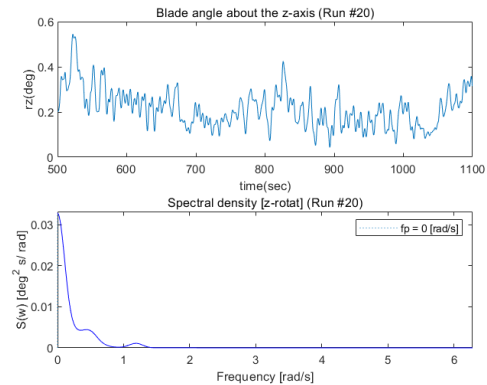
(c) Displacement in the z-direction



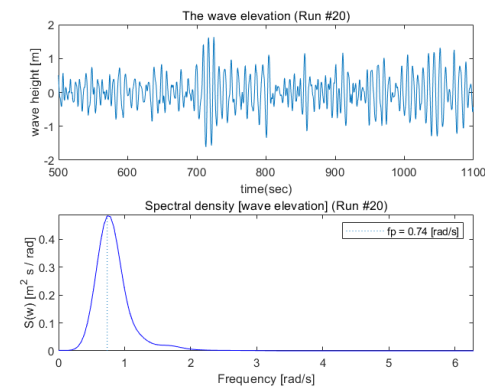
(d) Rotational angle about the x-axis



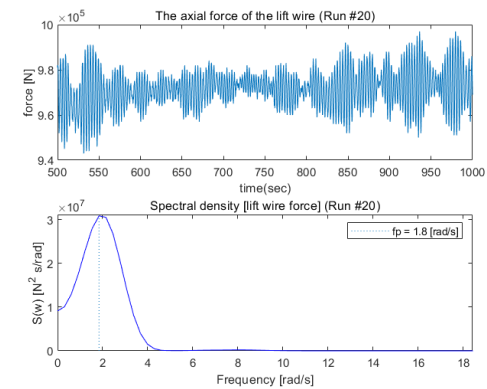
(e) Rotational angle about the y-axis



(f) Rotational angle about the z-axis



(g) Wave elevation



(h) Lift wire axial force

Figure 7.20: Time series and spectral density plots of run #20

Appendix 2: MATLAB scripts

1. Spectral analysis script of section. 4.1.6

```
clear all; close all; clc;

% x translational motion
xx=load("01surge.txt");
XX = dat2spec2(xx);
figure(1);
subplot(2,1,1);
plot(xx(:,1),xx(:,2));
xlabel('time(sec)');
ylabel('x (m)');
title('Blade COG x postion(Run #01)')
subplot(2,1,2);
plotspec(XX);
title("Spectral density [x-trans](Run #01)");

% y translational motion
yy=load("02sway.txt");
YY = dat2spec2(yy);
figure(2);
subplot(2,1,1);
plot(yy(:,1),yy(:,2));
xlabel('time(sec)');
ylabel('y(m)');
title('Blade COG y postion(Run #01)');
subplot(2,1,2);
plotspec(YY);
title("Spectral density [y-tras](Run #01)");

% z translational motion
zz = load("03heave.txt");
ZZ = dat2spec2(zz);
figure(3);
subplot(2,1,1);
plot(zz(:,1),zz(:,2));
xlabel('time(sec)');
ylabel('y(m)');
title('Blade COG z postion(Run #01)');
subplot(2,1,2);
plotspec(ZZ);
title("Spectral density [z-tras](Run #01)");

% rotational motion about x-axis
rx = load("04roll.txt");
RX = dat2spec2(rx);
figure(4);
subplot(2,1,1);
plot(rx(:,1),rx(:,2));
xlabel('time(sec)');
ylabel('rx(deg)');
title('Blade angle about the x-axis (Run #01)');
subplot(2,1,2);
plotspec(RX);
title("Spectral density [x-rotat] (Run #01)");
ylabel("S(w) [deg^2 s/ rad]");

% rotational motion about y-axis
ry = load("05pitch.txt");
RY = dat2spec2(ry);
figure(5);
subplot(2,1,1);
plot(ry(:,1),ry(:,2));
xlabel('time(sec)');
ylabel('ry(deg)');
title('Blade angle about the y-axis (Run #01)');
subplot(2,1,2);
plotspec(RY);
title("Spectral density [y-rotat]");
ylabel("S(w) [deg^2 s/ rad]");

% rotational motion about z-axis
rz = load("06yaw.txt");
RZ = dat2spec2(rz);
```

```

figure(6);
subplot(2,1,1);
plot(rz(:,1),rz(:,2));
xlabel('time(sec)');
ylabel('rz(deg)');
title('Blade angle about the z-axis (Run #01)');
subplot(2,1,2);
plotspec(RZ);
title("Spectral density [z-rotat] (Run #01)");
ylabel("S(w) [deg^2 s/ rad]")

% Lift wire
lift = load("07liftWire.txt");
LIFT = dat2spec2(lift);
figure(7);
subplot(2,1,1);
plot(lift(:,1),lift(:,2));
xlabel('time(sec)');
ylabel('force [N]');
title("The axial force of the lift wire (Run #01)");
subplot(2,1,2);
plotspec(LIFT);
title("Spectral density [lift wire force] (Run #01)");
ylabel("S(w) [N^2 s/rad]")

% Wave elevation
wave = load("08wave.txt");
WAVE = dat2spec2(wave);

figure(8);
subplot(2,1,1);
plot(wave(:,1),wave(:,2));
xlabel('time(sec)');
ylabel('wave height [m]');
title("The wave elevation (Run #01)");
subplot(2,1,2);
plotspec(WAVE);
title("Spectral density [wave elevation] (Run #01)");

```

2. The Gumbel distribution analysis

```
% Extreme analysis
clear all; close all; clc;

% surge
figure(1);
x = load('01surge_max.txt');
X = plotgumb(x)
title('Gumbel Probaility Plot [max surge]');
xlabel('x[m]');

% sway
figure(2);
y = load('02sway_max.txt');
Y = plotgumb(y)
title('Gumbel Probaility Plot [max sway]');
xlabel('y[m]');

% heave
figure(3);
z = load('03heave_max.txt');
Z = plotgumb(z)
title('Gumbel Probaility Plot [max heave]');
xlabel('z[m]');

% roll
figure(4);
rx = load('04roll_max.txt');
RX = plotgumb(rx)
title('Gumbel Probaility Plot [max roll]');
xlabel('rx[deg]');

% pitch
figure(5);
ry = load('05pitch_max.txt');
RY = plotgumb(ry)
title('Gumbel Probaility Plot [max pitch]');
xlabel('ry[deg]');

% yaw
figure(6);
rz = load('06yaw_max.txt');
RZ = plotgumb(rz)
title('Gumbel Probaility Plot [max yaw]');
xlabel('rz[deg]');
```

